A New Route to Poly(*p*-phenylene): Stereoregular Precursors via Transition-Metal-Catalyzed Polymerization

Thesis by

Douglas L. Gin

In Partial Fulfillment of the Requirements

For the Degree of

Doctor of Philosophy

California Institute of Technology

Pasadena, California

1993

(Submitted November 23, 1992)

To my mother and father.

Without their support over the years,

none of this would have been possible.

ACKNOWLEDGMENT

In retrospect, I can honestly say that my time at Caltech has been both an exciting and rewarding experience. The person I have to thank most for making it so is my advisor Bob Grubbs. He gave me direction and encouragement whenever I needed it, and he had enough confidence in my abilities to allow me to pursue my research in my own fashion. I do not think that I could have worked for a better advisor or for a nicer person. Thanks Bob.

There are many people who have been directly involved in this project that I must thank for their help. First, I would like to thank Vince Conticello, my partner in this endeavor for the past two years. We made a good team, and the project would never have gotten this far without his help. A special note of thanks goes out to Denis Ballard, Dave Haddleton, Andy Muir, Alan Nevin, and Evan Roberts at ICI Chemicals and Polymers Ltd., Runcorn, U. K. for providing us with starting materials and specialized polymer analysis over the past four years. Their expertise in the area of poly(*p*-phenylene) precursors was a vital component in the success of this project. I would also like to thank each of them personally for their generous hospitality during my visits to Runcorn. My thanks also to Dave Wheeler, Phil Hampton, and Tammy Ulibarri for their help and advice when I first started out here at Caltech.

There are also many people in the Caltech community who may not have been directly involved in the poly(*p*-phenylene) project but have provided invaluable help over the past four years. I would like to acknowledge their assistance with many aspects of my research. David Baselt and Rik Blumenthal taught me about STM and were invaluable in obtaining STM images of my polymers. In particular, I am indebted to David for all of the STM image processing and for showing me how to get the most out of a Macintosh computer for presentations. The exceptional STM figures in the following chapters of this

thesis are his handiwork. My thanks to Nat Finney for helping me out with many difficult NMR experiments and to Robert Lee for assistance with the solid-state NMR studies. I am also grateful to Jim Armstrong and Paul Carpenter in the Caltech Geology Dept. for allowing me to use their powder X-ray diffractometer and for assistance with the scanning electron microscope. My thanks to Josh Jacobs for performing the magnetic measurements on my polyphenylene samples and for reading over that section of my thesis for me. I would also like to thank Bob Kumpf, Brad Morgan, and Kevin Condroski for advice on computer molecular modeling. Thanks also to the members of the Grubbs research group. I do not believe there is a single person in the group who has not given me a hand or some helpful suggestions at one time or another. I would also like to thank the following people for proofreading this thesis: Vince, Greg Fu, SonBinh Nguyen, and my brother Dave.

To the many friends I have made here at Caltech, thank you for making my graduate career an enjoyable experience. Finally, I would like to thank my parents for their support and encouragement over the years.

A predoctoral fellowship from the
Natural Sciences and Engineering Research Council of Canada
is gratefully acknowledged.

ABSTRACT

Poly(*p*-phenylene) (PPP) is an insoluble rigid-rod polymer that possesses remarkable thermal stability, chemical resistance, and electrical conductivity when doped. The structural properties that make PPP such an attractive engineering material also make it very difficult to synthesize and process. Although many direct and precursor routes to PPP have been developed they have generally afforded low molecular weight material containing a substantial amount of structural defects that are detrimental to the properties of the final product. We have developed a new precursor route to PPP which offers processability as well as a high molecular weight, high quality polymer.

1,4-Linked, stereoregular precursors to PPP were synthesized by transition-metal-catalyzed polymerization of heteroatom-functionalized 1,3-cyclohexadienes. *cis*-5,6-Bis(trimethylsiloxy)-1,3-cyclohexadiene (TMS-CHD), a derivative of a microbial oxidation product of benzene, is polymerized stereospecifically by bis[(η^3-allyl)trifluoroacetatonickel(II)] with yields up to 96%. Not only does this polymerization system afford a highly 1,4-linked, stereoregular polymer, but it also has the potential for molecular weight control. The resulting polymer, [1,4-poly(TMS-CHD)], is a soluble, processable, semicrystalline material. Although 1,4-poly(TMS-CHD) cannot be pyrolyzed to yield PPP directly, the trimethylsilyl ethers on the polymer can be transformed to better leaving groups such as acetates to give the corresponding stereoregular acetoxy polymer (100% acetylation; 93% overall yield). Due to the low thermal stability of the stereroregular backbone, aromatization of this acetoxy polymer to PPP requires Lewis or Brønsted acid catalysts. Acids lower the onset temperature of the acid elimination process to a temperature regime well below that at which depolymerization can occur. The high quality PPP produced by the acid-catalyzed aromatization of the stereoregular acetoxy polymer exhibits properties comparable to those of PPP samples in the literature.

However, it is completely amorphous whereas PPP samples made by other routes are almost always semicrystalline. Since the physical and chemical properties of PPP and many other conjugated polymers depend highly on sample morphology, processing techniques for this material will have to be developed before its optimum properties can be realized.

TABLE OF CONTENTS

LIST OF FIGURES

CHAPTER 1

CHAPTER 2

CHAPTER 3

LIST OF TABLES

CHAPTER 2

CHAPTER 3

CHAPTER 1

Introduction:
Synthetic Approaches to Poly(*p*-phenylene)

Poly(*p*-phenylene)

Poly(*p*-phenylene) (PPP) (Figure 1) is a conjugated, rigid-rod polymer with unique structural and electronic properties.[1-4]

PPP

Figure 1. Poly(*p*-phenylene).

As an engineering material, its attractiveness arises from its relatively low density, high mechanical strength, excellent thermal stability, solvent resistance, and chemical inertness. Even though PPP only has a density of approximately 1.1–1.2 g/cm^3, the sintered material has a tensile strength of up to 5000 psi under optimum fabrication conditions.[5] In fact, the mechanical properties of PPP are ranked with those of the commercial polyimides and carbon fibers, the premier engineering polymers.[5] PPP is also thermally stable to approximately 450 °C in air and to 500–550 °C under argon.[2] Inside an oxidizing flame, the material glows and slowly decomposes but does not burn.[1] In addition, PPP is completely insoluble and intractable, and only extremely harsh reaction conditions are able to effect chemistry on the polymer.[1] Because of its excellent structural properties, PPP has already been used in ceramic and carbon fiber composites, as a lubricant additive, and in forming high strength, light-weight, sintered parts.[6]

As an electronic material, PPP's attractiveness arises from its conjugated π-electron system which allows it to be converted from an insulator to a highly conducting polymer upon doping. In its pristine state, PPP is a highly insulating material ($\sigma \leq 10^{-12}$ S/cm)[1,2] with a theoretical UV/visible absorption maximum of 339 nm and a band gap of 3.8 eV.[7] However, when doped with n-type (e.g., Li) or p-type (e.g., AsF_5) dopants, PPP forms highly conducting charge–transfer complexes with conductivities up to 500

S/cm.[1,2] Because of these electronic properties, current attention on doped PPP has focused on its use as electrodes in light-weight rechargeable batteries, as polymer-based wires, and as solar cell components.[6] Undoped PPP has been proposed for use as an electromagnetic shielding material and as an insulating layer in semiconductors.[6] PPP has also recently been utilized as the active component in a new type of polymer-based blue light emitting diode.[8]

Other potentially useful properties of PPP are its radiation resistance and its magnetic behavior. Pressed pellets of PPP can withstand high doses of β-radiation without significant degradation in their mechanical properties.[1,4] PPP is also intrinsically paramagnetic. Depending on the method of synthesis, the material contains unpaired electrons with spin densities of 10^{16}–10^{21} spins/gram.[1] The radical species present in the PPP matrix are extremely stable since storage of the polymer in air for over 10 years has little effect on the spin concentration.[1]

Clearly, there is a wide spectrum of applications for PPP as both a structural material and a conducting polymer. Unfortunately, the development of PPP for commercial applications has been hampered by two factors: (1) The structural properties that make PPP such an attractive engineering polymer also make it difficult to synthesize and process. (2) The excellent mechanical and electronic properties of PPP are highly dependent on its structural regularity and molecular weight. All previous synthetic routes to PPP have been unable to produce a high molecular weight polymer with a completely 1,4-linked (*para*) structure.

Direct Synthetic Routes to Poly(*p*-phenylene)

Many direct synthetic routes to PPP have been developed over the years, but they have all met with only limited success. For example, step growth polymerizations of 1,4-disubstituted benzenes and 4,4'-disubstituted biphenyls have been employed as direct avenues to PPP. The earliest approaches involved the coupling of 1,4-dihalobenzenes using alkali metals (the Wurtz–Fittig reaction),[9,10] activated copper, or silver (the Ullmann reaction) (Figure 2).[11-13]

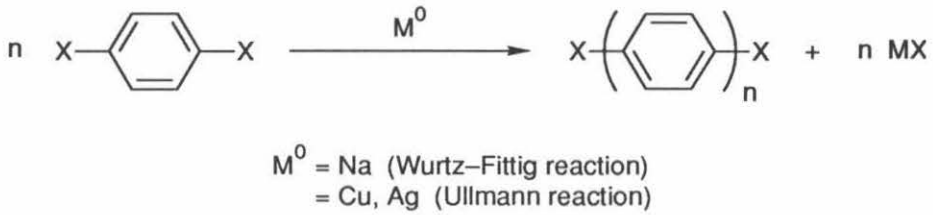

Figure 2. The synthesis of PPP via the Wurtz–Fittig and Ullmann reactions.

However, the polyphenylenes made by these processes are not strictly linear.[13] Generally, oligomers containing halogen impurities and structural defects in the form of sidechains and non-linear 1,3-linkages are obtained.[10] Polyphenylene has also been obtained by the coupling of 4,4'-diazobiphenyls using Cu^+ salts (Figure 3), but the polymers contain a substantial number of azo groups and branches due to the radical coupling mechanism of the reaction.[13-16]

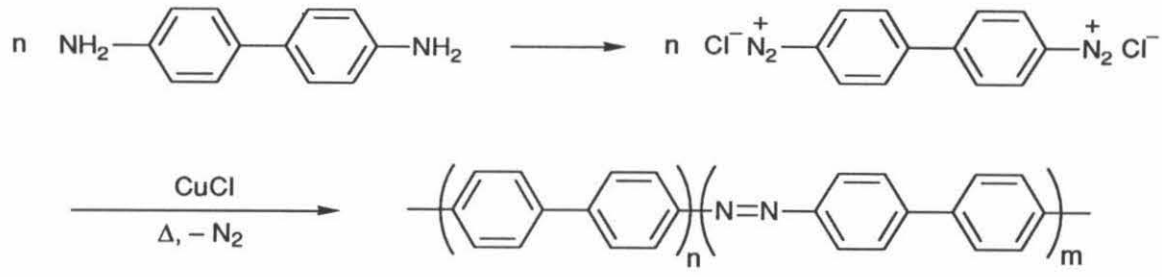

Figure 3. The synthesis of PPP via the coupling of 4,4'-diazobiphenyls.

More recently, attempts to synthesize PPP directly from 1,4-dihalobenzenes have focussed on catalyzed Grignard coupling (Figure 4),[17-19] Ni-catalyzed electropolymerization,[20-22] and Ni-catalyzed polycondensation (Figure 5).[23]

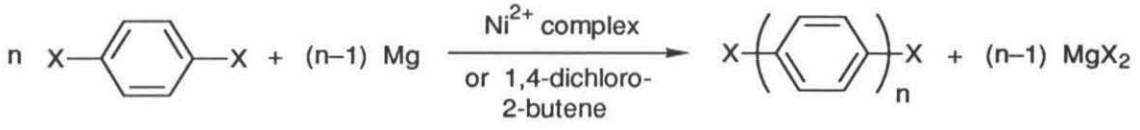

Figure 4. The synthesis of PPP via the catalyzed Grignard coupling of 1,4-dihalobenzenes.

Figure 5. The synthesis of PPP via the Ni-catalyzed polycondensation of 1,4-dihalobenzenes.

Although these reactions give entirely 1,4-linked products, only oligomers are produced because the inherent insolubility of the growing PPP chains causes them to precipitate out of solution before high molecular weight materials form. PPP with a number average degree of polymerization (DP) of approximately 24–38 has been claimed,[17,23] but it is more likely that only 14–16-mers are formed because extreme insolubility is reached in the *p*-oligophenyl series with only seven or eight rings.[1] A modification of the Wurtz–Fittig type reaction using lithium reagents has also been recently employed (Figure 6);

however, the final product is soluble and contains a considerable amount of 1,3-linkages.[24]

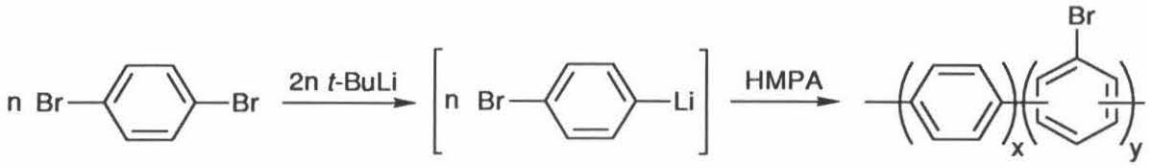

Figure 6. The synthesis of PPP by Li–HMPA promoted coupling of 1,4-dibromobenzene.

Poly(*p*-phenylene) has also been directly synthesized by high temperature Diels–Alder coupling of 1,4-phenyl-bis(pyrones) with 1,4-dialkynylbenzenes (Figure 7).[25,26] However, model reactions of the Diels–Alder polycondensation process indicate that this step growth polymerization yields approximately 10% 1,3-linkages [26] In addition, the PPP produced by this method has structural defects in the form of residual pyrone or carboxylic acid as indicated by the presence of a weak carbonyl band in the IR spectrum of the PPP formed.[25,26]

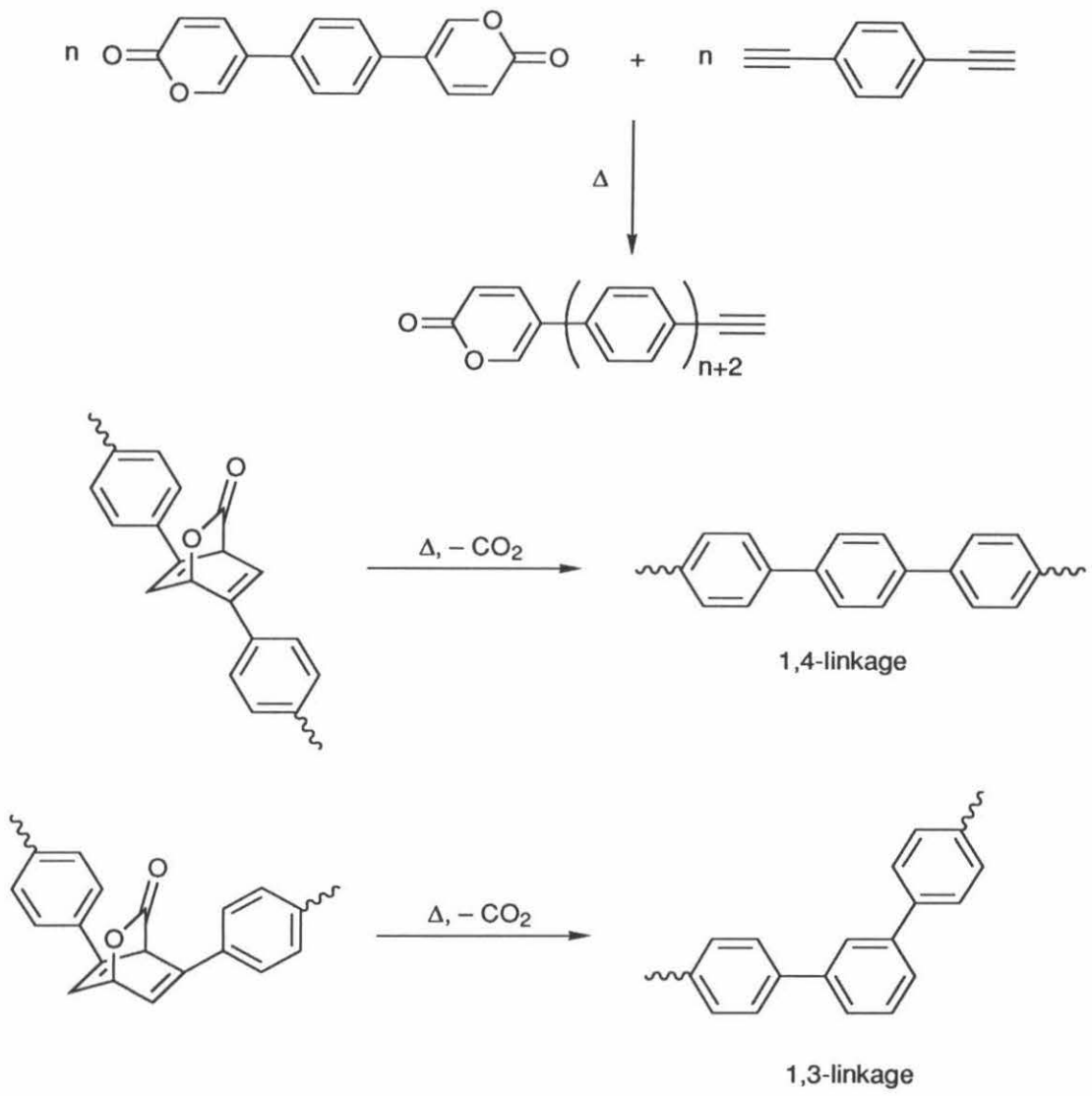

Figure 7. The synthesis of PPP by Diels–Alder polycondensation of 1,4-phenylbis(pyrone) with 1,4-diethynylbenzene.

A third direct synthetic approach to PPP is the direct polymerization of benzene and *p*-oligophenyls. For example, electrochemical polymerization of benzene in strong acids or liquid SO_2 has been used to obtain PPP.[27-29] Oxidative cationic polymerization of benzene using a variety of Lewis acid/oxidizing agent combinations (e.g., $AlCl_3/CuCl_2$) has also been employed (Figure 8).[1]

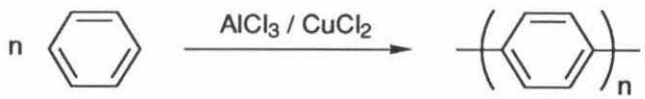

Figure 8. The synthesis of PPP by oxidative cationic polymerization of benzene.

Again, the polymers obtained from these two routes quickly precipitate out of solution before high molecular weight materials are formed. The PPP made from the electropolymerization of benzene has been claimed to have a DP of approximately 38[29] whereas the material formed by oxidative cationic polymerization has been found to have only a DP of 13–15.[1,2] In addition, the PPP materials made by both these routes contain structural defects in the form of polynuclear aromatic regions (Figure 9).[1,29]

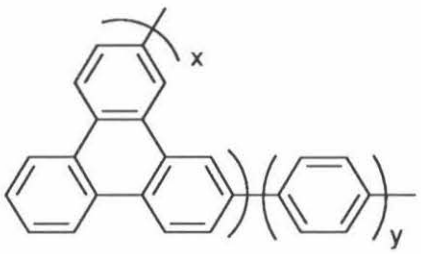

Figure 9. Polynuclear aromatic structures produced by the direct polymerization of benzene.

Similarly, oxidative cationic polymerization of *p*-oligophenyls also yields low molecular weight material but with a large percentage of 1,3-linkages.[1]

In general, direct synthetic routes to PPP suffer from either the lack of 1,4-regiochemical control during the polymerization, or the premature precipitation of the growing PPP chains. Also, post-synthesis processing of the PPP's obtained from even the more successful direct methods is difficult if not impossible due to the material's inherent insolubility and intractability. In order to overcome these problems, soluble substituted PPP's have also been synthesized by the coupling of substituted 1,4-functionalized benzenes,[30-36] by Diels–Alder polycondensation,[37-40] and by oxidative cationic

polymerization of substituted benzenes.[1] Substituents permit the formation of higher molecular weight polymers by allowing the growing chains to remain in solution. Although the direct syntheses of substituted PPP's offer higher molecular weight materials with improved processability, many of these routes still do not give entirely linear polyphenylene.[30,31,37-40] In addition, the improved molecular weights and processability are achieved at the cost of many of the desirable properties of parent PPP. For example, the presence of pendant groups on PPP often reduces the material's thermal stability and chemical inertness compared to parent PPP.[37-40] In addition, the steric effects of sidechains on the polymer backbone increases the ring torsion angle between adjacent phenylene units and reduces the extent of conjugation necessary for high electrical conductivity in the doped material.

Precursor Routes to Poly(*p*-phenylene)

In order to circumvent the synthetic limitations that result from the inherent insolubility of PPP, several precursor strategies have also been developed. By using a high molecular weight, processable intermediate polymer that can be converted to PPP, these strategies offer processability without sacrificing any of the desirable properties of the final material.

The first precursor route to PPP employed polycyclohexadiene as a processable intermediate.[41-44] In this strategy, the precursor polymer is obtained by cationic,[42] anionic,[44] or Ziegler–Natta[41,42] polymerization of 1,3-cyclohexadiene. By heating the polycyclohexadiene with choranil,[41,42] or by brominating the polymer and then thermally eliminating HBr and H_2,[42-44] aromatic units are produced (Figure 10).

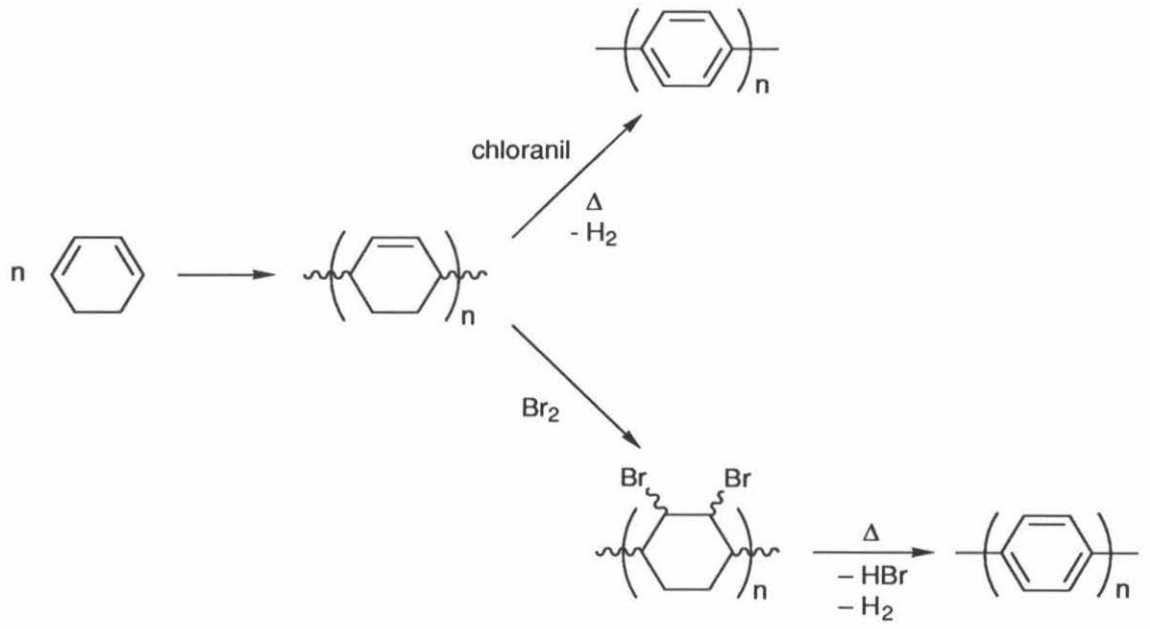

Figure 10. Precursor route to PPP using polycyclohexadiene.

Unfortunately, these polymerization reactions produce precursors with low molecular weights,[41] or with a mixture of 1,4- and 1,2-linkages.[42-44] In addition, the aromatization processes employed have been found to be inefficient in forming phenylene units.[41,42,44]

A more efficient precursor route to 90% *para*-linked polyphenylene has recently been developed by Ballard and co-workers at ICI Chemicals and Polymers.[45,46] This process involves the radical polymerization of monomers obtained by the microbial oxidation of benzene. The resulting soluble polymers are subsequently converted to PPP by thermally-induced acid elimination (Figure 11).[46]

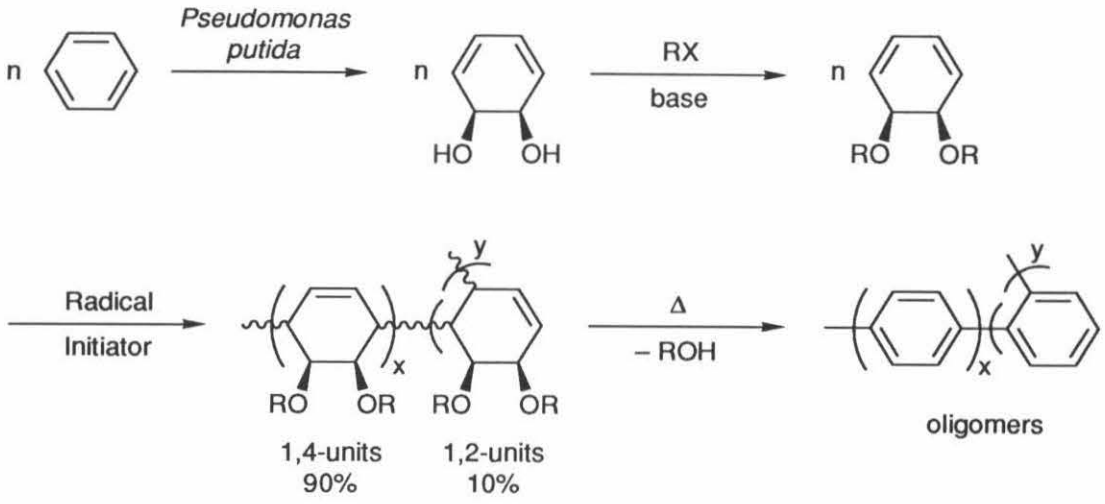

Figure 11. The ICI precursor route to PPP.

This process, however, only yields phenylene oligomers due to extensive chain fracturing during the pyrolysis step.[47] Backbone fracturing is believed to arise from the 10% 1,2-units and/or random backbone stereochemistry that result from the nonstereospecific nature of the radical polymerization process.

A similar PPP precursor route to the ICI process was also developed by McKean and Stille.[48] This route utilizes the same type of monomers, polymerization techniques, and aromatization methods as the ICI process; however, the monomers are chemically synthesized from 1,4-cyclohexadiene in a multistep procedure rather than microbially synthesized from benzene. Unfortunately, this PPP precursor route suffers from the same drawbacks as the ICI process. In addition, the synthesis of the monomers in this route is less efficient.

Summary

PPP is a valuable engineering polymer and electronic material. Unfortunately, its full potential has not been realized due to the quality of the material available. All previous synthetic routes to PPP—both direct and indirect—have been unable to produce a high molecular weight polymer with a completely 1,4-linked (*para*) structure. They have either afforded either phenylene oligomers or polyphenylenes with significant amounts of structural defects detrimental to the properties of the final polymer. What is sought is a synthetic route to PPP which not only yields high molecular weight, completely 1,4-linked material but also permits processability without sacrificing any of the excellent properties of the final product.

References and Notes

(1) For reviews on poly(*p*-phenylene), see: Kovacic, P.; Jones, M. B. *Chem. Rev.* **1987**, *87*, 357, and references 2–4.

(2) Elsenbaumer, R. I.; Shacklette, L. W. In *Handbook of Conducting Polymers*; Skotheim, T. A., Ed.; Marcel–Dekker: New, York, 1986; Vol. 1, Chapter 7.

(3) Speight, J. G.; Kovacic, P.; Koch, F. W. *J. Macromol. Sci., Rev. Macromol. Chem.* **1971**, *C5*(2), 295.

(4) Noren, G. K.; Stille, J. K. *Macromol. Rev.* **1971**, *5*, 385.

(5) Gale, D. M. *J. Appl. Polym. Sci.* **1978**, *22*, 1971.

(6) For a review of the current and proposed applications of poly(*p*-phenylene), see references 1 and 3.

(7) Suzuki, H. *Bull. Chem. Soc. Jpn.* **1960**, *33*, 109.

(8) Grem, G.; Leditzky, G.; Ullrich, B.; Leising, G. *Adv. Mater.* **1992**, *4*(1), 36.

(9) Goldfinger, G. *J. Polym. Sci.* **1949**, *9*, 93.

(10) Edwards, G. A.; Goldfinger, G. *J. Polym. Sci.* **1955**, *16*, 589.

(11) Sircar, A. C.; Majumbar, J. N. *J. Indian Chem. Soc.* **1928**, *5*, 417.

(12) Pummerer, R.; Seligsberger, L. *Chem. Ber.* **1931**, *64*, 2477.

(13) Berlin, A. A.; *J. Polym. Sci.* **1961**, *55*, 621.

(14) Berlin, A. A.; Liogon'kii, V. I.; Parini, V. P. *J. Polym. Sci.* **1961**, *55*, 675.

(15) Hayama, S.; Niino, S. *J. Polym. Sci., Polym. Chem. Ed.* **1974**, *12*, 357.

(16) Tanaka, M.; Watanabe, A.; Fujimoto, H.; Tanaka, J. *Chem. Lett.* **1980**, 907.

(17) Yamamoto, T.; Yamamoto, A. *Chem. Lett.* **1977**, 353.

(18) Yamamoto, T.; Hayashi, Y.; Yamamoto, A. *Bull. Chem. Soc. Jpn.* **1978**, *51*, 2091.

(19) Taylor, S. K.; Bennett, S. G.; Khoury, I.; Kovacic, P. *J. Polym. Sci., Polym. Lett. Ed.* **1981**, *19*, 85.

(20) Fauvarque, J. F.; Petit, M. A.; Pfluger, F.; Jutrand, A.; Chevrot, C.; Troupel, M.

Makromol. Chem., Rapid Commun. **1983**, *4*, 455.

(21) Froyer, G.; Maurice, F.; Goblot, J. Y.; Fauvarque, J. F.; Petit, M. A.; Digua, A. *Mol. Cryst. Liq. Cryst.* **1985**, *118*, 267.

(22) Fauvarque, J. F.; Digua, A.; Petit, M. A.; Savard, J. *Makromol. Chem.* **1985**, *185*, 2415.

(23) Yamamoto, T.; Morita, A.; Miyazaki, Y.; Maruyama, T.; Wakayama, H.; Zhou, Z. -H.; Nakamura, Y.; Kanbara, T.; Sasaki, S.; Kubota, K. *Macromolecules* **1992**, *25*, 1214.

(24) Tour, J. M.; Stephens, E. B. *J. Am. Chem. Soc.* **1991**, *113*, 2309.

(25) Stille, J. K.; Gilliams, Y. *Macromolecules* **1971**, *4*(4), 515.

(26) VanKerckhoven, H. F.; Gilliams, Y. K.; Stille, J. K. *Macromolecules* **1972**, *5*(5), 541.

(27) Brilmyer, G.; Jasinski, R. *J. Electrochem. Soc.* **1982**, *129*(9), 1950.

(28) Delamar, M.; Lacaze, P. -C.; Dumousseau, J. -Y.; Dubois, J. -E. *Electrochim. Acta* **1982**, *27*(1), 61.

(29) Soubiran, P.; Aeiyach, S.; Aaron, J. J.; Delamar, M.; Lacaze, P. -C. *J. Electroanal. Chem.* **1988**, *251*, 89.

(30) Claesson, S.; Gehm, R.; Kern, W. *Makromol. Chem.* **1951**, *7*, 46.

(31) Wirth, H. O.; Müller, R.; Kern, W. *Makromol. Chem.* **1963**, *77*, 90.

(32) Rehahn, M.; Schlüter, A.; Wegner, G.; Feast, W. J. *Polymer* **1989**, *30*(6), 1054.

(33) Rehahn, M.; Schlüter, A.; Wegner, G.; Feast, W. J. *Polymer* **1989**, *30*(6), 1060.

(34) Rehahn, M.; Schlüter, A.; Wegner, G. *Makromol. Chem.* **1990**, *191*, 1991.

(35) Noll, A.; Siegfried, N.; Heitz, W. *Makromol. Chem., Rapid Commun.* **1990**, *11*, 485.

(36) Wallow, T. I.; Novak, B. M. *J. Am. Chem. Soc.* **1991**, *113*, 7411.

(37) Stille, J. K.; Harris, F. W.; Rakutis, R. O.; Mukamal. H. *J. Polym. Sci., Part B* **1966**, *4*, 791.

(38) Schilling, C. L.; Reed, J. A.; Stille, J. K. *Macromolecules* **1969**, *2*, 85.

(39) Stille, J. K.; Noren, G. J. *J. Polym. Sci., Part B* **1969**, *7*, 525.

(40) Stille, J. K. *J. Macromol. Sci., Chem.* **1969**, *3*, 1043.

(41) Marvel, C. S.; Hartzell, G. E. *J. Am. Chem. Soc.* **1959**, *81*, 488.

(42) Frey, D. A.; Hasegawa, M.; Marvel, C. S. *J. Polym. Sci., Part A* **1963**, *1*, 2057.

(43) Dawans, F.; LeFebvre, G. *J. Polym. Sci., Part A* **1964**, *2*, 3277.

(44) Cassidy, P. E.; Marvel, C. S.; Ray, S. *J. Polym. Sci., Part A* **1965**, *3*, 1553.

(45) Ballard, D. G. H.; Courtis, A.; Shirley, I. M.; Taylor, S. C. *J. Chem. Soc., Chem. Commun.* **1983**, 954.

(46) Ballard, D. G. H.; Courtis, A.; Shirley, I. M.; Taylor, S. C. *Macromolecules* **1988**, *21*, 294.

(47) Internal report from ICI Chemicals and Polymers Ltd., Runcorn, U. K., based on neutron scattering analysis of PPP performed at Durham University.

(48) McKean, D. R.; Stille, J. K. *Macromolecules* **1987**, *20*, 1787.

CHAPTER 2

Transition-Metal-Catalyzed Polymerization of Heteroatom-Functionalized 1,3-Cyclohexadienes: Stereoregular Precursors to Poly(*p*-phenylene)

Introduction

The objective of this research was to develop an efficient precursor methodology for the synthesis of high quality poly(*p*-phenylene) (PPP). In a precursor methodology, there are two principal steps: (1) the synthesis of suitable, processable precursor polymers, and (2) the conversion of these precursors to the final polymer. Ideally, such a route should permit processability without sacrificing any of the properties of the final material. The most successful precursor route to PPP to date is the ICI process developed by Ballard et al. (Figure 1).[1,2] This process involves the synthesis of soluble precursor polymers (**3a,b**) by the radical polymerization of monomers (**2a,b**) derived from *cis*-5,6-dihydroxy-1,3-cyclohexadiene (**1**), a microbial oxidation product of benzene. The precursors are subsequently converted to PPP by thermally-induced acid elimination.

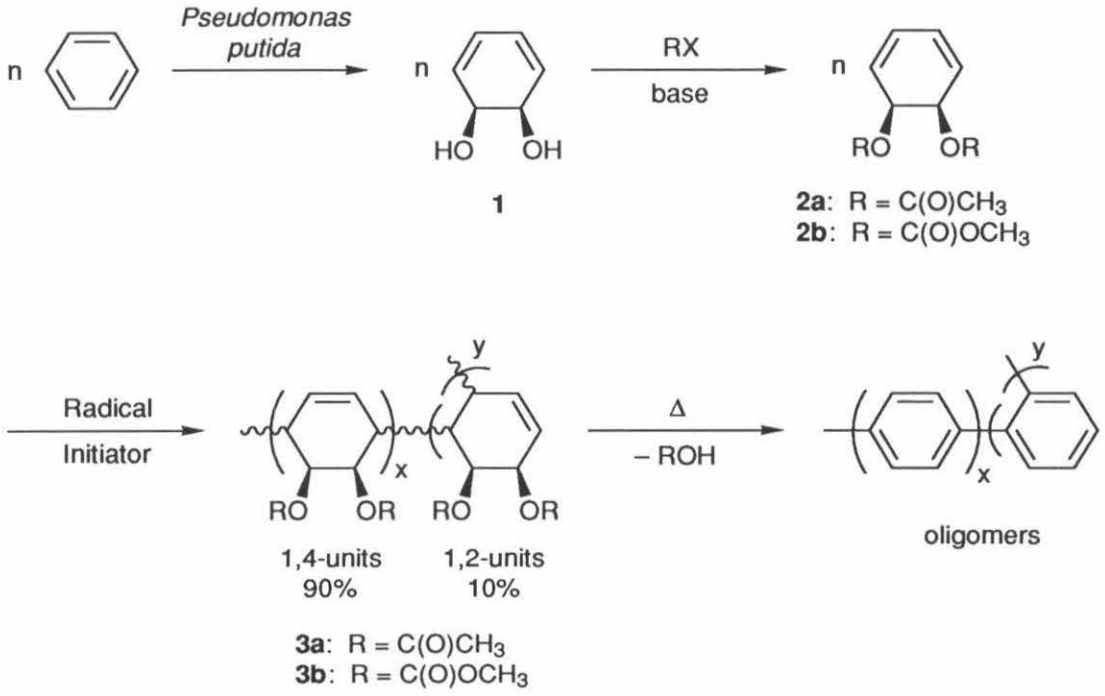

Figure 1. The ICI precursor route to PPP.

However, the ICI process suffers from two inherent problems as a result of the nonstereospecific nature of the radical polymerization process: (1) The radically polymerized precursors contain approximately 10% 1,2-linkages that introduce nonlinear defects in the final PPP.[2] (2) The precursors fracture during the final pyrolysis step as a result of the random backbone stereochemistry and/or the presence of the 1,2-linkages.[3] In addition, the radical polymerization process provides little if any control over the molecular weight of the polymers.

Our goal was to develop a superior precursor route to PPP based on the ICI process by synthesizing completely 1,4-linked, stereoregular precursor polymers. Specifically, what we sought was a method for polymerizing derivatives of compound **1** that would provide three things: (1) regiochemical control to give completely 1,4-linked precursor polymers for 100% *para*-linked polyphenylene, (2) stereochemical control to give precursors with the optimum stereochemistry for facile acid elimination without chain degradation, and (3) molecular weight control during the synthesis of the polymers. The optimum stereochemistry for acid elimination in this case would be the 1,4-*SSRR* repeat unit structure[4] depicted in Figure 2. Since the pyrolytic acid elimination from these precursors is believed to involve a cis-six-membered ring transition state,[2] the precursor repeat unit should not only be 1,4-linked but also have the bridging C–C bonds in a cis relationship on the face of the cyclohexenyl ring opposite that of the pendant functional groups (Figure 2).

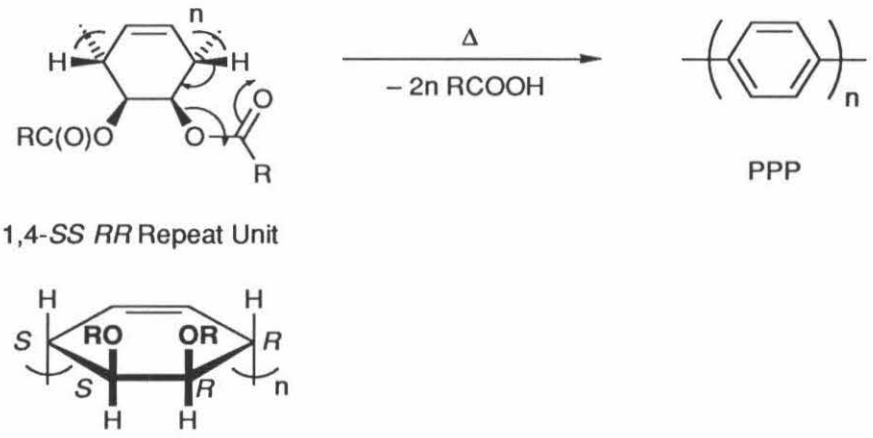

Figure 2. Thermally-induced acid elimination via a cis-six-membered ring transition state.[2]

Unfortunately, few initiators offer the combination of high 1,4-regioselectivity, high cis stereospecificity, and the capability for molecular weight control in the polymerization of 1,3-dienes. As demonstrated in the original ICI process (Figure 1)[1,2] and in a similar synthetic approach used by McKean and Stille,[5] conventional radical polymerization initiators are unable to provide this unique combination of properties in the polymerization of **2a** and **2b**. Anionic and cationic initiators have also proven to be unequal to the task since both of these types of initiators afford polymers with mixtures of 1,4- and 1,2-linkages when used to polymerize 1,3-cyclohexadiene.[6-8] Our strategy was to apply the stereochemical and regiochemical control afforded by transition-metal catalysts to the polymerization of derivatives of **1**. The result is a high-yield, multistep synthesis of 1,4-linked stereoregular precursors to PPP which utilizes a transition-metal catalyst to provide stereochemical and molecular weight control, protecting group chemistry to provide catalyst/functional group compatibility, and functional group interconversion chemistry to provide precursors that can be easily aromatized to PPP.

Results and Discussion

In the development of a transition-metal catalyst polymerization system that would perform stereospecific polymerization of derivatives of compound **1**, two primary issues needed to be addressed: (1) stereochemical control during the polymerization, and (2) catalyst/functional group compatibility. Many transition-metal polymerization catalysts such as Ziegler–Natta type systems afford highly 1,4-linked polymers of 1,3-butadiene[9,10] and 1,3-cyclohexadiene.[6] However, the Lewis acid co-catalysts in these Ziegler–Natta systems generally cannot tolerate the types of heteroatom functionalities on the monomers required for efficient conversion of the corresponding precursor polymers to PPP. Metal-π-allyl catalyst systems are also known to give highly 1,4-linked polymers of 1,3-dienes.[9,10] Although much work has been done with these catalysts using purely hydrocarbon 1,3-dienes (e.g., 1,3-butadiene and 1,3-cyclohexadiene),[11,12] little has been done with heteroatom-functionalized 1,3-dienes. In fact, the only examples of successful polymerizations of heteroatom-functionalized 1,3-dienes by transition-metal complexes have been copolymerizations with 1,3-butadiene.[13,14] The corresponding homopolymerizations of the highly functionalized monomers were unsuccessful with these metal-π-allyl catalysts. Since the most successful of these copolymerizations employed bis[(η^3-allyl)trifluoroacetatonickel(II)] [$(ANiTFA)_2$] as the catalyst system, $(ANiTFA)_2$ was an excellent starting point for our investigations (Figure 3).[14]

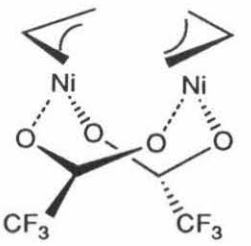

Figure 3. Bis[(η^3-allyl)trifluoroacetatonickel(II)] [$(ANiTFA)_2$].

(A) The Catalyst Bis(η^3-allyl)trifluoroacetatonickel(II)] [$(ANiTFA)_2$]

$(ANiTFA)_2$ is an air- and water-sensitive compound that can easily be prepared by the oxidative addition of allyl trifluoroacetate to bis(1,5-cyclooctadienyl)nickel(0) [$Ni(COD)_2$] (Figure 4).[15,16]

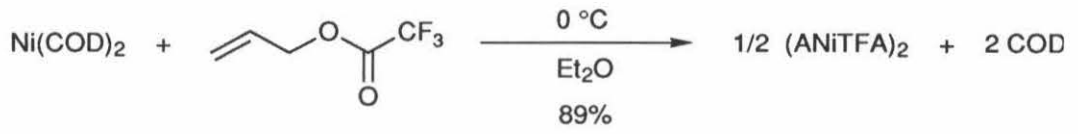

Figure 4. The synthesis of $(ANiTFA)_2$.

Not only does this catalyst exhibit a partial tolerance to heteroatom functionalities in 1,3-butadiene polymerizations,[14] but it has also been used for the "living" polymerization of butadiene, exhibiting >98% 1,4-regioselectivity.[17] In addition, the polymerization of 1,3-dienes by nickel-π-allyl complexes such as $(ANiTFA)_2$ has been found to exhibit high cis stereospecificity and to proceed by a syn-coordinative insertion mechanism.[18-20] This unique combination of characteristics makes $(ANiTFA)_2$ ideal for the synthesis of highly 1,4-linked, stereoregular precursors to PPP from derivatives of compound **1**. However, no work has yet been done with this catalyst with cyclic 1,3-dienes or highly functionalized cyclic dienes.

(B) Polymerization of 1,3-Cyclohexadiene by $(ANiTFA)_2$ as a Model System

Initial experiments with $(ANiTFA)_2$ focussed on its ability to polymerize 1,3-cyclohexadiene (CHD). The purpose of these initial experiments was two-fold: (1) to determine whether the catalyst could polymerize the 1,3-cyclohexadiene moiety, the polymerizable functionality of derivatives of **1**, and (2) to determine whether the high

1,4-regioselectivity exhibited by the catalyst in butadiene polymerizations[17] is retained in the polymerization of 1,3-cyclohexadienes. CHD was found to be readily polymerized by $(ANiTFA)_2$ at a temperature of 50 °C or higher in a variety of non-coordinating aromatic solvents with yields between 70 and 90%. The resulting polycyclohexadiene [poly(CHD)] is an insoluble white powder that precipitates rapidly out of the reaction mixture during the course of the polymerization. In general, the more polar aromatic solvents (e.g., chlorobenzene and *o*-dichlorobenzene) were found to enhance catalyst activity and provide the highest yields of poly(CHD).

The regiochemistry of the poly(CHD) synthesized using $(ANiTFA)_2$ was determined by ^1H NMR analysis on soluble oligomers extracted from the mostly insoluble polymer matrix. The relative amounts of 1,4-and 1,2-linkages in poly(CHD)s can be determined by examining the integrals of the proton resonances at approximately 1.6 and 2.0 ppm, which are due to methylene protons in non-allylic (β) and allylic (α) environments, respectively (Figure 5).[12]

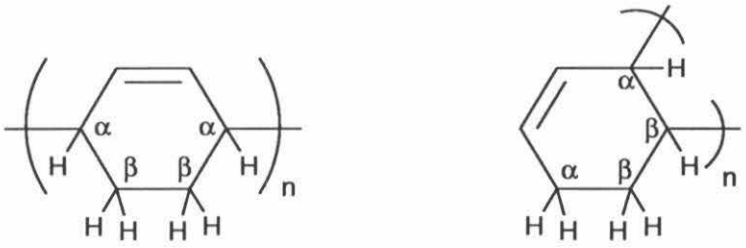

Figure 5. The 1,4- and 1,2-linked repeat units possible for poly(CHD).

For example, a polymer comprised of entirely 1,2-units would be expected to have a ratio of β to α protons of 1:1, whereas a completely 1,4-linked polymer would be expected to have a ratio of 2:1. Thus, the fraction of 1,4-units (m) can be deduced from the integrals of the peaks at 1.6 and 2.0 ppm (N) by using Eq. 1.[12]

$$m = \frac{3(N-1)}{(N+1)} \quad ; \; N = \frac{I_\beta}{I_\alpha} \qquad (1)$$

The ^{1}H NMR spectrum of the soluble oligomers obtained using $(ANiTFA)_2$ (Figure 6) indicates approximately 90–95% 1,4-linkages in the poly(CHD).

The highly 1,4-linked structure for the poly(CHD) made using $(ANiTFA)_2$ inferred from ^{1}H NMR analysis was also supported by powder X-ray diffraction (PXRD) and thermal analysis of the polymer. PXRD analysis of the insoluble poly(CHD) revealed three sharp reflections at 5.291, 4.517, and 3.907 Å, indicating a highly crystalline material (Figure 7). Differential scanning calorimetry (DSC) and thermal gravimetric analysis (TGA) on the poly(CHD) revealed that the polymer is thermally stable under inert atmosphere to approximately 320 °C and possesses no observable glass transition (T_g) or melting point (T_m) prior to that temperature. Such high thermal stability in poly(CHD) has only been exhibited by material containing >90% cis-1,4-linkages made using a similar nickel catalyst.[10,11] In contrast, poly(CHD) containing structural irregularities is typically a soluble, amorphous material with a significantly lower thermal stability.[6,7,11,12] Clearly, not only can $(ANiTFA)_2$ polymerize the 1,3-cyclohexadiene moiety, but the high 1,4-regioselectivity exhibited by the catalyst in 1,3-butadiene polymerizations is also retained in the polymerization of 1,3-cyclohexadienes.

(C) Catalyst/Functional Group Compatibility Studies

Once it was determined that $(ANiTFA)_2$ could polymerize the 1,3-cyclohexadiene moiety with very high 1,4-regioselectivity, experiments were then performed to determine whether the catalyst could polymerize the bis(acetyl) (**2a**) and bis(methoxycarbonyl) (**2b**) derivatives of compound **1**. All attempts to polymerize these two monomers using $(ANiTFA)_2$ under similar conditions to those employed in the CHD

Figure 6. 400 MHz ^1H NMR spectrum (in $CDCl_3$) of soluble poly(CHD) oligomers made using $(ANiTFA)_2$.

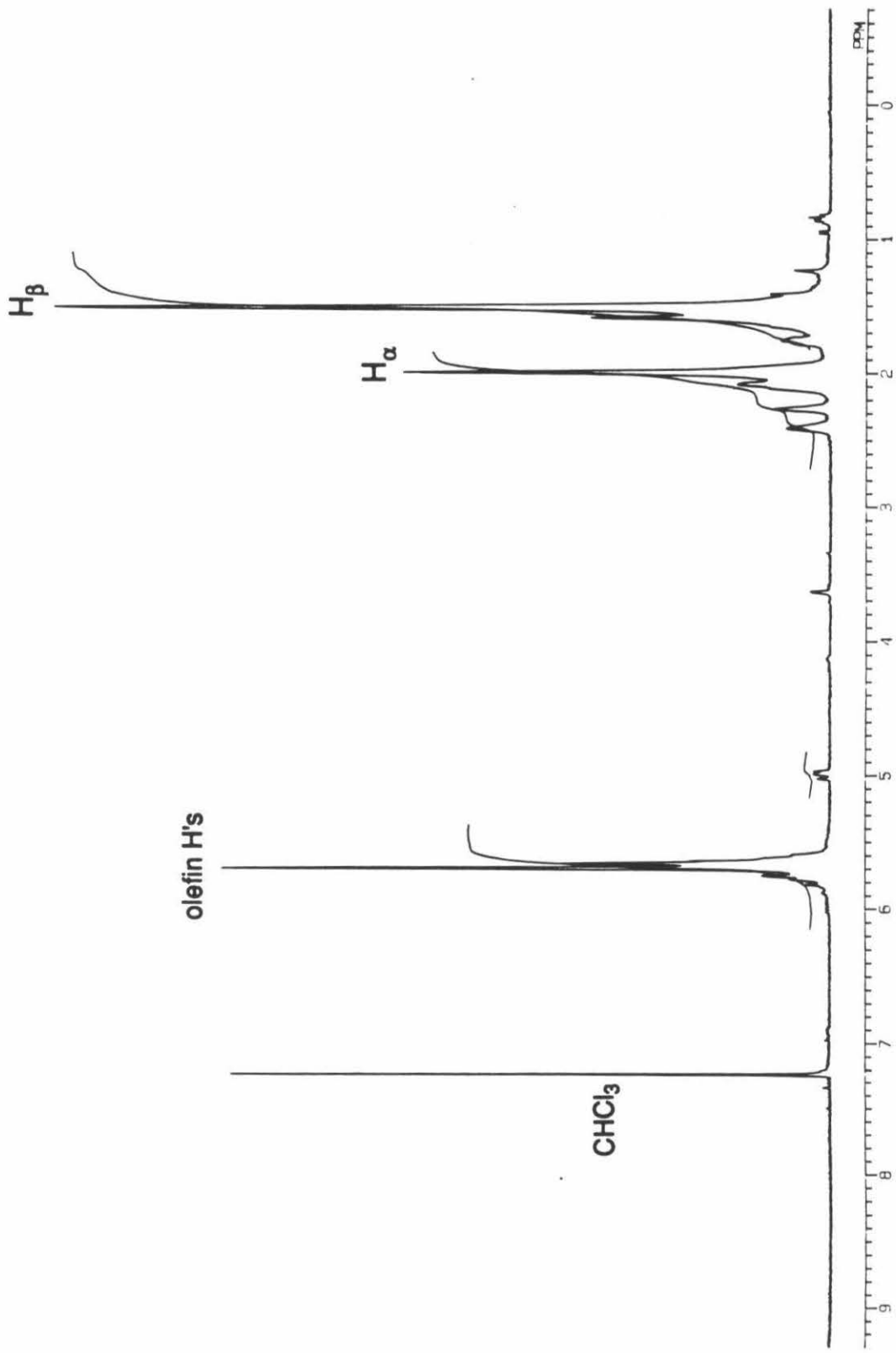
H_β
H_α
olefin H's
$CHCl_3$
PPM
9
8
7
6
5
4
3
2
1
0

Figure 7. PXRD profile of poly(CHD) made using $(ANiTFA)_2$. The weak reflection at 4.110 Å is a diffractometer artifact.

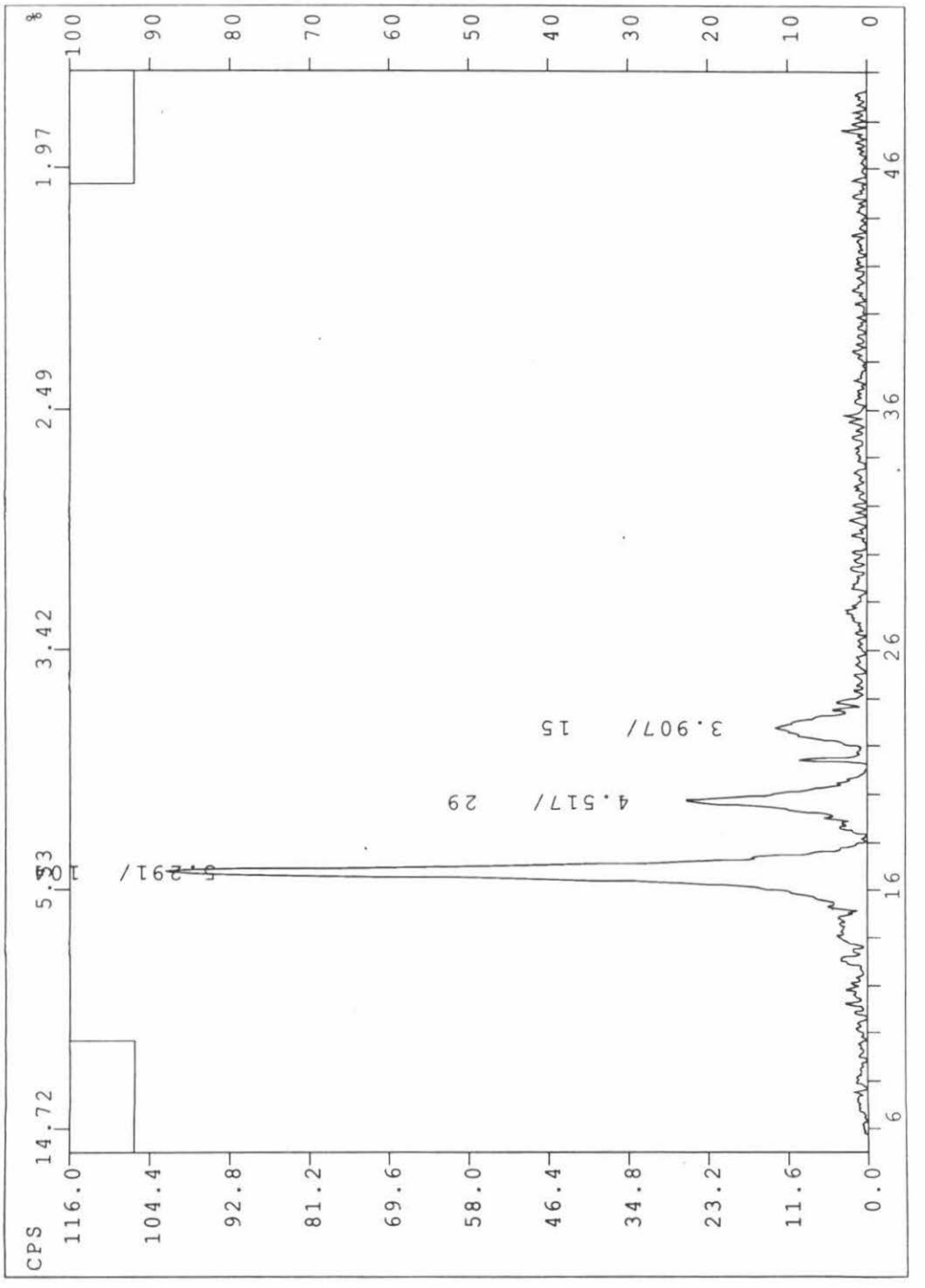
d (Å)
CPS
14.72
5.53
3.42
2.49
1.97
116.0
104.4
92.8
81.2
69.6
58.0
46.4
34.8
23.2
11.6
0.0
100
90
80
70
60
50
40
30
20
10
0
6
16
26
36
46
2θ (degrees)
4.517/ 29
3.907/ 15

polymerizations proved unsuccessful. ^{1}H NMR analysis of the resulting reaction mixtures revealed that instead of initiating polymerization, the catalyst aromatizes a stoichiometric amount of the monomers **2a** and **2b**. It is believed that the acid or alcohol eliminated during the aromatization of these monomers decomposes the catalyst (Figure 8).

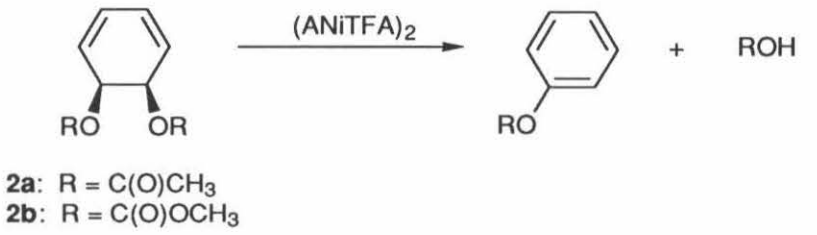

2a: R = $C(O)CH_3$
2b: R = $C(O)OCH_3$

Figure 8. Aromatization of the monomers **2a** and **2b** leading to decomposition of $(ANiTFA)_2$.

Subsequent investigations revealed that not only is the aromatization of **2a** and **2b** a problem for $(ANiTFA)_2$, but carbonyl containing groups in general are incompatible with the catalyst. For example, the addition of a small amount of purified ethyl acetate to the active CHD/$(ANiTFA)_2$ polymerization system resulted in dramatically lower polymer yields or no polymer formation at all. Most likely, the Lewis basic carbonyl groups compete with the 1,3-diene moieties to coordinate to the electrophilic nickel centers of the catalyst. Evidently, the functionalities best suited for facile conversion of the precursor polymers to PPP (i.e., esters and carbonates) are completely incompatible with the catalyst.

Additional catalyst/functional group compatibility studies revealed that compound **1** itself and many of its other common derivatives are also incompatible with the $(ANiTFA)_2$ catalyst. Attempts to polymerize **1** directly using $(ANiTFA)_2$ were unsuccessful and only resulted in aromatizing the monomer to phenol and water. Use of the acetonide (**2c**) and silyl acetonide (**2d**) derivatives of **1** (Figure 9) did not result in immediate decomposition of the catalyst; however, the two monomers could not be

polymerized.

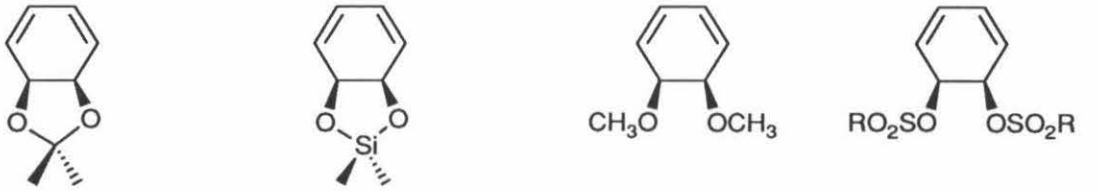

Figure 9. Other derivatives of **1** that cannot be polymerized by $(ANiTFA)_2$.

Attempts to synthesize simple alkyl ether derivatives of **1** (e.g., **2e**) in sufficient purity for polymerization/compatibility studies with $(ANiTFA)_2$ were unsuccessful using literature preparations.[2] Hence, simple compatibility studies of 1,2-diethers with the catalyst were performed by adding small amounts of purified 1,2-dimethoxyethane (DME) to an active CHD/$(ANiTFA)_2$ polymerization reaction. The addition of DME to a CHD polymerization reaction quickly resulted in catalyst decomposition and afforded only very low polymer yields. A plausible rationale for this incompatibility is that 1,2-diethers chelate to the electrophilic nickel centers to deactivate the catalyst (Figure 10).

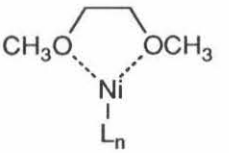

Figure 10. Possible chelation of $(ANiTFA)_2$ by 1,2-dimethoxyethane.

Due to the difficulty of synthesizing bis(sulfonic ester) derivatives of compound **1** (**2f**), similar compatibility studies were performed for sulfonic esters using ethyl tosylate as an additive. Only a small amount of poly(CHD) formed, probably because of a similar coordination effect by the S=O groups to the electrophilic metal catalyst.

More exotic derivatization of **1** (e.g., substitution of the hydroxy groups with

halides) was not attempted due to the thermal and hydrolytic instability of the material. Compound **1** spontaneously aromatizes to form phenol and water in the presence of acid or at temperatures in excess of 60 °C.[2] In fact, **1** must be stored as a solid at sub-zero temperatures or as solution in organic base (e.g., pyridine) to minimize aromatization. As a result, derivatization of this substrate is limited to procedures using relatively low temperatures under basic or near neutral conditions.[2]

(D) *cis*-5,6-Bis(trimethylsiloxy)-1,3-Cyclohexadiene: A Compatible Monomer via Protecting Group Chemistry

A derivative of **1** which is compatible with $(ANiTFA)_2$ was synthesized by applying protecting group chemistry to the parent monomer. *cis*-5,6-Bis(trimethylsiloxy)-1,3-cyclohexadiene (**4**) was prepared by reacting compound **1** with two equivalents of chlorotrimethylsilane (TMSCl) in a mixture of pyridine and methylene chloride using 4-dimethylaminopyridine (DMAP) as a catalyst (Figure 11).

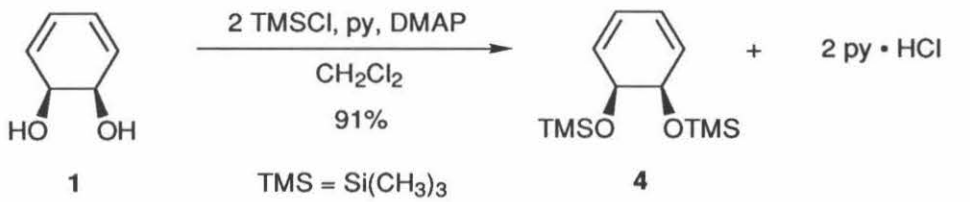

Figure 11. Preparation of *cis*-5,6-bis(trimethylsiloxy)-1,3-cyclohexadiene (**4**), a derivative of **1** which is compatible with $(ANiTFA)_2$.

By masking the hydroxy groups on **1** as trimethylsilyl (TMS) ethers, monomer **4** can be polymerized in high yields by $(ANiTFA)_2$ at a temperature of 50 °C or higher in a variety of aromatic solvents or in neat monomer.[21] Chlorobenzene was found to be the best solvent system for the polymerization reaction in terms of polymer yield and catalyst activity. Typically with a monomer-to-catalyst ratio of 80:1 and a monomer

concentration of 1.5 M in chlorobenzene, the polymer is obtained in 93% yield with a number average degree of polymerization (M_n) of 38,000 and a polydispersity index (PDI) of 1.64, as determined by Viscotek GPC analysis.[22] Under these reaction conditions, the initial clear orange solution of $(ANiTFA)_2$ and **4** in chlorobenzene changes first to a dark red solution and then to an opaque coffee-colored mixture over a period of approximately 15–20 minutes at 50 °C. The active reaction mixture then remains black for the duration of the polymerization, becoming progressively more viscous until a gel forms (usually after 24 hours). The resulting TMS ether polymer (**5**) is a white powder which is completely soluble in solvents such as hexanes and THF.

Monomer **4** is believed to be compatible with the catalyst unlike the other derivatives of compound **1** for two reasons: (1) the steric bulk of the large TMS protecting groups effectively prevents the oxygen atoms of the monomer from coordinating to the catalyst and interfering with the polymerization, and (2) the TMS ethers are very poor leaving groups compared to the esters and carbonates so monomer aromatization leading to catalyst decomposition is inhibited. It is also believed that the bulky TMS groups play a secondary role in the polymerization by directing the attack of the catalyst on the monomer. The bulky TMS groups not only sterically shield the oxygen atoms, but they also effectively block one face of the cyclohexadiene ring of monomer **4**, thus permitting approach of the catalyst from only the unhindered opposite face away from the TMS ethers. These steric shielding effects can clearly be seen by examining the computer-generated space-filling model of **4** presented in Figure 12. This π-facial selectivity afforded by the TMS ethers on the monomer, together with the cis stereospecificity in butadiene polymerization[18-20] and the 1,4-regioselectivity in cyclohexadiene polymerization afforded by the $(ANiTFA)_2$ catalyst, should yield the resulting polymer **5** as a completely 1,4-linked, stereoregular polymer with the 1,4-*SSRR* repeat unit depicted in Figure 13.

Figure 12. Edge-on view of a space-filling (CPK) model of **4**. The oxygen atoms are in red.

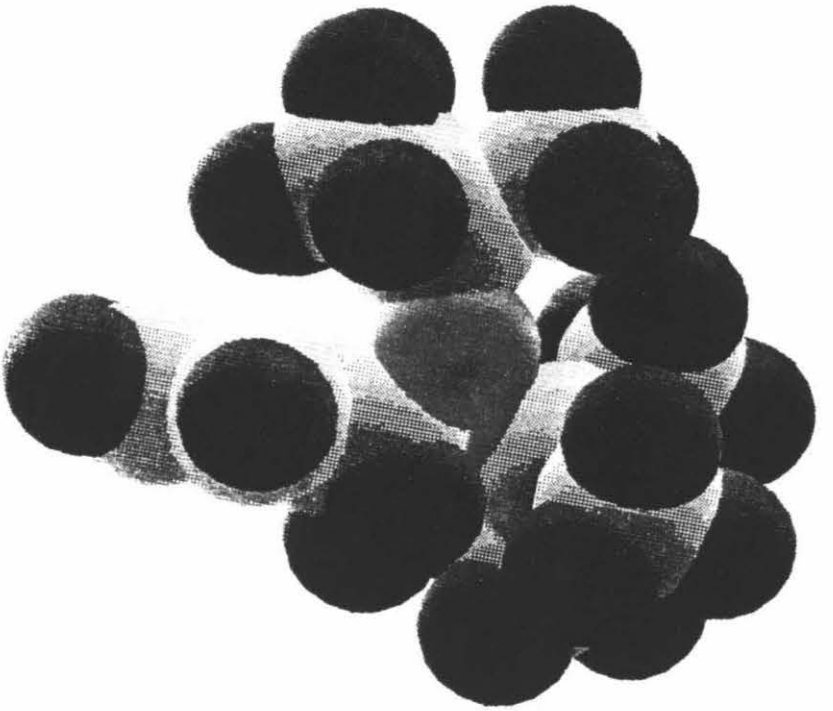

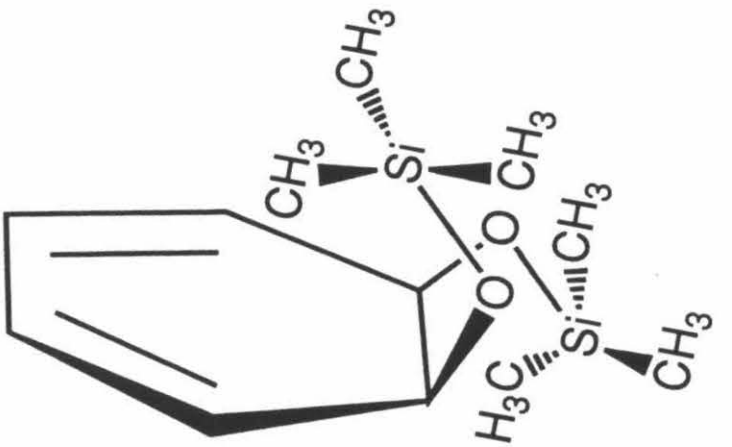
CH3
Si
CH3
CH3
O
O
Si
CH3
H3C
CH3

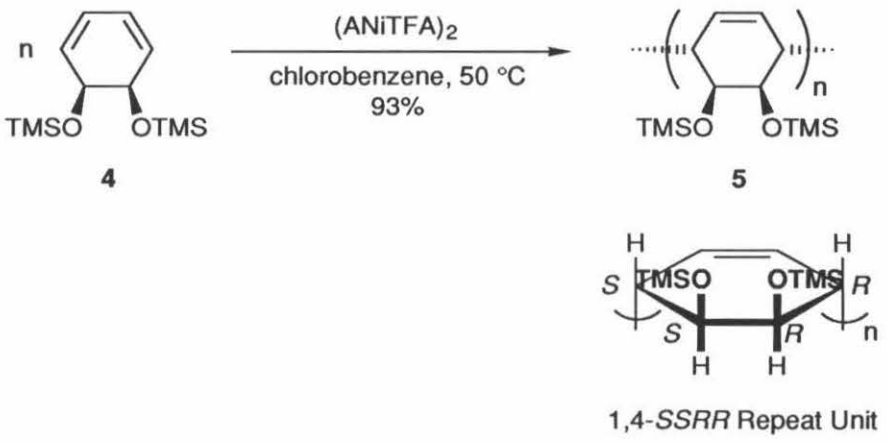

Figure 13. Stereospecific polymerization of monomer **4** using $(ANiTFA)_2$.

(E) Characterization of Polymer 5: Confirmation of the Inferred 1,4-Stereoregular Structure for the Polymer

The completely 1,4-linked structure for **5** as inferred from the factors discussed above was confirmed by ^1H NMR analysis. ^1H NMR analysis is the primary method of determining the relative amounts of 1,4- and 1,2-linkages in PPP precursor polymers.[2,5] 1,2-Units in radically synthesized polymers of compound **1** derivatives typically exhibit a proton resonance at 1.8–2.1 ppm that is not found in 1,4-units. This assignment is inferred from ^1H NMR analysis of a model compound of a 1,2-unit (Figure 14).[5]

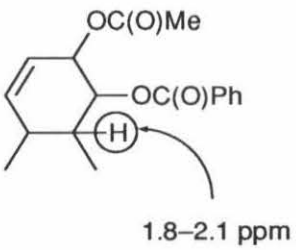

Figure 14. Model compound of a 1,2-linkage in polymers of compound **1** derivatives.[5]

As can be seen from the ^{1}H NMR spectrum of **5** (Figure 15), the polymer does not exhibit any proton signals in this region, thus suggesting a completely 1,4-linked structure for the polymer. Further support for this assignment was provided by comparing the ^{1}H NMR spectrum of **5** made using $(ANiTFA)_2$ (Figure 16a) with the ^{1}H NMR spectrum of radically polymerized oligomers of **4** (Figure 16b).[23] Only the radically polymerized oligomers exhibit a proton signal at 1.9 ppm indicative of 1,2-units.

Although ^{1}H NMR analysis suggests a highly 1,4-linked regioregular structure for **5**, this technique was not able to furnish any further information on the tacticity (stereochemistry) of the polymer backbone. For a completely stereoregular polymer, the symmetric 1,4-*SSRR* repeat unit inferred for polymer **5** (Figure 13) can be connected in two ways: (1) the same throughout (an isotactic structure), and (2) a perfectly alternating fashion (a syndiotactic structure) (Figure 17).[24] Since there is usually rapid half-chair–half-chair conformational interconversion (i.e., "ring-flipping") for cyclohexene molecules in solution,[25] there should be a plane of symmetry passing through each repeat unit of the two possible stereoregular structures on the NMR timescale (Figure 17). The number of nonequivalent ^{1}H and ^{13}C NMR signals should be the same in both cases from symmetry arguments: four unique carbons in total and three unique protons on the cyclohexene ring. Consequently, NMR spectroscopy would not be able to distinguish between the isotactic and syndiotactic structures possible for polymer **5** simply from the number of unique ^{1}H and ^{13}C signals exhibited. However, the ^{1}H NMR spectrum of **5** (Figure 15) shows different chemical environments for each of the six protons on the cyclohexenyl ring of the repeat units. In addition, variable temperature ^{1}H NMR analysis of **5** in d_8-toluene revealed no coalescence of the six ring proton resonances even up to 100 °C. Attempts to use ^{13}C NMR analysis to obtain more information on the stereochemistry of **5** were completely unsuccessful. ^{13}C NMR analysis of polymer **5** using a variety of different solvents (e.g., C_6D_6, $CDCl_3$, d_8-THF) and concentrations only yielded spectra with extremely poor signal-to-noise and poor resolution.

Figure 15. 400 MHz ^{1}H NMR spectrum of polymer **5** in $CDCl_3$.

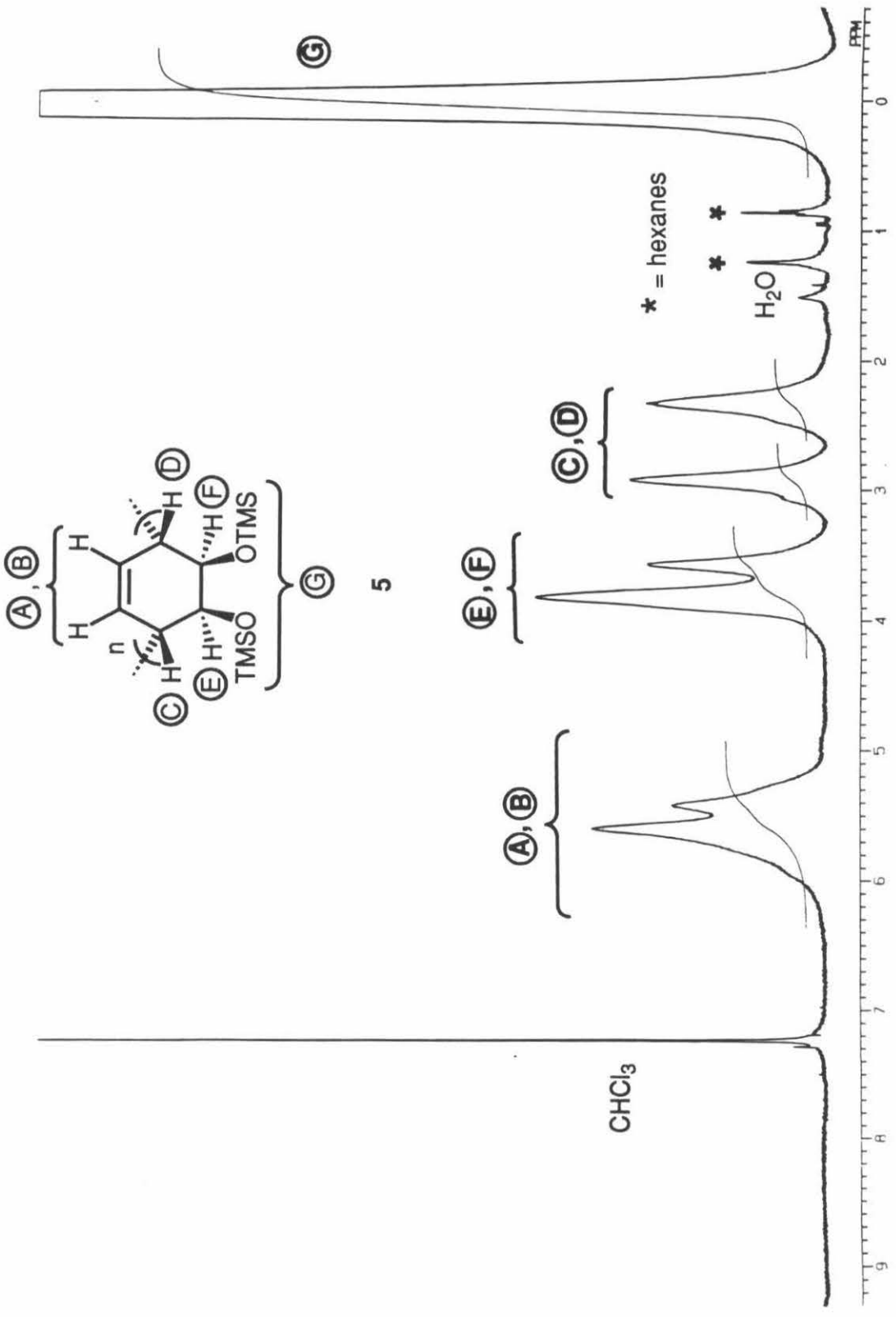
Ⓐ, Ⓑ
H
H
n
Ⓒ H
Ⓓ H
Ⓔ H
Ⓕ H
TMSO
OTMS
Ⓖ
5
Ⓐ, Ⓑ
Ⓔ, Ⓕ
Ⓒ, Ⓓ
Ⓖ
CHCl3
* = hexanes
* *
H2O
PPM

Figure 16. 500 MHz ^{1}H NMR spectra of (a) polymer **5** and (b) radically polymerized oligomers of **4** in d_8-THF.

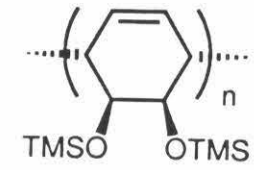

Ni Catalyzed Polymerization

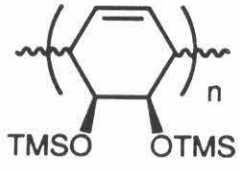

Radical Polymerization

1,4-*SSRR* Repeat Unit for **5**

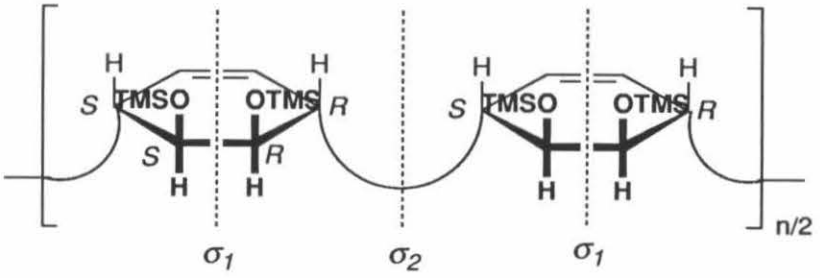

Isotactic structure

By symmetry: (a) All junctions are identical: *RS*.
(b) Three chemically nonequivalent ring protons.

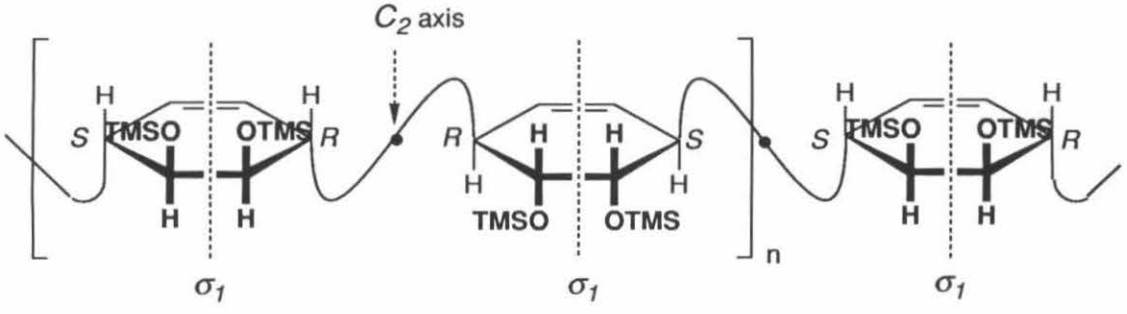

Syndiotactic structure

By symmetry: (a) *RR* and *SS* junctions are enantiomers and therefore equivalent by NMR spectroscopy.
(b) Three chemically nonequivalent ring protons.

Figure 17. The symmetry of the isotactic and syndiotactic structures for a conformationally nonrigid, polymer **5** with the 1,4-*SSRR* repeat unit.

In order to further elucidate the structure of polymer **5**, the material was also analyzed by a combination of secondary analytical techniques. Wide angle PXRD analysis of **5** revealed that the material is partially ordered, exhibiting a single diffraction peak at 9.725 Å (Figure 18). This PXRD profile is typically exhibited by rodlike molecules such as nematic liquid crystals.[26] Additional support for a rodlike secondary structure was provided by STM imaging of **5** on highly oriented pyrolytic graphite (HOPG).[27] STM imaging showed rodlike polymer chains on the surface of the substrate (Figures 19a and 19b) with longitudinal dimensions that agree well with chain lengths inferred from Viscotek GPC analysis.[28,29] This unexpected rodlike secondary structure for polymer **5** is likely the source of the difficulties encountered in obtaining a good ^{13}C solution NMR spectrum of the polymer. The rodlike conformation of the polymer chains probably makes tumbling in solution extremely slow on the NMR timescale, resulting in severe chemical shift anisotropy and poor signal-to-noise and resolution. This assumption is supported by the fact that solutions of polymer **5** are often thixotropic. That is, the initially nonviscous polymer solution often forms a gel upon standing, but returns to its original fluid state with subsequent agitation.

What we infer from all these results is that polymer **5** probably has a stereoregular structure (either isotactic or syndiotactic) with the symmetric 1,4-*SSRR* repeat unit expected from the stereospecificity of the polymerization catalyst (Figure 13). However, the polymer chains adopt a rodlike secondary structure in which each polymer repeat unit is conformationally locked into a half-chair conformation. The loss of the normally rapid conformational (i.e., "ring-flipping") equilibrium removes the expected plane of symmetry in the repeat units of these two stereoregular structures on the NMR timescale, resulting in six types of ring protons in the ^{1}H NMR spectrum instead of the three expected. Both the rodlike secondary structure and the resulting locked half-chair repeat unit inferred for **5** are most likely the result of large steric interactions from the

Figure 18. PXRD profile of polymer **5**. The reflections at 4.110 and 3.723 Å are diffractometer artifacts.

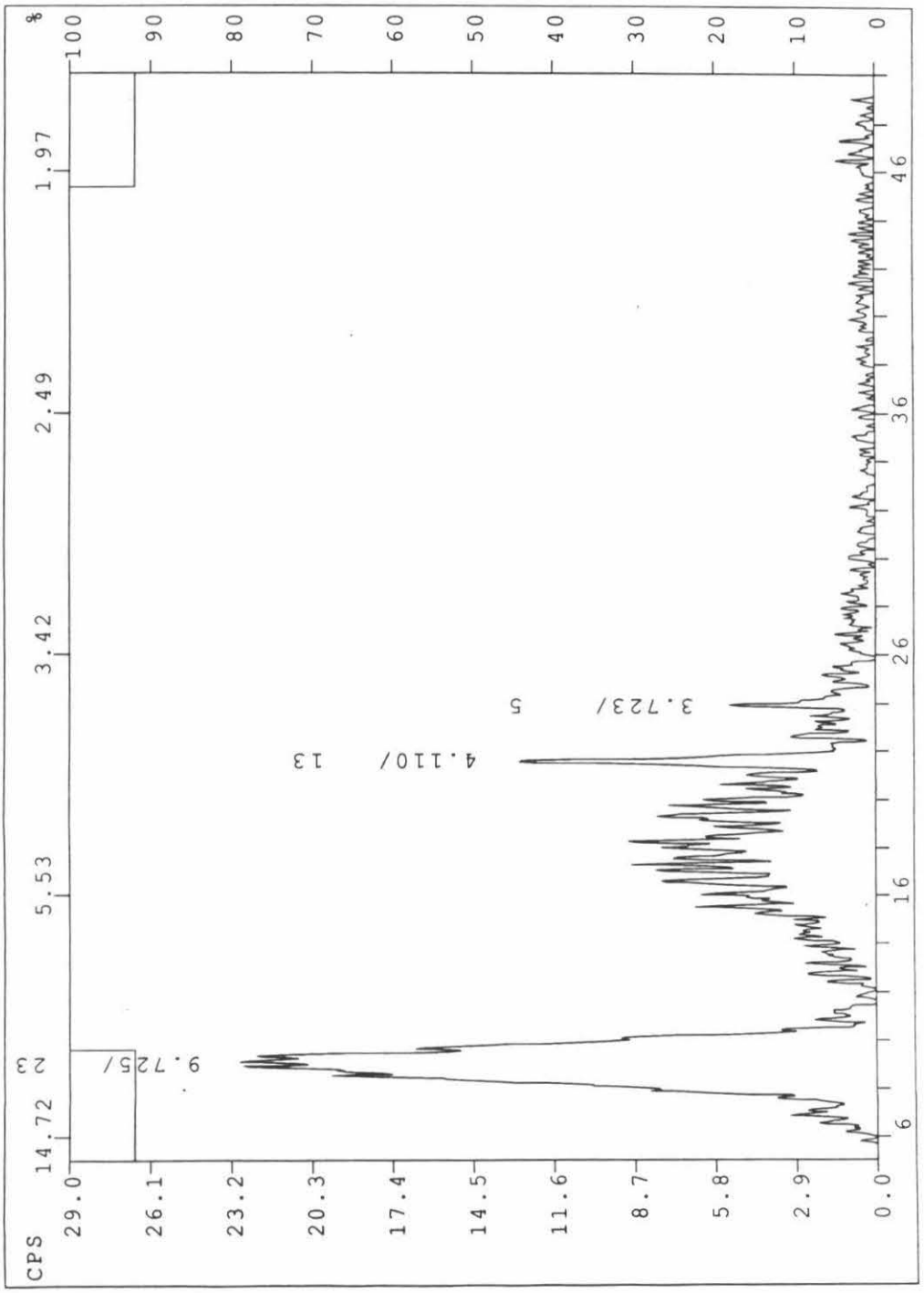
d (Å)
CPS
14.72
5.53
3.42
2.49
1.97
%
100
90
80
70
60
50
40
30
20
10
0
29.0
26.1
23.2
20.3
17.4
14.5
11.6
8.7
5.8
2.9
0.0
9.725/
4.110/ 13
3.723/ 5
6
16
26
36
46
2θ (degrees)

Figure 19a. STM image of rodlike chains of polymer **5** on highly oriented pyrolytic graphite (image dimensions: 280 x 280 nm).

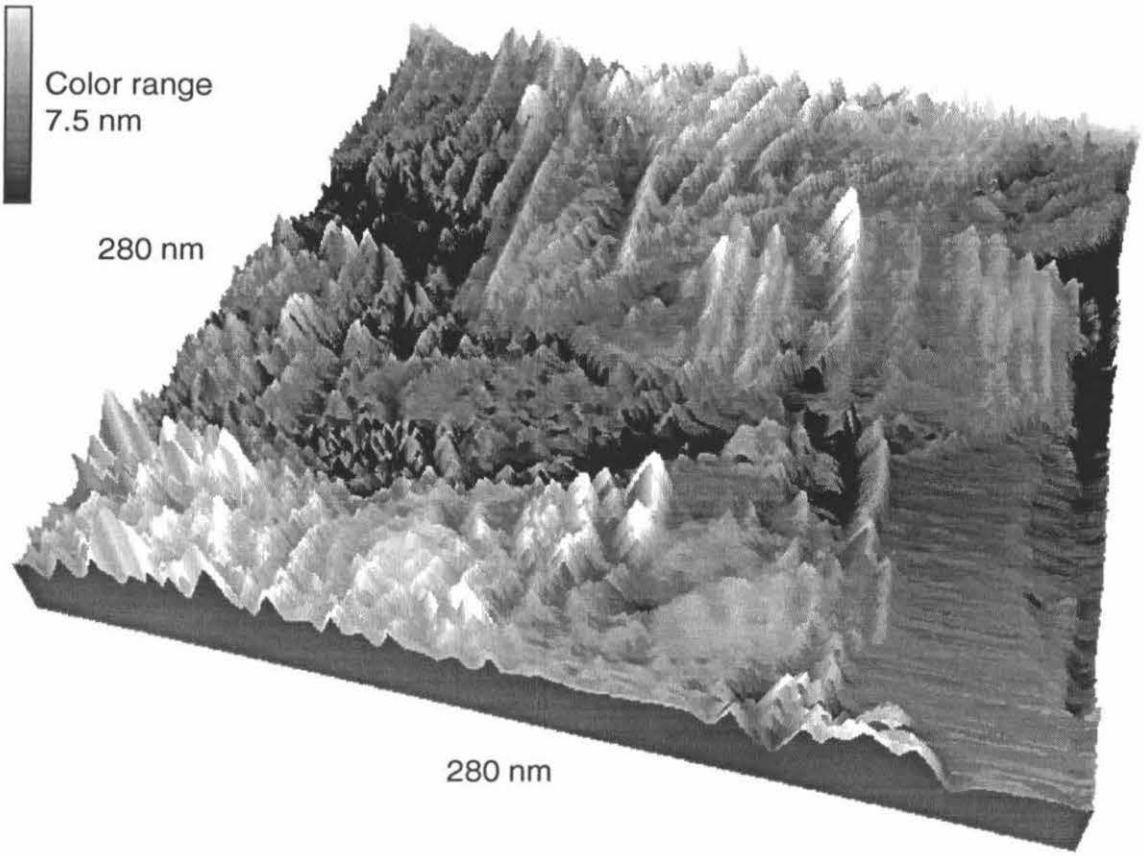
Color range
7.5 nm
280 nm
280 nm

Figure 19b. STM image of a small cluster of chains of polymer **5** on highly oriented pyrolytic graphite. (image dimensions: 880 x 880 nm).

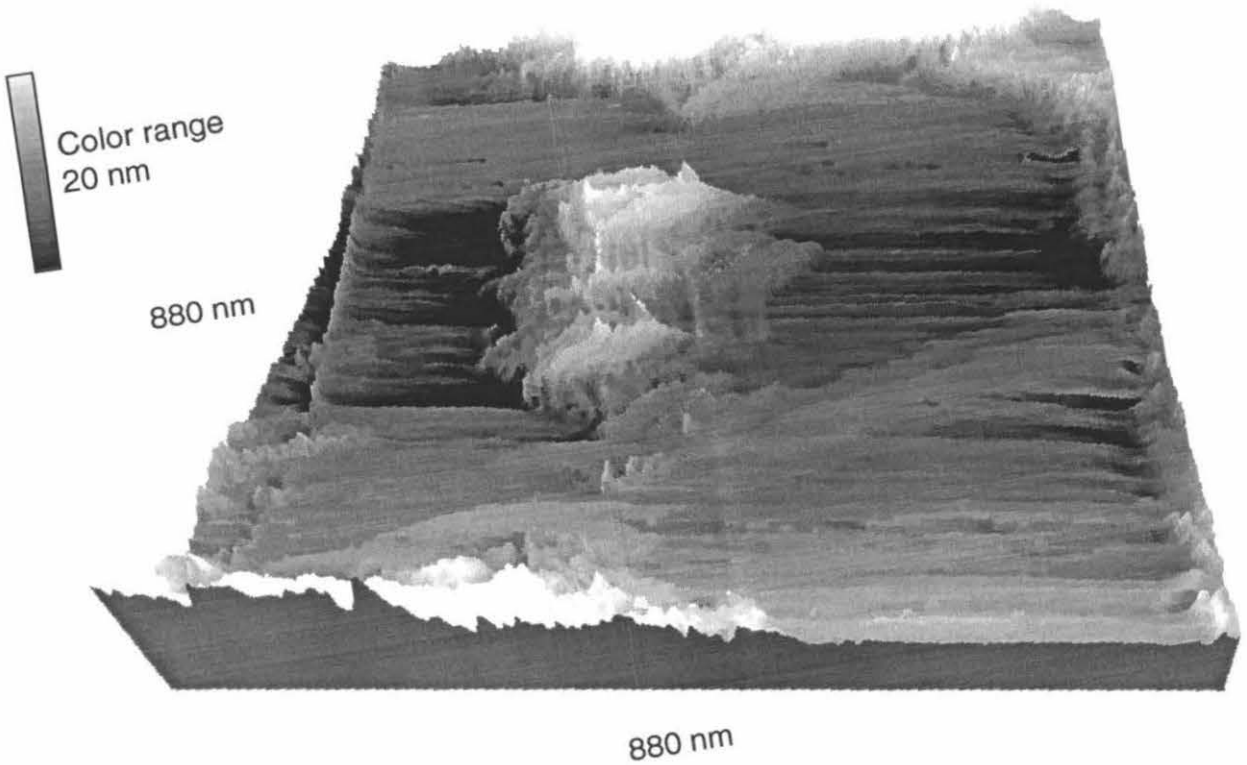
Color range
20 nm
880 nm
880 nm

bulky TMS ethers on the polymer. (These assumptions on the stereoregular structure and conformation of polymer **5** are all confirmed in a subsequent section in this chapter.)

Computer-modeled images of the locked 1,4-*SSRR* repeat unit and the rodlike secondary structure suggested by NMR, PXRD, and STM analysis of polymer **5** are presented in Figures 20 and 21, respectively. It should be noted that the images presented in Figures 20 and 21 are of a local energy minimum conformation for the isotactic structure of **5** shown in Figure 17, modeled using Biograf and MM2 force-field parameters.[30] Similar modeling of the corresponding 1,4-*SSRR* syndiotactic structure of **5** (Figure 17) afforded an elongated helix rather than a rod as in the isotactic case. Although molecular modeling at this very simple level cannot be used to deduce the actual tacticity of **5**, the fact that one of the possible stereoregular structures has a local energy minimum that is a rodlike molecule helps to substantiate our initial assumptions on the structure and conformation of the polymer.

(F) Preliminary Kinetic Analysis of the $(ANiTFA)_2$/Monomer 4 Polymerization System

The $(ANiTFA)_2$/monomer **4** polymerization system in chlorobenzene exhibits a strong dependence on monomer concentration. At a monomer-to-catalyst ratio of 80:1, the yield of polymer **5** increases asymptotically (up to 93%) with increasing initial monomer concentration. Below a critical monomer concentration (0.14 M), however, polymerization does not proceed (Figure 22).

Figure 20. The locked half-chair conformation for polymer **5** with the 1,4-*SSRR* isotactic structure, as suggested by computer modeling.

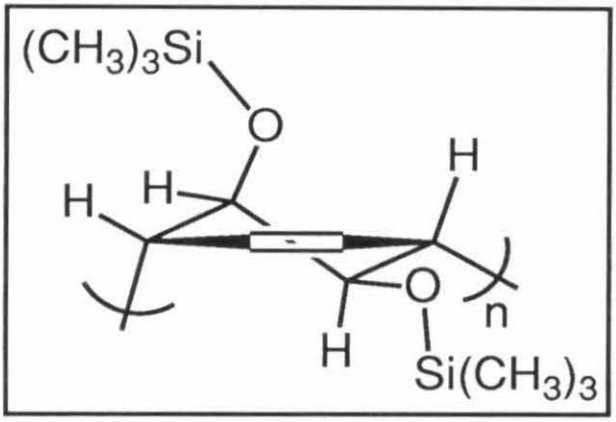
(CH3)3Si
O
H
H
H
O
n
H
Si(CH3)3

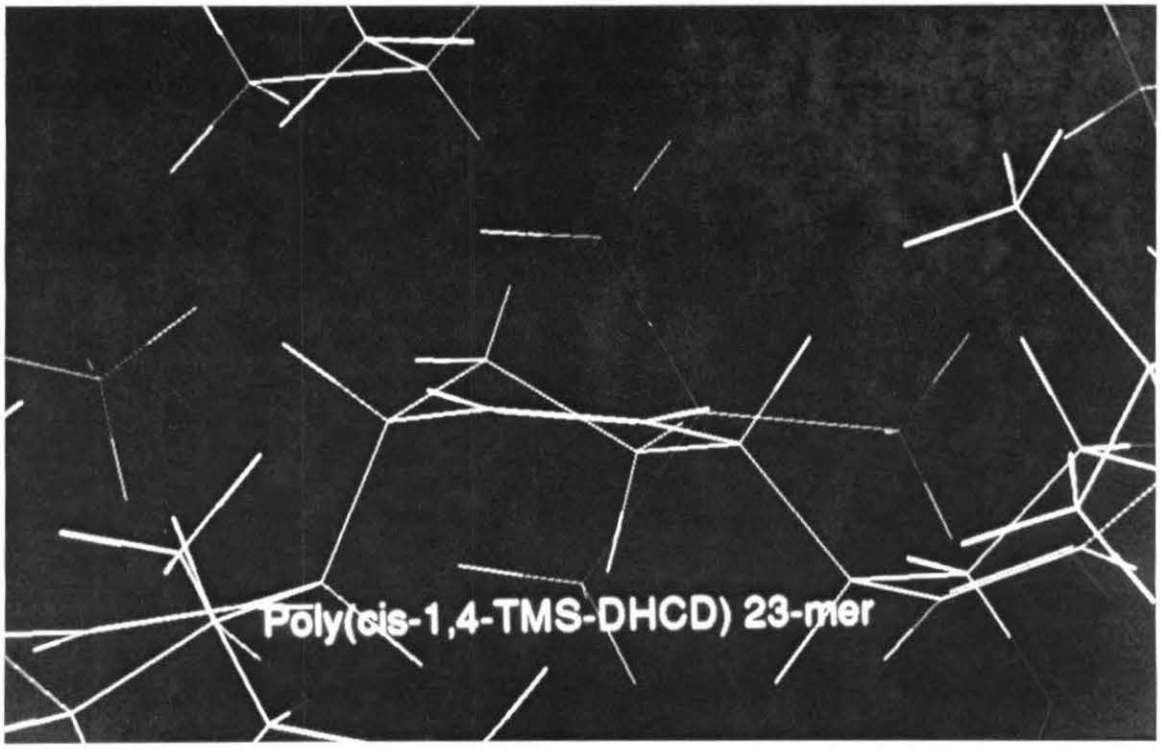
Poly(cis-1,4-TMS-DHCD) 23-mer

Figure 21. The rodlike secondary structure for the 1,4-*SSRR* isotactic structure of polymer **5**, as suggested by computer modeling.

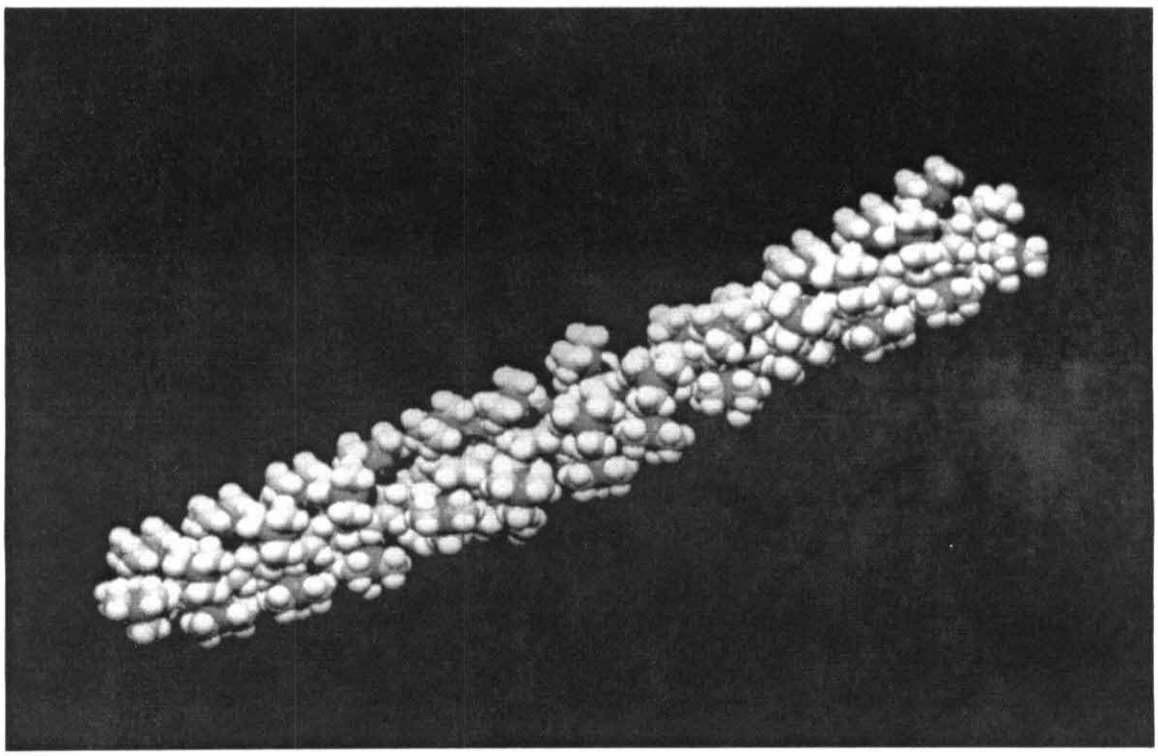

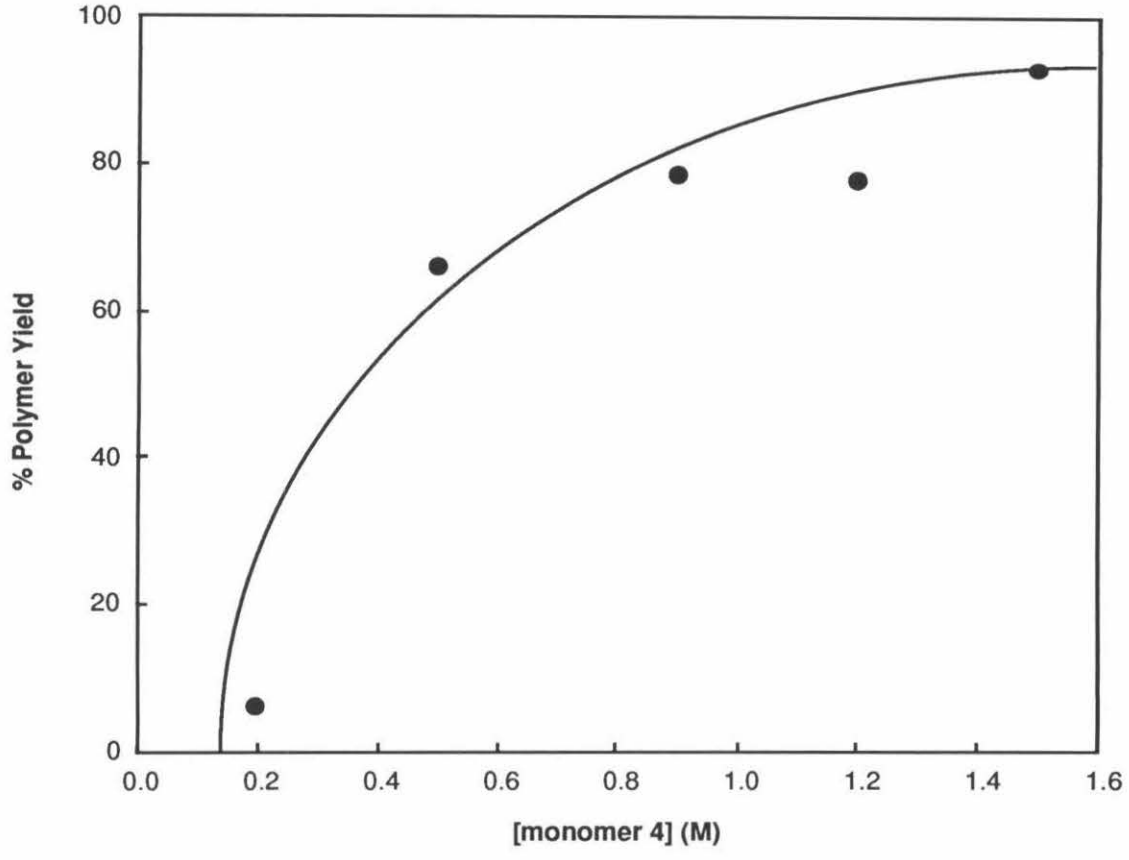

Figure 22. Plot of % polymer yield vs. initial monomer concentration for the $(ANiTFA)_2$/monomer **4** polymerization system in chlorobenzene. (Polymerization temperature = 50 °C; monomer-to-catalyst ratio = 80:1; reaction time = 24 h.)

The kinetic behavior of the $(ANiTFA)_2$/monomer **4** polymerization system in chlorobenzene, toluene, and neat monomer was investigated by examining the % conversion of **4** as a function of time and the M_n of the polymer as a function of % conversion of monomer, using a constant monomer-to-catalyst ratio of 75:1. The two sets of relationships for the polymerization system are presented in Figures 23 and 24.

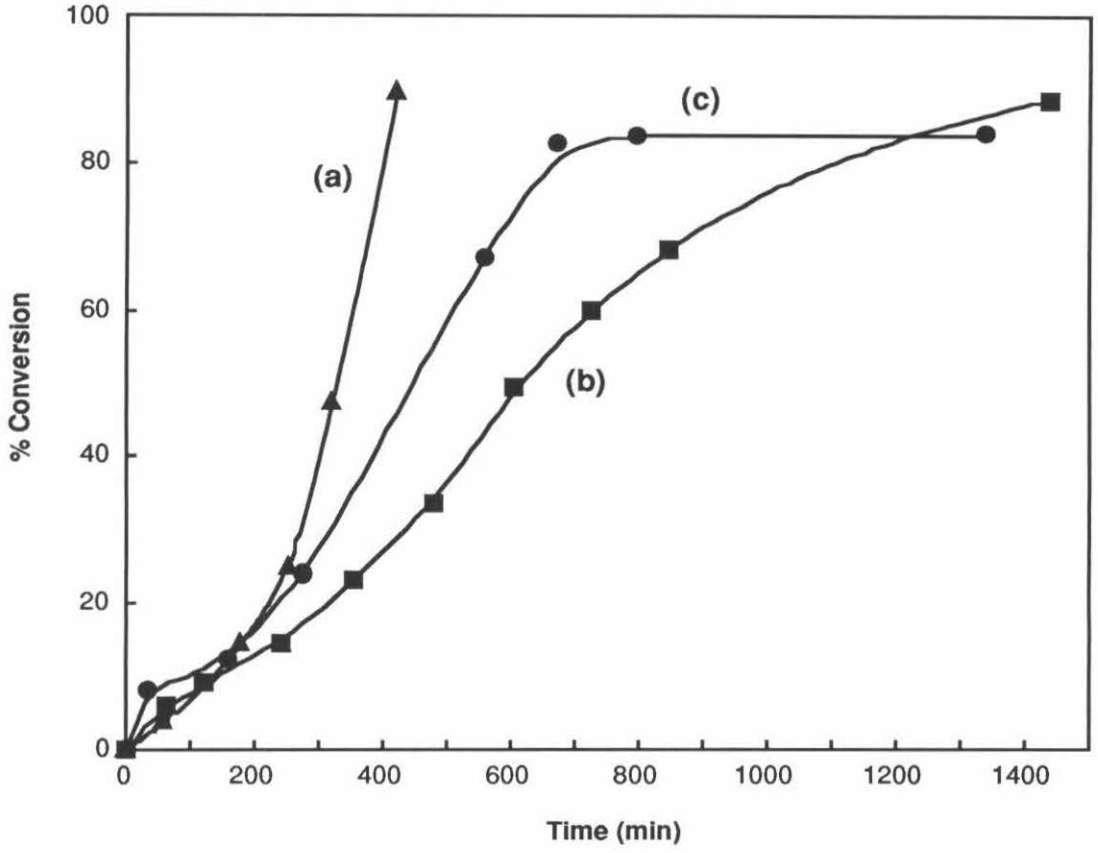

Figure 23. Plots of % conversion vs. time for the $(ANiTFA)_2$/monomer **4** polymerization system: (a) neat; (b) in toluene, [**4**] = 2.0 M; (c) in chlorobenzene, [**4**] = 0.7 M. All polymerizations were performed at 50 °C with a monomer-to-catalyst ratio of 75:1.

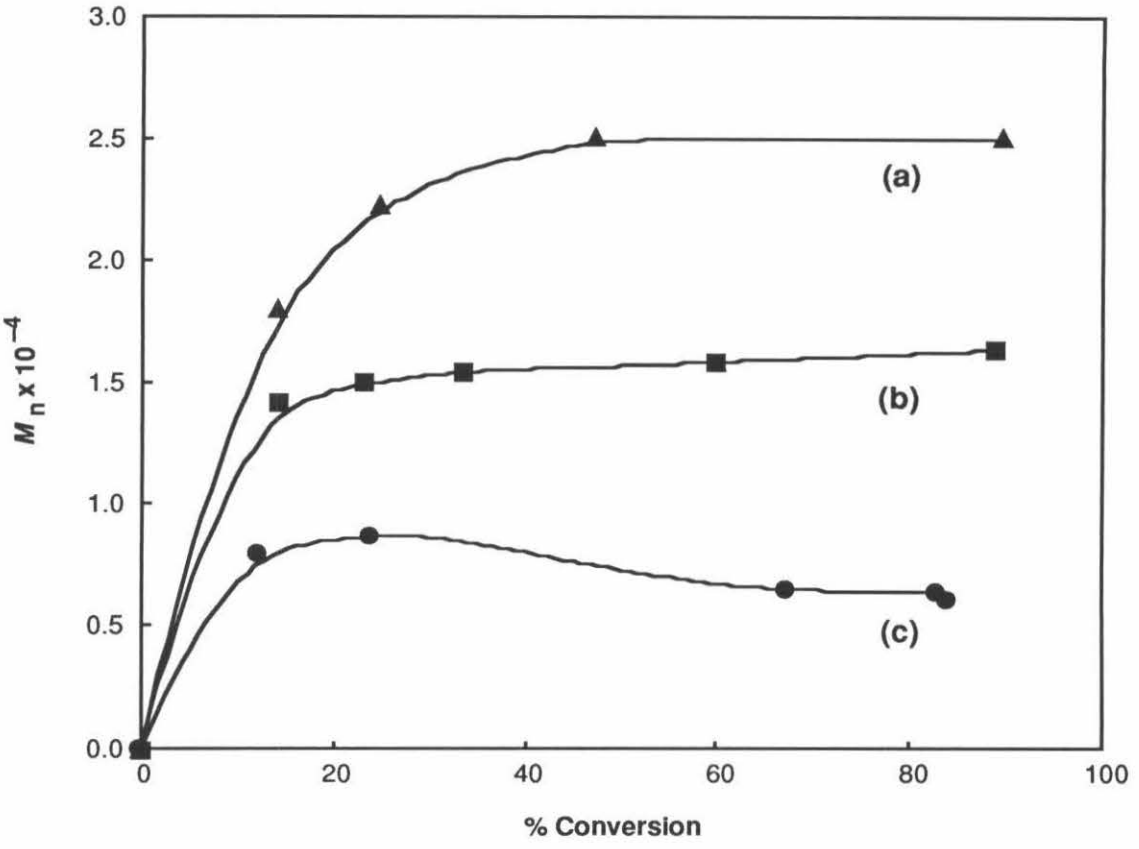

Figure 24 Plots of M_n of polymer **5** vs. % monomer conversion for the $(ANiTFA)_2$/monomer **4** polymerization system: (a) neat; (b) in toluene, [**4**] = 2.0 M; (c) in chlorobenzene, [**4**] = 0.7 M. All polymerizations were performed at 50 °C with a monomer-to-catalyst ratio of 75:1. M_n values were determined by Viscotek GPC, except for those of (c), which are referenced to polystyrene molecular weight standards.

As can be seen from Figure 24, the M_n vs % conversion relationship in each case is not linear, but rather the polymer M_n rises quickly at small % conversion and levels out for the remainder of the polymerization. These M_n vs. % conversion relationships are characteristic of a typical chain addition polymerization, suggesting a non-"living" process.[31,32]

Despite its non-"living" kinetics, this system does appear to have the potential for molecular weight control. Blocking experiments, performed by fresh aliquots of

monomer to the propagating system at approximately 75% conversion, resulted in predictable molecular weight increases in the resulting polymer *without* broadening the PDI or producing a multimodal molecular weight distribution (Table I).

Table I. Blocking experiment: The effect of adding fresh aliquots of monomer to the active $(ANiTFA)_2$ /monomer **4** polymerization system in chlorobenzene.

Equiv. of Fresh Monomer 4 Added [a]	Polymer 5		
	M_n (Viscotek GPC)	DP	PDI
75	1.78×10^4	69	2.06
70	3.31×10^4	129	1.84
247 [b]	5.14×10^4	200	2.03

(a) Addition of fresh aliquots of monomer performed at approx. 75% conversion of previous aliquot. The monomer aliquots were diluted to maintain an initial monomer concentration of 0.7 M at each addition.
(b) A larger amount of **4** was required at this point in the experiment due to increasing viscosity in the reaction mixture. The lower than expected M_n from this final blocking experiment is a result of gel formation stopping the reaction prematurely before all the added monomer can be consumed.

This observation suggests the presence of a "living" endgroup during the course of the reaction. Additional evidence for a "living" endgroup was obtained by examining the molecular weight of the polymer as a function of increasing monomer-to-catalyst ratio at a constant monomer concentration. The M_n of the polymer increases with increasing monomer-to-catalyst ratio (Table II). However, the relationship is not a direct one, and lower polymer yields are generally obtained with increasing monomer-to-catalyst ratios at a constant monomer concentration of 1.5 M.

Table II. The effect of increasing monomer-to-catalyst ratio on the M_n and % yield of polymer **5** for the $(ANiTFA)_2$/monomer **4** polymerization system in chlorobenzene. ([**4**] = 1.5 M; reaction time = 24 h; polymerization temp. = 50 °C)

Monomer-to-Catalyst Ratio	Polymer 5			
	M_n (Viscotek GPC)	DP	PDI	% Yield
50:1	2.22×10^4	87	1.75	80
100:1	2.73×10^4	106	2.00	83
200:1	3.47×10^4	135	1.84	66

These lower than expected M_n values and lower polymer yields are likely due to the rapid gel formation observed during the reaction. This gel formation results from the rapid buildup of polymer under the concentrated reaction conditions employed, and it stops the reactions prematurely before all of the monomer can be polymerized. By diluting the reaction mixtures with more solvent, not only can this same trend of increasing M_n with monomer-to-catalyst ratio be observed more definitively, but higher polymer yields can also be obtained as result of reduced gelling (Table III).

Table III. The effect of increasing monomer-to-catalyst ratio on the M_n of **5** for the $(ANiTFA)_2$/monomer **4** polymerization system in chlorobenzene under optimum yield conditions. (reaction time = 48 h; polymerization temp. = 50 °C)

Monomer 4 to $(ANiTFA)_2$ Ratio	[monomer 4] (M)	Polymer 5			
		M_n (Viscotek GPC)	DP	PDI	% Yield
80:1	1.5	2.09×10^4	81	1.53	93
140:1	1.2	5.31×10^4	207	1.31	96

The exact nature of this system's unique combination of non-"living" and "living" characteristics has not yet been determined. We do know that the rate-determining step in chain-transfer and termination in this system is not a conventional β-H elimination of a

propagating metal-allyl species, as suggested by Teyssié et al. for the $(ANiTFA)_2$/butadiene system.[17] If β-H elimination were the rate-determining step in chain transfer and termination, a difference in M_n should be observed in the two polymers made from ring deuterated **4** and perprotio **4** as a result of a kinetic isotope effect. The M_n and PDI of the polymers made by the $(ANiTFA)_2$-catalyzed polymerization of ring-deuterated **4** and perprotio **4** under identical reaction conditions are identical (Figure 25).[33]

Unfortunately, a more detailed examination of the dark brown–black active species responsible for this behavior was not possible. Attempts to analyze the propagating species by ^1H NMR spectroscopy only afforded spectra with extremely broad lines and poor signal-to-noise. Possibly, the active species is a paramagnetic nickel complex or a fluxional species which is responsible for the difficulties during NMR analysis. Attempts to isolate the black active species were also unsuccessful due to its high solubility in solvents typically used precipitate organometallic intermediates (e.g., pentane and hexanes) and its instability in coordinating solvents.

(G) Thermal Analysis and Pyrolysis of Polymer 5

Although the $(ANiTFA)_2$/monomer **4** polymerization system produces a completely 1,4-linked polymer and possesses the potential for molecular weight control, the resulting polymer **5** does not yield PPP upon pyrolysis. DSC and TGA of **5** revealed that the polymer is thermally stable up to approximately 327 °C under argon, exhibiting neither a T_g nor a T_m prior to its decomposition temperature. IR analysis of the pyrolysis product after heating **5** past its decomposition temperature revealed the absence of any bands indicative of PPP in the 650–850 cm^{-1} region.[34,35] In addition, elemental analysis of the pyrolysis residue of **5** revealed a substantial amount of Si remaining in the material. Apparently, the poor leaving ability of the TMS ethers prevents monomer **4**

Figure 25. Viscotek GPC plots of the polymers made by the $(ANiTFA)_2$-catalyzed polymerization of ring-deuterated **4** and perprotio **4** under identical reaction conditions. ([d_6-**4**] = [**4**] = 1.6 M in chlorobenzene; monomer-to-catalyst ratio = 40:1; reaction time = 24 h; polymerization temperature = 50 °C.)

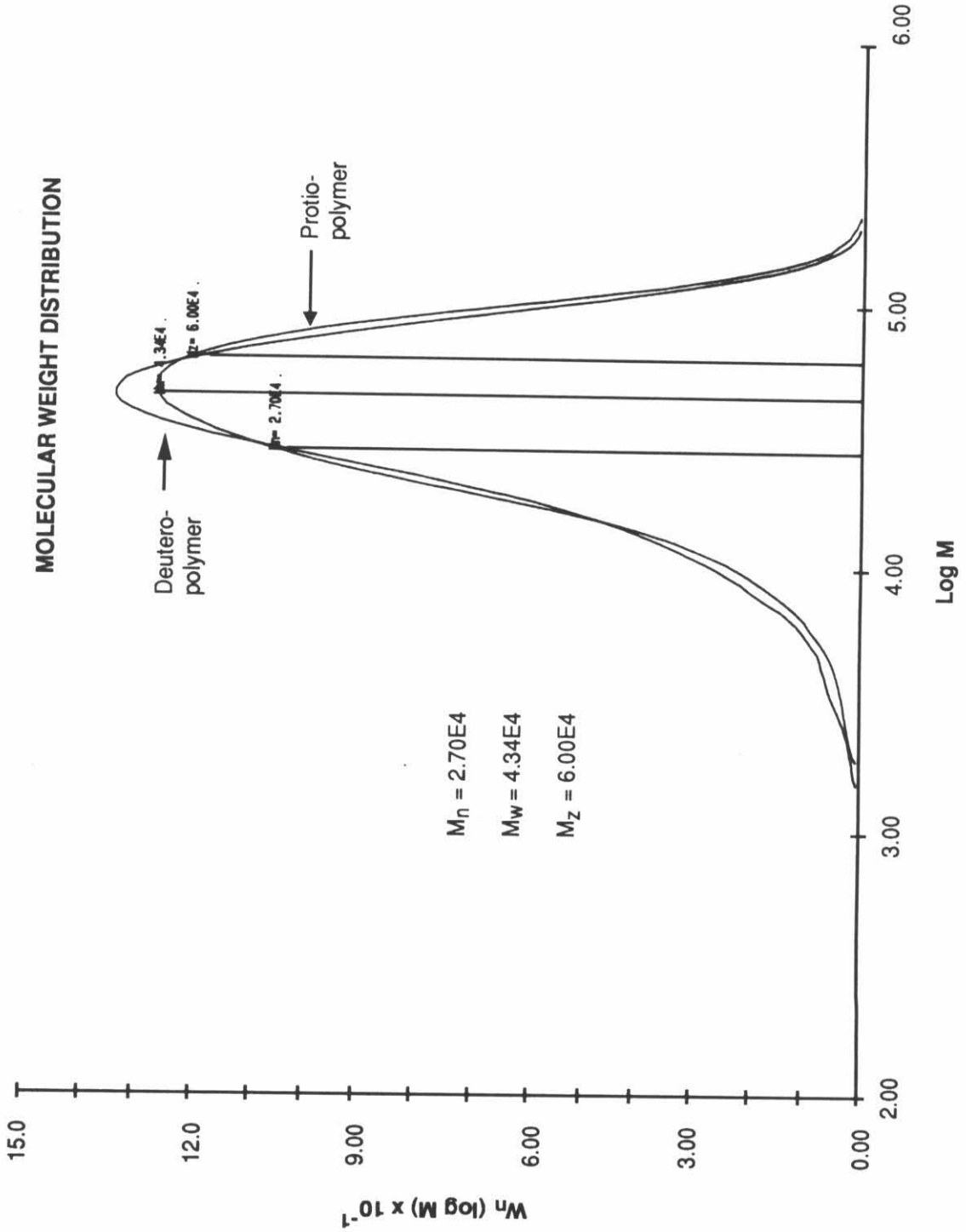
MOLECULAR WEIGHT DISTRIBUTION
Deutero-polymer
Protio-polymer
M_n = 2.70E4
M_w = 4.34E4
M_z = 6.00E4
W_n (log M) x 10^{-1}
Log M
15.0
12.0
9.00
6.00
3.00
0.00
2.00
3.00
4.00
5.00
6.00

from aromatizing under the polymerization conditions, but it hinders the pyrolytic aromatization of the resulting polymer **5** to form PPP. In order to overcome this obstacle, the TMS protecting groups on polymer **5** were transformed to better leaving groups.

(H) Functional Group Transformations on Polymer 5

Few efficient functional group interconversions on polymers are documented;[36-38] however, two methods were found to completely convert the TMS ethers of polymer **5** to more facile leaving groups such as acetates. The first method involved treating the polymer with acetyl chloride using $ZnCl_2$ as a catalyst (Figure 26).

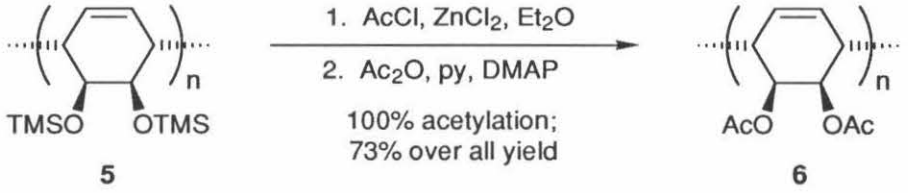

Figure 26. Acetylation of polymer **5** using acetyl chloride and $ZnCl_2$.

The combination of an acid chloride and $ZnCl_2$ has been used to provide almost quantitative conversion of TMS ethers to ester groups in one step in the case of small molecules.[39] When applied to polymer **5**, these reagents completely transform the TMS ethers to approximately 96% acetate groups and 4% unreacted TMS ether groups that are hydrolyzed to hydroxy groups upon workup. The fully acetylated polymer (**6**), is obtained by treating the crude material with acetic anhydride in the presence of pyridine and DMAP. Complete acetylation is indicated by the disappearance of the proton signal at 3.9 ppm due to residual hydroxy groups in the ^1H NMR spectrum of the polymer. The overall yield of this two-step procedure is 70% with 100% acetylation.

The second procedure for transforming the TMS ether groups of **5** to acetate

groups was inspired by the retreatment process employed in the first procedure. Instead of attempting to convert the TMS ethers to acetates in one step, **5** is first deprotected by tetra(*n*-butyl)ammonium fluoride (TBAF) and methanol to give the corresponding hydroxy polymer **7**.[36,37] Polymer **7** is then completely acetylated to give polymer **6** by treatment with a mixture of pyridine, acetic anhydride, and DMAP at 80 °C (Figure 27). This second procedure affords polymer **6** with 93% recovered yield over two steps.

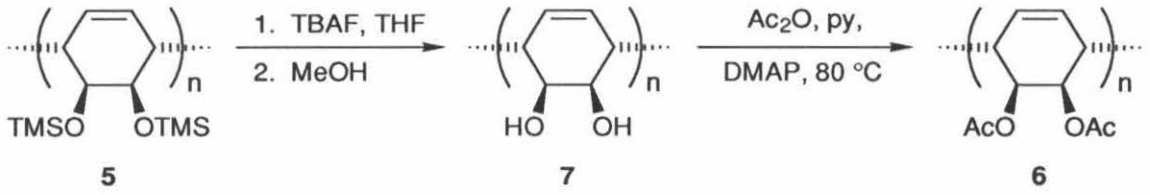

Figure 27. Conversion of polymer **5** to polymer **6** by deprotection followed by acylation.

Both procedures result in 100% conversion of the TMS ethers to acetate groups without affecting any of the stereocenters on the polymer. The acetoxy polymer **6** is, in fact, a completely 1,4-linked, stereoregular analogue to the radically polymerized acetoxy functionalized PPP precursor **3a,** originally used in the ICI process (Figure 1). Unfortunately, the first procedure (Figure 26) appears to be limited to acetyl substitution. The use of other acyl chlorides such as benzoyl chloride did not produce the corresponding benzoate polymer from **5**. The second procedure (Figure 27) appears to be a much more general process for the synthesis of ester derivatives of **4**. Treatment of polymer **7** with pyridine, DMAP, and the appropriate acid anhydride afforded the corresponding 1,4-linked benzoate, propionate, and hexanoate polymers (Figure 28).[40]

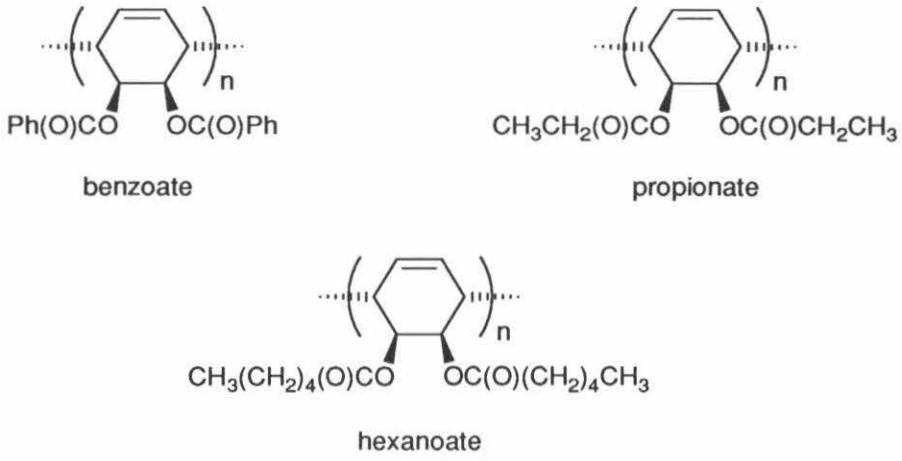

Figure 28. Other ester-functionalized stereoregular PPP precursors accessible via the acylation of polymer **7**.

The synthesis of the latter two derivatives has not yet been optimized. It was not possible to synthesize the stereoregular analogue to the radically polymerized methoxycarbonyl polymer **3b** using methyl chloroformate or dimethyl pyrocarbonate by either of the aforementioned procedures.

(I) Characterization of Polymer 6: Confirmation of the 1,4-Stereoregular Structure

Polymer **6** was characterized by a combination of NMR spectroscopy, Viscotek GPC analysis, low angle laser light scattering (LALLS) analysis, PXRD analysis, and STM imaging.

Unlike in the case of polymer **5**, a highly 1,4-linked, stereoregular structure for polymer **6** (Figures 26 and 27) could be confirmed by NMR analysis. Superficially, a stereoregular structure for polymer **6** is suggested by comparison of its ^{1}H and ^{13}C NMR spectra with those of its radically polymerized counterpart **3a**, which has 10% 1,2-units and random backbone stereochemistry. As can be seen from comparing Figures 29a,b

and 30a,b, **6** has ^{1}H and ^{13}C resonances with chemical shifts identical to those of its radically polymerized analogue **3a**; however, the individual resonances are much narrower and more symmetric as would be expected for a stereoregular polymer.

Unfortunately, ^{1}H NMR analysis of polymer **6** cannot directly detect the presence of any 1,2-units in the polymer. The proton signal from the acetate protons masks the 1.8–2.1 ppm region where protons from 1,2-linkages normally appear (see Figure 29a).[5] However, the ^{1}H NMR spectrum of the stereoregular benzoate polymer, which was similarly derived from polymer **5**, does not exhibit any proton signals in this region (Figure 31). This observation further confirms that polymer **5** and its derivatives such as **6** are completely 1,4-linked.

With respect to the stereoregularity of the polymer, both the sharpness and the number of unique signals in the ^{1}H and ^{13}C NMR spectra of **6** suggest two things about the polymer: (1) It has a highly tactic (i.e., stereoregular) structure with a plane of symmetry within each repeat unit. (2) It is conformationally nonrigid. As can be seen from Figures 29a and 30a, polymer **6** exhibits four sharp ^{1}H NMR signals and five sharp ^{13}C NMR signals, thus indicating the presence of only four unique protons and five unique carbons in the polymer. This fact implies that there must be a plane of symmetry bisecting *each* repeat unit of the polymer in order make both halves of the cyclohexene rings equivalent by NMR analysis throughout the polymer. There are only two possible regular tacticities for polymer **6** with the 1,4-*SSRR* type repeat unit (as inferred from the parent polymer **5**) that maintains a symmetry plane through each repeat unit: (1) an isotactic structure, and (2) a syndiotactic structure (Figure 32).[24] If the polymer is conformationally flexible and the repeat units undergo rapid half-chair–half-chair conformational interconversion (i.e., "ring-flipping") as expected for cyclohexene molecules in solution,[25] each repeat unit of these two structures would possess a plane of symmetry on the NMR timescale (Figure 32).[41] This conformational flexibility and repeat unit symmetry would make the protons and carbons on each half of each

Figure 29. 400 MHz ^{1}H NMR spectra of (a) stereoregular acetoxy polymer **6** and (b) its radically polymerized analog **3a** in $CDCl_3$.

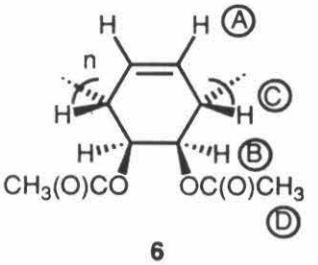
H
H
A
n
C
H
H
H
H
B
CH3(O)CO
OC(O)CH3
D

6

(a)
CHCl3
A
B
C
D
PPM
9
8
7
6
5
4
3
2
1
0

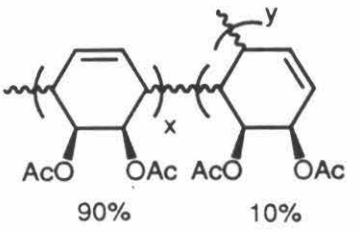
y
x
AcO
OAc
AcO
OAc
90%
10%

3a

(b)
PPM
9
8
7
6
5
4
3
2
1
0

Figure 30. 100 MHz ^{13}C NMR spectra of (a) stereoregular acetoxy polymer **6** and (b) its radically polymerized analog **3a** in $CDCl_3$.

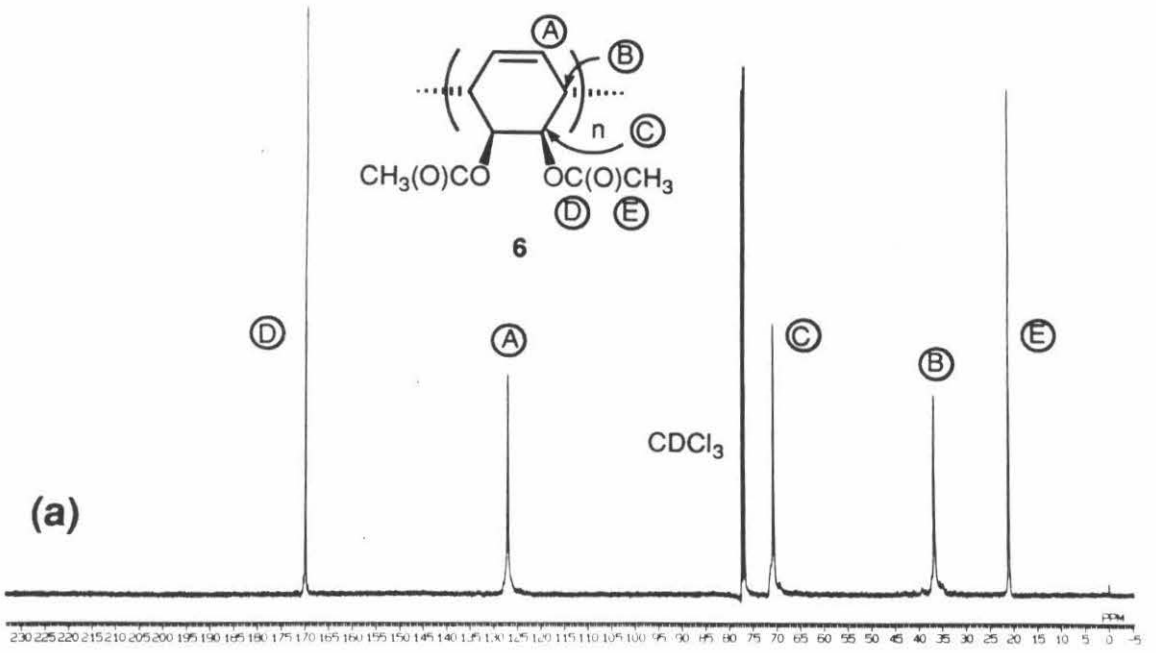
A
B
n
C
CH3(O)CO
OC(O)CH3
D
E
6
D
A
C
B
E
CDCl3
(a)

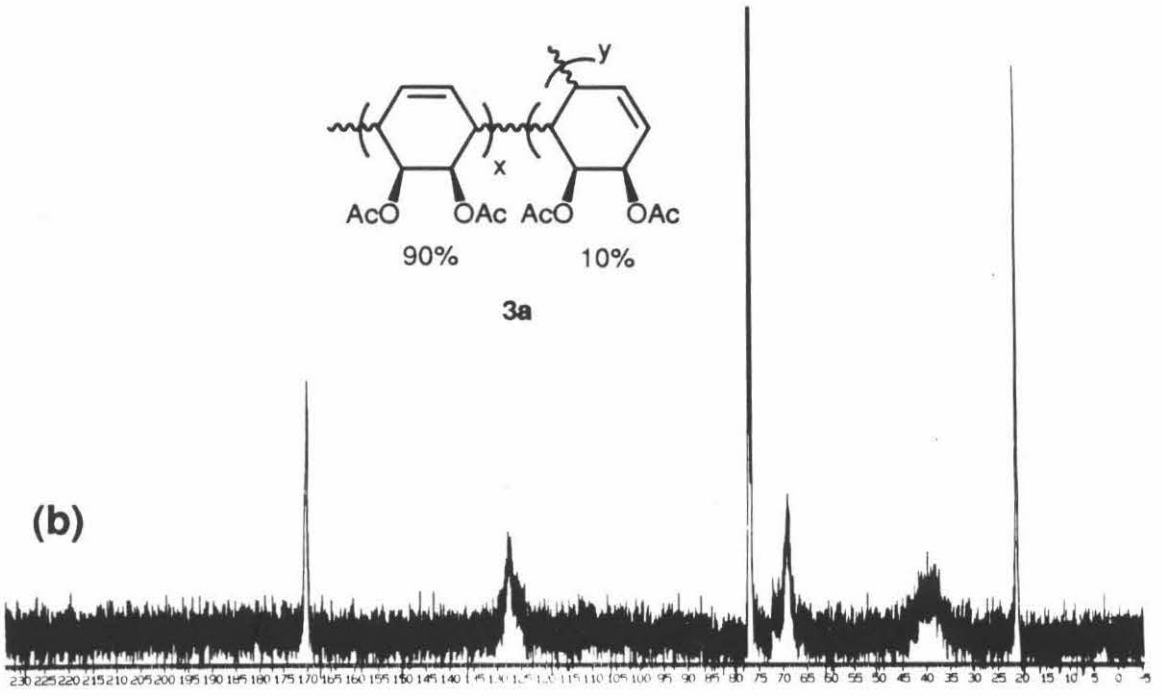
y
x
AcO
OAc
AcO
OAc
90%
10%
3a
(b)

Figure 31. 400 MHz ^{1}H NMR spectrum of the benzoate derivative of polymer **5** in CD_2Cl_2.

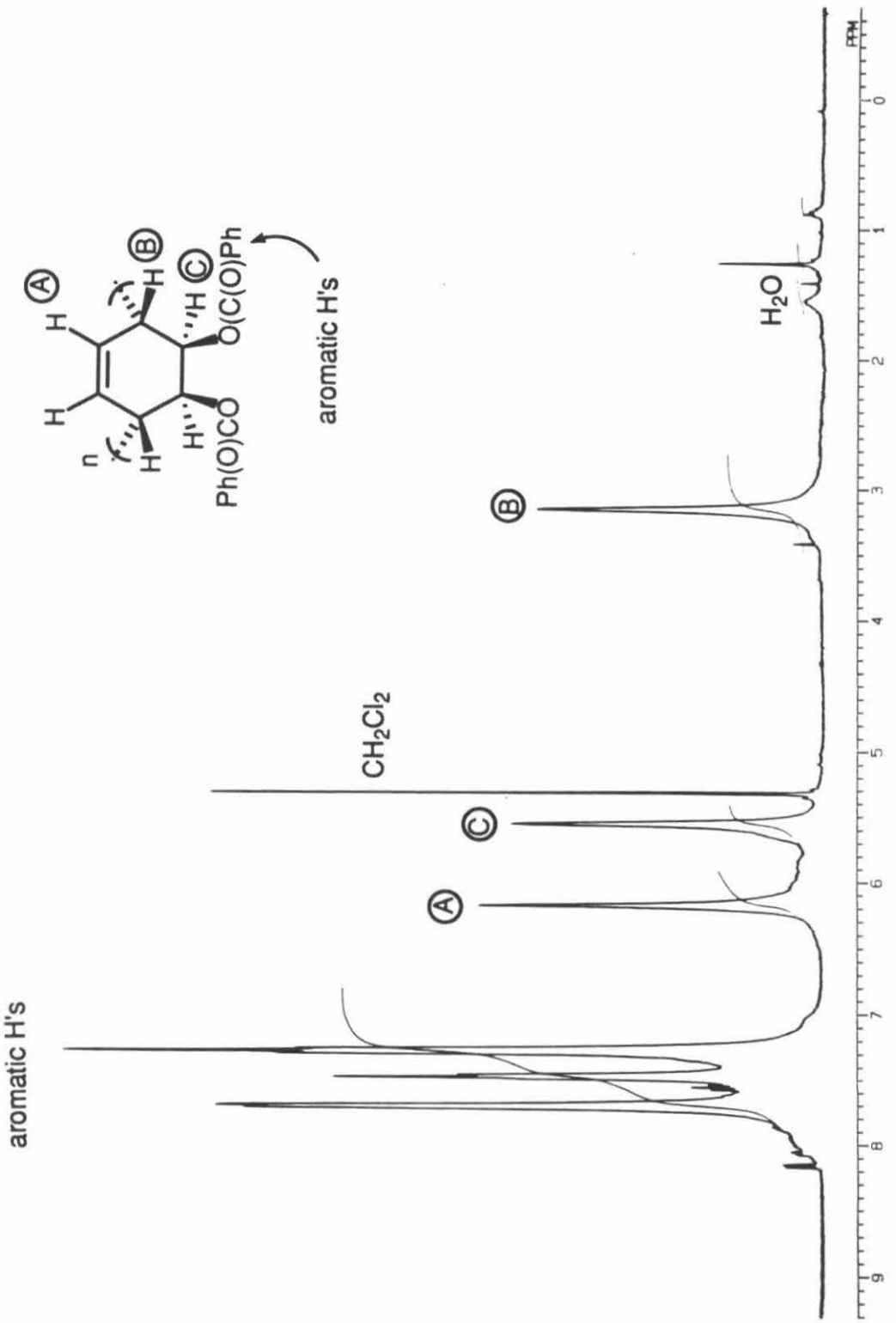
aromatic H's
CH2Cl2
A
C
B
H2O
PPM
9
8
7
6
5
4
3
2
1
0
A
B
C
H
H
H
H
n
H
O(C(O)Ph
Ph(O)CO
aromatic H's

1,4-*SSRR* Repeat Unit for **6**

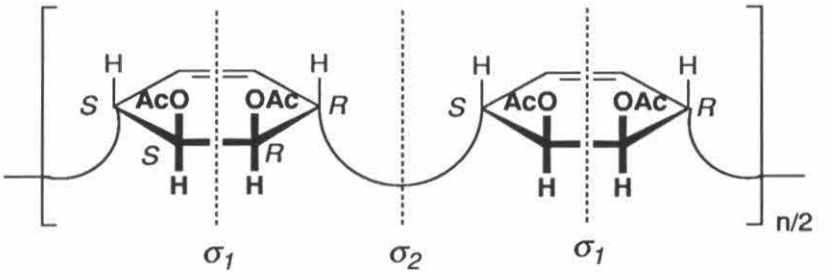

Isotactic structure

By symmetry: (a) All junctions are identical: *RS*
(b) Four chemically nonequivalent protons.
(c) Five chemically nonequivalent carbons.

Ac = $C(O)CH_3$

σ = plane of symmetry

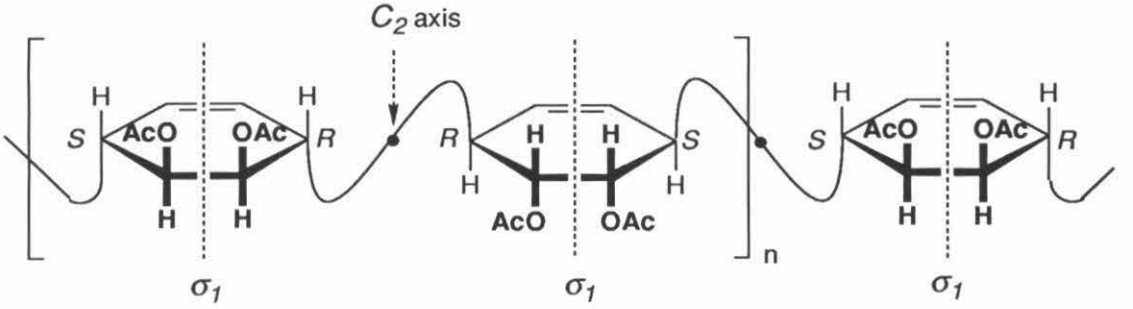

Syndiotactic structure

By symmetry: (a) *RR* and *SS* junctions are enantiomers and therefore equivalent by NMR spectroscopy.
(b) Four chemically nonequivalent protons.
(c) Five chemically nonequivalent carbons.

Figure 32. The symmetry of the isotactic and syndiotactic structures for a conformationally flexible polymer **6** with the 1,4-*SSRR* repeat unit.

cyclohexene ring equivalent throughout the polymer. Thus, the ^{1}H and ^{13}C NMR spectra of these two structures would exhibit exactly four chemically nonequivalent protons and five chemically nonequivalent carbons, as is observed experimentally for the polymer.

All other possible repeat sequences containing the 1,4-*SSRR* repeat unit for **6** would not exhibit the four unique protons and five unique carbons observed for the polymer by NMR analysis. Although many other possible regular sequences with the same repeat unit would possess symmetry planes and C_2 axes, they all would not have the plane of symmetry within *each* repeat unit required to make the two halves of the cyclohexene rings equivalent throughout the entire molecule (Figure 33). Consequently, they would all exhibit more chemically nonequivalent protons and carbons than the four and five observed. Although an isotactic or a syndiotactic structure consisting of 1,4-*RSRS* repeat units (Figure 34) would give the same number of observed NMR signals, it is highly unlikely that polymer **6** consists of these 1,4-*RSRS* repeat units, considering the π-facial selectivity afforded by the TMS ethers of **4** during the synthesis of the parent polymer **5** (see Section D).

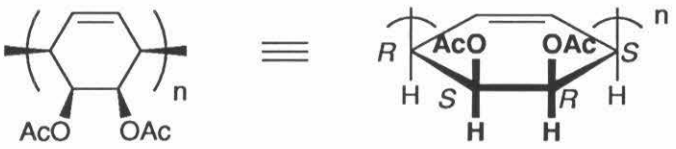

Figure 34. Two representations of a 1,4-*RSRS* repeat unit for **6**.

Polymer **6** definitely cannot be an atactic polymer (random backbone stereochemistry) with the 1,4-*SSRR* repeat unit, or a polymer containing a substantial amount of 1,2-units or trans (1,4-*SSRS* or 1,4-*RSRR*) repeat units if it exhibits the observed NMR spectra. These structures would have many more chemically nonequivalent protons and carbons than that observed for the 1,4-*SSRR* isotactic and syndiotactic cases because the symmetry of these systems would be considerably lower (Figure 35).

Figure 33. Examples of repeating sequences with the 1,4-*SSRR* repeat unit for **6** that would not have the symmetry observed in the ^{1}H and ^{13}C NMR spectra of the polymer.

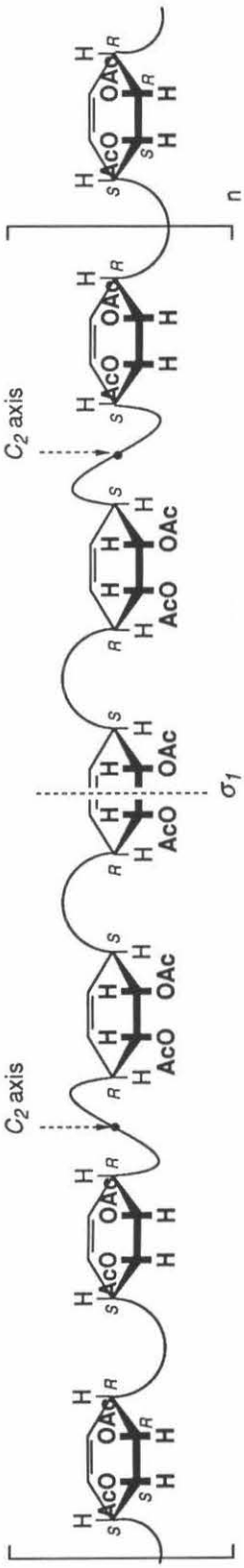
C_2 axis
σ_1
n

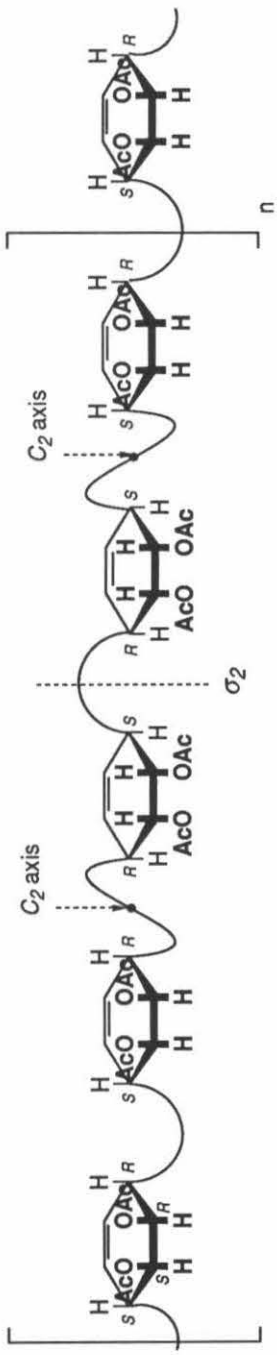
C_2 axis
σ_2
n

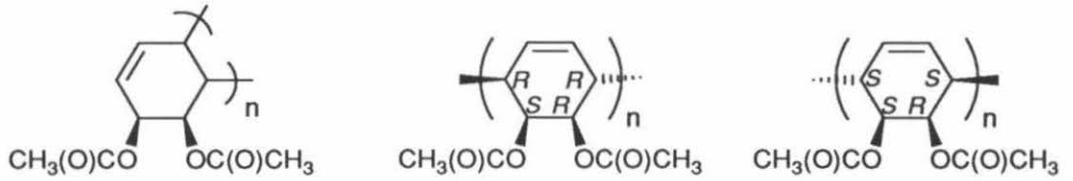

1,2-unit

No symmetry in repeat unit,
10 unique carbons

1,4-*RSRR* repeat unit

1,4-*SSRS* repeat unit

No symmetry in repeat unit,
10 unique carbons each

Figure 35. Repeat units that do not possess the symmetry to generate the ^{1}H and ^{13}C NMR spectra observed for polymer **6**.

Thus, the ^{1}H and ^{13}C NMR spectra for these latter structures would be much broader and more asymmetric. This is indeed the case for radically polymerized **3a**, which is atactic and has a combination of all three structures as a result of the nonstereospecific nature of the radical polymerization process (see Figures 29b and 30b). Consequently, polymer **6** must have a highly isotactic or syndiotactic structure with the 1,4-*SSRR* repeat unit, as shown in Figure 32.

In order to confirm that the sharpness and symmetry of the signals in the ^{1}H and ^{13}C NMR spectra of **6** (Figures 29a and 30a) are the result of a stereoregular structure and not the result of very low molecular weight material, the absolute molecular weight of the polymer **6** was determined by Viscotek GPC and LALLS analysis.[42] The results of these analyses are presented in Table IV and compared to similar data obtained from radically polymerized **3a**.

Table IV. Comparison of absolute molecular weight data for polymers **6** and **3a**.

Polymer	Viscotek GPC analysis			LALLS analysis
	M_n	M_w	PDI	M_w
6	2.68×10^4	4.17×10^4	1.56	4.94×10^4
3a	3.57×10^4	9.32×10^4	2.61	1.10×10^5

The molecular weight of **6** is approximately one-half the molecular weight of **3a**. These molecular weight values for **6** are in good agreement with the number average degree of polymerization obtained for polymer **5** from which it was derived. Consequently, the differences observed between the ^{1}H and ^{13}C NMR spectra of **6** and **3a** cannot be attributed to low molecular weight material but instead must be attributed to differences in stereochemistry.

The conformationally flexible secondary structure inferred for **6** from the symmetry of its NMR spectra was also supported by both PXRD analysis and STM imaging of the polymer. Whereas the rodlike structure of **5** was supported by the presence of nematic order in its PXRD profile (Figure 18), PXRD analysis of **6** revealed an absence of reflections, thus suggesting that the polymer has an amorphous, flexible backbone instead. In fact, the PXRD profile of **6** is similar to that of its radically polymerized analogue **3a**, which is reported to be completely amorphous and have a coiled chain structure.[2] In addition, STM imaging of **6** on HOPG[43] did not show any of the rodlike structures seen during the STM imaging of **5**. Instead, only amorphous, globular structures were observed which appear to have been swept aside by the scanning tip (Figures 36a and 36b). Unfortunately, computer molecular modeling[44] of the 1,4-*SSRR* isotactic and syndiotactic structures inferred from NMR analysis of **6** provided little information on the secondary structure of the polymer. At a low level of theory (MM2), elongated helical chains were generated by modeling. Without performing detailed dynamic molecular mechanics analysis, these simple structures cannot be used to deduce any information on the conformational flexibility of the polymer.

The fact that NMR, PXRD, and STM analysis all support a conformationally flexible, highly 1,4-stereoregular structure for polymer **6** also supports all of our original assumptions made for the structure and conformation of the parent TMS ether polymer **5**. It was originally assumed that the parent polymer **5** is completely stereoregular with either a 1,4-*SSRR* isotactic or syndiotactic structure (Figure 17) and that its unusual ^{1}H

Figure 36a. STM image of amorphous, globular structures observed during STM imaging of polymer **6** on highly oriented pyrolytic graphite (image dimensions: 210 x 210 nm).

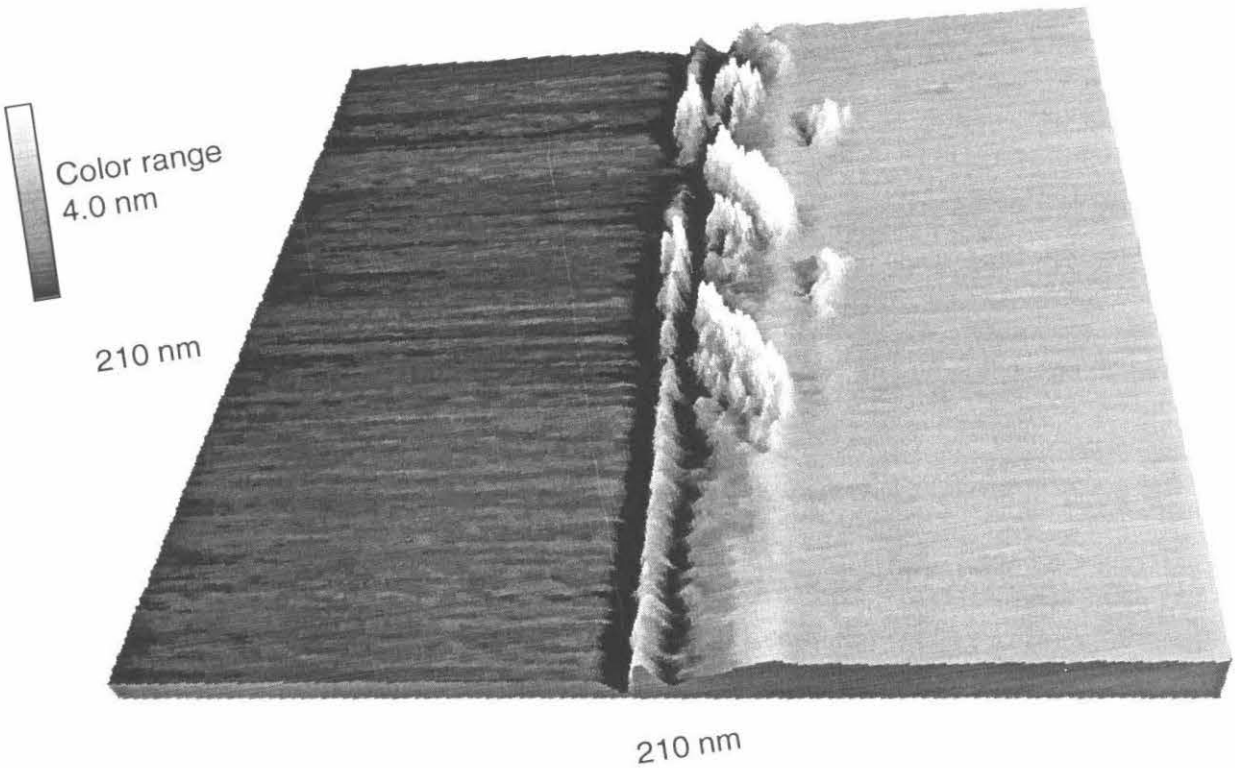
Color range
4.0 nm
210 nm
210 nm

Figure 36b. Close-up view of the globular structure observed during STM imaging of polymer **6** on highly oriented pyrolytic graphite (image dimensions: 52 x 52 nm).

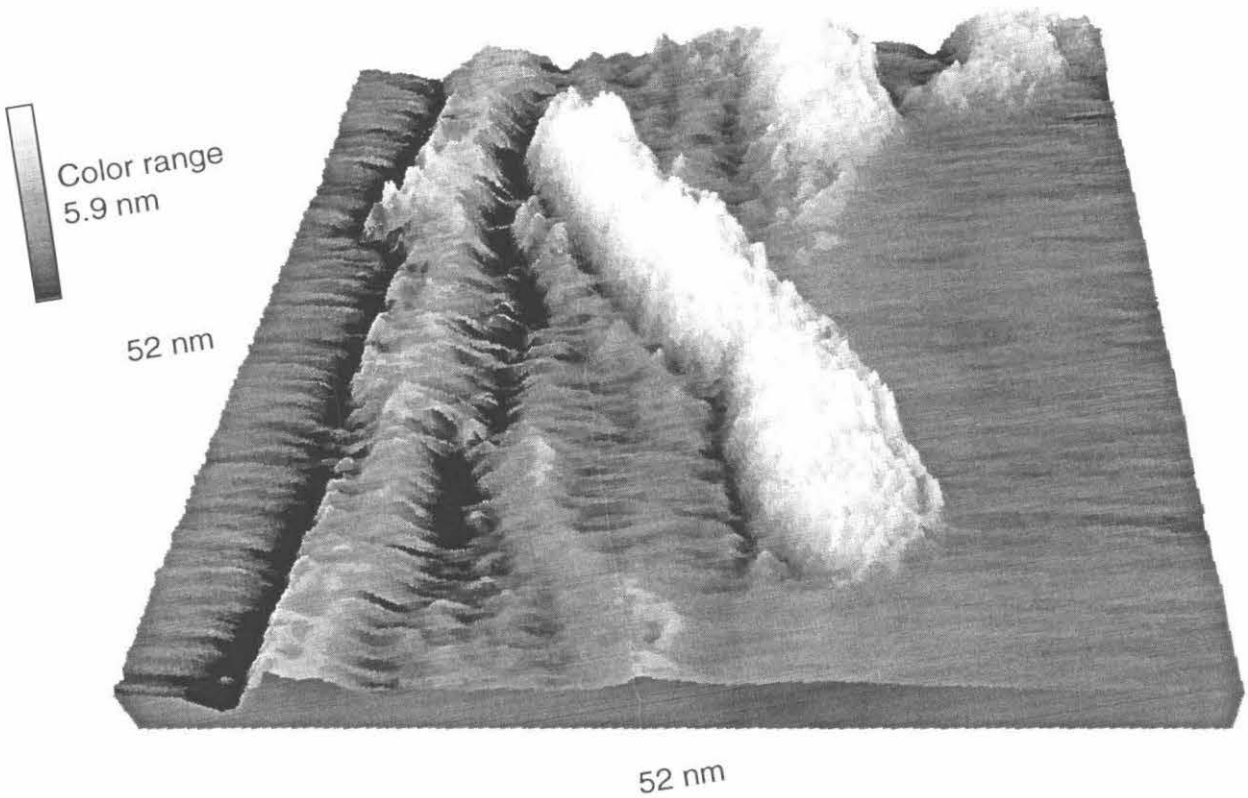
Color range
5.9 nm
52 nm
52 nm

NMR spectrum and physical properties are due to a rodlike secondary structure in which all the 1,4-*SSRR* repeat units are conformationally locked (Figures 20 and 21). By simply changing the bulky TMS ethers on the polymer to acetate groups, the resulting polymer exhibits spectroscopic properties expected for a conformationally flexible, stereoregular polymer, despite the fact that the backbone stereochemistry remains the same. This observation clearly indicates that the unusual ^{1}H NMR spectrum and physical properties of **5** are not the result of an unusual backbone stereochemistry but rather the result of conformational effects due to the TMS ether sidechains. The increase in conformational flexibility upon transformation of **5** to **6** is probably the result of a reduction in steric interactions on going from bulky TMS ethers to less sterically demanding acetate groups.

In summary, NMR, PXRD, and STM analysis all suggest that **6** is a conformationally flexible, highly 1,4-linked, stereoregular polymer with one of the two tacticities shown in Figure 32. Unfortunately, there is no simple spectroscopic method for directly determining which of the two tacticities the polymer backbone actually has because of the similar symmetry of the two structures. Fortunately, in the production of high quality PPP, the actual tacticity of the polymer is not important as the 1,4-regioregularity of the polymer and stereochemical relationships within each precursor repeat unit. The linear structure of the PPP depends entirely on the 1,4-regioregularity of the precursor polymer, whereas the ease of the acid elimination should depend on just the stereochemical (cis) relationship between the pendant ester group and the adjacent bridgehead proton within each repeat unit (the 1,4-*SSRR* repeat unit; see Figure 2). The stereocenters on the precursor polymer backbone are lost upon pyrolytic acid elimination to PPP regardless. All spectroscopic analyses performed on **5** and **6** suggest that the polymers are highly 1,4-linked and have repeat units with the optimum geometry for conversion to PPP. Both the 1,4-*SSRR* isotactic and syndiotactic structures for polymer **6** (Figure 32) meet these two criteria for the formation of high quality PPP.

(J) Preliminary Pyrolysis Studies on Polymer 6

In order to demonstrate that the stereoregular acetoxy polymer **6** could be easily converted to PPP, preliminary pyrolysis experiments were conducted on thin films of the material. Thin films of **6** were coated onto NaCl crystals and aromatized by heating under argon at 310–340 °C. The IR spectra of the resulting brown films (Figure 37) did not show any band at 1745 cm^{-1} due to residual acetate groups. Instead, they were dominated by a strong band at 807 cm^{-1}, which is characteristic of the C–H out-of-plane bending of the 1,4-linked repeat units of PPP.[34,35] The relative intensity of this band was much stronger than the intensities of the two bands at 760 and 696 cm^{-1}, which are characteristic of the C–H bending modes of monosubstituted aromatic endgroups. This observation is a qualitative indication that the PPP films made from **6** consist of long polymer chains.

In contrast, IR analysis of thin films made from the pyrolysis of **3a** gave inconsistent results. Occasionally, the IR spectra of the pyrolyzed films revealed repeat unit and endgroup bands with relative intensities indicative of 1,4-phenylene chains (Figure 38a). At other times, the IR spectra of the pyrolyzed thin films exhibited relative intensities of repeat unit and endgroup bands characteristic of PPP oligomers plus an additional band at 789 cm^{-1} attributable to the C–H bending of 1,2-phenylene units[35] (Figure 38b).

Figure 37. IR spectrum of a PPP film obtained by the pyrolysis of a thin film of **6** on NaCl.

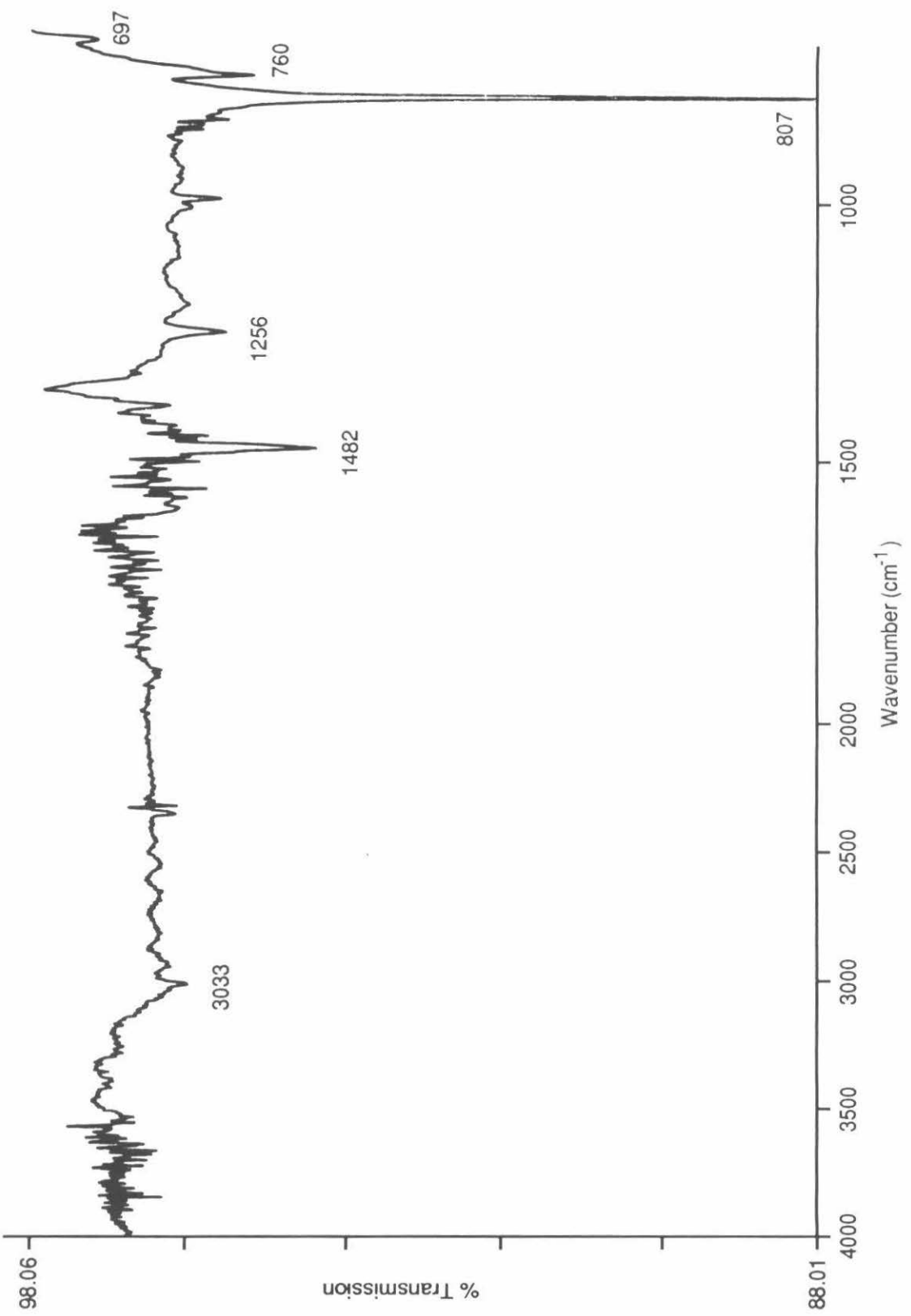
98.06
88.01
% Transmission
4000
3500
3000
2500
2000
1500
1000
Wavenumber (cm-1)
3033
1482
1256
807
760
697

Figure 38. Two IR spectra of polyphenylene thin films made by pyrolysis of thin films of **3a** on NaCl, showing (a) PPP oligomer and (b) polyphenylene oligomers with a substantial fraction of 1,2-units.

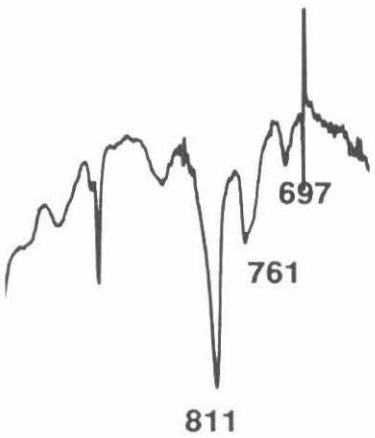

(a)

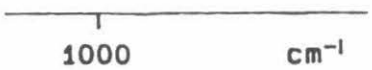

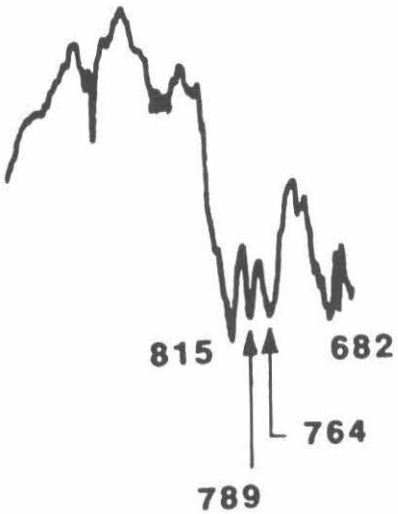

(b)

Summary

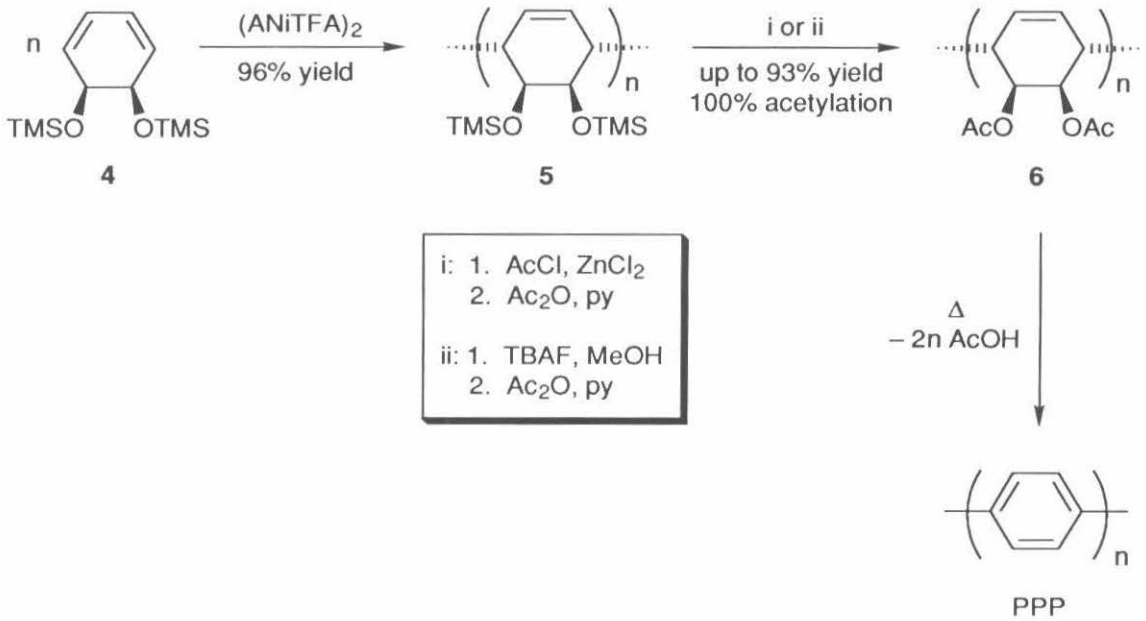

Figure 39. Stereoregular precursors to PPP via transition-metal-catalyzed polymerization: Summary of the process.

1,4-Linked stereoregular precursor polymers to poly(*p*-phenylene) (PPP) were synthesized by the transition-metal-catalyzed polymerization of heteroatom-functionalized 1,3-cyclohexadienes (Figure 39). *cis*-5,6-Bis(trimethylsiloxy)-1,3-cyclohexadiene (**4**), a derivative of a microbial oxidation product of benzene, was polymerized exclusively in a syn-1,4-fashion by bis[(η^3-allyl)trifluoroacetatonickel(II)] [$(ANiTFA)_2$] with yields up to 96%. This polymerization system not only affords a highly 1,4-linked, stereoregular polymer, but it also has the potential for molecular weight control. The resulting stereoregular polymer **5** is a soluble, processable, partially crystalline material which unfortunately does not yield PPP upon direct pyrolysis. Polymer **5** was subsequently transformed to the corresponding stereoregular acetoxy polymer **6** (100% acetylation; up to 93% overall yields). NMR analysis of polymer **6**

confirms that the polymer has either a highly isotactic or syndiotactic structure with the symmetric repeat unit depicted. Preliminary pyrolysis studies on thin films of **6** cast on on NaCl crystals yielded PPP as indicated by IR analysis.

Experimental Section

General Considerations

All manipulations of air- and/or water-sensitive compounds were performed using standard high vacuum or Schlenk techniques. Argon was purified by passage through columns of BASF R3-11 catalyst (Chemlog) and 4Å molecular sieves (Linde). Solids were transferred and stored in a nitrogen-filled Vacuum Atmospheres drybox. All distillations were performed under argon flush. All solvents and liquid reagents were degassed by repeated freeze–pump–thaw cycles and stored under argon in flasks fitted with PTFE valves. Solid reagents and monomers were degassed in vacuo and stored in the drybox prior to use.

Materials

(a) Solvents

All solvents were purchased from Aldrich, EM Science, or Fisher Scientific. *n*-Pentane, toluene, benzene, diethyl ether, THF, and DME were vacuum transferred from sodium/benzophenone. *n*-Pentane and *n*-dodecane were made olefin-free prior to vacuum transferring by successively stirring over concentrated H_2SO_4 and washing with deionized water until the acid layer became colorless. *n*-Dodecane was vacuum-distilled prior to use. Methylene chloride was vacuum transferred from calcium hydride. Chlorobenzene, and *o*-dichlorobenzene were distilled from calcium hydride. Ethyl acetate was purified by distillation. Anhydrous methanol was obtained by distilling over Mg powder. Methanol and hexanes for polymer precipitations, and HPLC grade hexanes and THF for STM sample preparations were all used without further purification.

(b) Reagents

1,3-Cyclohexadiene, chlorotrimethylsilane, acetyl chloride, acetic anhydride,

tetrabutylammonium fluoride (TBAF) monohydrate, 2,6-di-*tert*-butyl-4-methylphenol (BHT), 4-dimethylaminopyridine (DMAP), and $ZnCl_2$ were all purchased from Aldrich. 1,3-Cyclohexadiene was distilled from sodium borohydride or calcium hydride prior to use. Chlorotrimethylsilane was purified by distillation from magnesium filings. Acetyl chloride was simply distilled prior to use whereas acetic anhydride was distilled from anhydrous sodium sulfate. TBAF monohydrate (98%), BHT (99+%), DMAP (99%), and $ZnCl_2$ (99.999%) were all used without further purification. Benzoic anhydride (97%) was obtained from Sigma and just degassed in vacuo prior to use. Pyridine was purchased from Baker Chemicals and purified by distillation from calcium hydride. Allyl trifluoroacetate was prepared according to a literature synthesis by refluxing distilled allyl alcohol and trifluoroacetic acid (Aldrich) together in a reverse Dean–Stark apparatus.[15] Bis(1,5-cyclooctadienyl)nickel(0) [$Ni(COD)_2$] was obtained from the Strem Chemical Company and recrystallized from toluene prior to use. *cis*-5,6-Dihydroxy-1,3-cyclohexadiene (**1**), its acetyl (**2a**) and methoxycarbonyl (**2b**) derivatives, and the corresponding radically polymerized polymers (**3a**, **3b**) were all donated by ICI Chemicals and Polymers Ltd., Runcorn, U. K. Compound **1** was obtained as a 50 wt % solution in pyridine. It was purified by removing the pyridine in vacuo, precipitating the crude material from pentane, and recrystallizing from 30 °C ethyl acetate using charcoal as a decolorizer. The acetyl and methoxycarbonyl derivatives **2a** and **2b** required no further purification. All three monomers were stored under anhydrous, sub-zero conditions and degassed in vacuo prior to use. The radically polymerized PPP precursors **3a** and **3b** also required no further purification prior to use.

(c) Filtration Materials

Basic alumina (Fluka) was dried under dynamic vacuum at 130 °C for 24 h prior to use. Millex-SR Luer-Lok syringe filter units for non-aqueous solutions were obtained from the Waters–Millipore company. Glass microfibre paper (Whatman) for cannula-

filtrations was oven-dried prior to use.

Instrumentation

NMR spectra were recorded using a JEOL GX-400 (399.65 MHz ^{1}H, 100.40 MHz ^{13}C) spectrometer. Infrared spectra were recorded using a Perkin-Elmer 1600 series FT-IR spectrometer. Gas chromatography was performed using a Hewlett–Packard HP 5890 Series II Gas Chromatograph equipped with 30 m SE-30 (OV-1) capillary column and an HP 3396 Series II Integrator. General gel permeation chromatograms were obtained on a home-built system consisting of two American Polymer Standards columns and a Waters Ultrastyragel column, an Altex Model 110A pump, and a Knauer differential refractometer using HPLC grade methylene chloride (Burdick and Jackson) as the eluant at a flow rate of 1.0 mL/min at room temperature. Viscotek gel permeation chromatograms were obtained on a system consisting of a set of three Polymer Labs mixed B columns (300 mm, 5 μm) and a Viscotek differential refractometer/viscometer detector using THF as the eluant at a flow rate of 1 mL/min at 35 °C. Low angle laser light scattering (LALLS) analysis was performed on a Chromatrix KMX-6 light scattering apparatus using THF as the solvent. Powder X-ray diffraction work was performed on a Scintag/USA PAD V powder X-ray diffractometer using CuK_{α} radiation. Differential scanning calorimetry and thermal gravimetric analysis were performed on a Perkin-Elmer PC Series DSC7 and TGA7, respectively. Scanning tunneling microscopy was performed using a Digital Instruments Nanoscope II. Molecular modeling calculations were performed on a Silicon Graphics Iris 4D/220GTX computer employing Biograf Version 2.20 and BatchMin Version 3.1d programs. Space-filling (CPK) images of the modeled structures were displayed using MacroModel. Elemental analysis was performed at Oneida Research Services Inc., Whitesboro, NY.

Preparation of Bis[(η^3-allyl)trifluoroacetatonickel(II)] [$(ANiTFA)_2$]

In the drybox, recrystallized bis(1,5-cyclooctadienyl)nickel(0) [$Ni(COD)_2$] (5.00 g, 18.2 mmol) was ground to a fine powder using a mortar and pestle and loaded into a 250-mL Schlenk flask containing a stirbar. The canary-yellow powder was suspended in 100 mL of rapidly stirred diethyl ether and then added to a 250-mL Schlenk flask containing allyl trifluoroacetate (5.60 g, 35.4 mmol) at 0 °C as 10-mL aliquots via a wide-bore cannula over a period of 10 min. The mixture was stirred in the absence of light at 0 °C for 90 min, or until all of the yellow $Ni(COD)_2$ was consumed. The resulting clear dark-red solution was then quickly filtered into another Schlenk flask using a cannula with a plug of glass microfibre at one end (cannula-filtration). Three-quarters of the solvent was pumped off with the mixture maintained below room temperature in order to induce precipitation of the $(ANiTFA)_2$. An equal volume of olefin-free pentane at –78 °C was then added to precipitate out the remainder of the catalyst as a red-brown powder. The product was washed with 2 x 10-mL aliquots of olefin-free pentane at –78 °C and dried in vacuo overnight. Yield: 3.43 g (89%) of $(ANiTFA)_2$. ^1H NMR (400 MHz, C_6D_6): δ 4.80–5.30 (1H), 2.45 (2H), 1.60–1.90 (2H). (It is important to perform this synthesis as quickly as possible in one session to minimize the amount of time the product remains in solution.)

A Typical Polymerization of 1,3-Cyclohexadiene using $(ANiTFA)_2$

In the drybox, $(ANiTFA)_2$ (0.010 g, 0.024 mmol) was weighed out into a vial and dissolved in 2.3 mL of solvent (e.g., benzene, chlorobenzene, or *o*-dichlorobenzene) to give a clear orange solution. (If the catalyst solution was slightly turbid, it was subsequently filtered through a 0.2 μm syringe filter unit (Millex-SR) using a gas-tight syringe.) This catalyst solution was then transferred to a 50-mL capacity, thick-walled glass Schlenk tube containing a stirbar and fitted with an 8 mm PTFE valve. 1,3-Cyclohexadiene (1.1 mL, 0.89 g, 0.011 mol) that had been filtered through a short plug of

basic alumina was then syringed into the orange catalyst solution. After approximately 5 min, the initially clear orange reaction mixture became turbid due to polymer formation at room temperature. The reaction vessel was then sealed, brought out of the drybox, and placed under an atmosphere of argon after repeated freeze–pump–thaw cycles. The turbid orange reaction mixture was placed in a 50–51 °C oil bath and rapidly stirred for 24 h. During that period, the polymerization mixture became progressively more difficult to stir due to the rapid buildup of insoluble polymer until finally at the end of the reaction, an immobile orange solid mass was obtained. The crude polymer was purified by first suspending it in methanol (25 mL) containing a grain of BHT and then isolated by suction-filtration. The resulting light orange powder was subsequently re-suspended in benzene (50 mL) and re-isolated from methanol as before. After drying overnight in vacuo, the polymer was obtained as an off-white powder. Yield: 0.79 g (88%) of polycyclohexadiene. ^{1}H NMR (400 MHz, C_6D_6): δ 5.6–5.8 (2H), 1.9–2.1 (2H), 1.4–1.7 (4H). PXRD: 5.292, 4.517, 3.907 Å. Anal. Calcd for $(C_6H_8)_n$: C, 90.00; H, 10.00. Found: C, 85.34; H, 9.49.

Preparation of *cis*-5,6-Bis(trimethylsiloxy)-1,4-cyclohexadiene (4)

cis-5,6-Dihydroxy-1,3-cyclohexadiene (**1**) (20.00 g, 0.178 mol) and a catalytic amount of DMAP were dissolved in a mixture of methylene chloride (650 mL) and pyridine (43.2 mL, 0.536 mol) in a 2-L round bottom flask containing a stirbar. While rapidly stirring under argon with the temperature moderated using a cool water bath, chlorotrimethylsilane (50.0 mL, 0.393 moles) was added dropwise to the pale yellow solution using a pressure-equalizing addition funnel. After stirring for 1.5 h, olefin-free pentane (200 mL) was cannulated into the cloudy white suspension to completely precipitate the pyridinium hydrochloride salts, which were subsequently removed by filtration. The solvent was removed from the filtrate in vacuo to yield a pale yellow oil. High vacuum distillation of the oil using a short path distillation apparatus and an 80 °C

oil bath yielded as a viscous, colorless, clear liquid (bp: 47 °C at ca. 10 μm Hg pressure). The final product was stored at sub-zero temperatures in the drybox freezer. Yield: 41.6 g (91%) of monomer **4**. ^{1}H NMR (400 MHz, C_6D_6): δ 5.73–5.88 (4H), 4.12 (2H), 0.14 (18H).

A Typical Polymerization of *cis*-5,6-Bis(trimethylsiloxy)-1,4-cyclohexadiene (4) using (ANiTFA)$_2$

In the drybox, (ANiTFA)$_2$ (0.140 g, 0.329 mmol) was dissolved in chlorobenzene (10.2 mL) to give a dark orange-red solution. This solution was filtered via a gas-tight syringe through a 0.5 μm porosity, Millex-SR, non-aqueous filter unit into a 50-mL capacity, thick-walled glass Schlenk tube containing a stirbar and topped with an 8 mm PTFE valve. To this catalyst solution was added monomer **4** (6.75 g, 26.3 mmol) that had been passed through equal volume of dry, basic alumina to remove trace impurities. (This monomer filtration step is optional with freshly distilled monomer that has been checked by GC analysis for purity.) The clear orange reaction mixture (monomer-to-catalyst ratio = 80:1; monomer concentration = 1.5 M) was freeze–pump–thaw degassed and sealed under an argon atmosphere. The reaction mixture was placed in a 50–51 °C oil bath and rapidly stirred for 24 hours. The initial clear orange solution became deep red-brown after a period of 5 min. After approximately 30 min, the reaction mixture became opaque and coffee-colored. After 48 h, a dark brown gel was usually obtained. The polymer gel was dissolved in an equal volume of hexanes or THF and precipitated into rapidly stirred methanol (800 mL) containing BHT. The resulting off-white powder was isolated by suction-filtration, washed with fresh methanol, and dried in vacuo overnight. Yield: 6.25 g (93%) of polymer **5**. ^{1}H NMR (400 MHz, $CDCl_3$): δ 5.1–6.2 (2H), 3.3–4.1 (2H), 2.7–3.2 (1H), 2.1–2.6 (1H), –0.4–0.5 (18H). IR (neat): 2957, 2898, 1251, 1111, 1087, 1046, 837, 748 cm^{-1}. PXRD: 9.725 Å and an amorphous halo centered at 5.5 Å. Anal. Calcd for $(C_{12}H_{24}O_2Si_2)_n$: C, 56.19; H, 9.43; Si, 21.90. Found:

C, 55.91; H, 9.34; Si, 22.21.

A Typical Experiment for Determining the M_n vs. % Conversion Relationship of the (ANiTFA)$_2$/Monomer 4 Polymerization System

For a typical molecular weight vs. % conversion experiment, a preliminary calibration for quantitative GC analysis was initially performed by determining the relative response factor for the monomer (**4**) and the internal standard (n-$C_{12}H_{26}$). A standard solution was made up by diluting a mixture of olefin-free n-$C_{12}H_{26}$ (0.0188 g, 0.110 mmol) and monomer **4** (0.0423 g, 0.165 mmol) with methanol to 1.00 mL in a volumetric flask. A range of diluted standards were made up from this stock solution by transferring 1–8 μL of the stock solution to several 1.00-mL volumetric flasks and diluting with methanol quantitatively to the marks. Each diluted standard was then analyzed by GC on a HP 5890 II using a 1.0-μL injection volume, an injector temperature of 160 °C, a detector temperature of 250 °C, an initial temperature of 80 °C, an initial time of 2 min, a ramp rate of 10 °C/min, a final temperature of 200 °C, and a final time of 4 min. The relative response factor (C) between the monomer and the internal standard (std) was determined by averaging the ratio of the integral of the monomer over that of the standard over several concentrations and several injections and then applying it to Eq. 2.

$$C = \left(\frac{[\text{monomer}]}{[\text{std}]}\right)\left(\frac{\text{area monomer}}{\text{area std}}\right) \qquad (2)$$

Using the GC conditions described, a typical relative response factor between the monomer and the internal standard was found to be 1.06 ± 5%.

A polymerization reaction was then set up by the procedure described previously on a scale large enough to permit repeated sampling. For example, for a polymerization

system in toluene with a [**4**] of 2.0 M, and a monomer-to-catalyst ratio of 75:1, $(ANiTFA)_2$ (0.110 g, 0.259 mmol), monomer **4** (5.00 g, 19.4 mmol, 5.43 mL), toluene (3.44 mL), and *n*-$C_{12}H_{26}$ (0.664 g, 3.90 mmol) were combined in a 50-mL Schlenk tube. After placing the reaction mixture in a 50–51 °C oil bath, aliquots of the reaction mixture containing varying proportions of polymer and unreacted monomer were withdrawn at various times. Typically, 0.6–0.7 mL samples were withdrawn under argon flush using a 1.00 mL gas-tight syringe and a long, wide-bore needle. Each aliquot was then injected into 10 mL of methanol with 0.1 wt % BHT to precipitate the polymer. After mixing the resulting suspension well and then allowing the polymer to settle, 5–10 μL of the green supernatant was transferred to a 1.00 mL volumetric flask and diluted with more methanol. The amount of unreacted monomer in each aliquot was then determined by quantitative GC analysis on each diluted supernatant solution using the GC conditions described above. The amount of unreacted monomer can be calculated using Eq. 3 by comparing the area of its GC trace with that of the internal standard.

$$\text{Moles of monomer remaining} = C\left(\frac{\text{area monomer}}{\text{area std}}\right)(\text{initial moles of std}) \qquad (3)$$

The precipitated polymer **5** from each sample aliquot was individually purified and isolated by first centrifuging the crude material, then washing it with fresh methanol, then redissolving it in THF (1 mL), and finally precipitating it into methanol and centrifuging it down. The M_n of each polymer sample was determined by Viscotek GPC analysis at ICI, Runcorn, U.K. By plotting the % conversion of **4** vs. time and the M_n of polymer **5** against the % conversion of monomer at that point, the relationships shown in Figure 23 and 24 were obtained.

Preparation of the Stereoregular Acetoxy Polymer 6: Method 1

A 500-mL capacity Schlenk flask was charged with polymer **5** (2.41 g), anhydrous zinc chloride (2.69 g, 19.7 mmol), and a stirbar in the drybox. On the Schlenk line, diethyl ether (250 mL) was cannulated into the reaction vessel under argon flush. The mixture was rapidly stirred at ambient temperature for 1 h to completely dissolve the zinc chloride. Then, acetyl chloride (5.62 mL, 79.0 mmol) was syringed in as a neat liquid to the colorless clear solution. The mixture was stirred at room temperature for 18 h during which time a pale yellow gelatinous solid formed. Subsequently, the reaction mixture was decanted into methanol (1600 mL) to precipitate the polymer as a white powder. The polymer was isolated by suction-filtration, washed with fresh methanol, and dried in vacuo overnight. Yield: 1.43 g (78%) of crude acetoxy polymer **6**.

This crude polymer **6** typically has a small percentage (4%) of hydroxy groups as indicated by a signal at 3.9 ppm in its ^{1}H NMR spectrum. These residual hydroxy groups were acetylated by treating the crude polymer with pyridine and acetic anhydride: A 50-mL capacity, thick-walled glass Schlenk tube fitted with a 8 mm PTFE valve was charged with a stirbar, the crude acetoxy polymer **6** (1.13 g), and a grain of DMAP. The solids were degassed in vacuo, placed under an argon atmosphere, and dissolved in methylene chloride (10 mL). To this clear pale yellow solution was added pyridine (1.72 mL, 21.2 mmol) and acetic anhydride (1.72 mL, 18.2 mmol) as neat liquids by syringe under argon flush. The flask was sealed, and the reaction mixture was stirred at 40 °C for 13 h. After the mixture was cooled to ambient temperature, the volatiles were removed in vacuo. The remaining light orange, glassy solid was dissolved in methylene chloride (50 mL) and washed sequentially with saturated aqueous $NaHCO_3$ (2 x 50 mL), saturated aqueous NaCl (2 x 50 mL), and deionized water (50 mL). The organic phase was dried over anhydrous Na_2SO_4, concentrated to approximately 10 mL, and added dropwise to stirred hexanes (100 mL) containing BHT to precipitate the polymer. The white precipitate was isolated by suction-filtration, washed with more hexanes, and dried in vacuo overnight. Yield: 1.02 g (90%, based on the crude material) of fully acetylated polymer **6**. The

resulting polymer **6** has the same ^1H NMR spectrum as the material made via acetylation of polymer **7**: no hydroxy proton signal at 3.9 ppm after retreatment of the impure polymer.

Preparation of the Stereoregular Acetoxy Polymer 6: Method 2

(a) Preparation of the Stereoregular Hydroxy Polymer 7 from Polymer 5

A 1-L Schlenk flask was charged with a stirbar and TBAF monohydrate (34.7 g, 0.133 mol). The TBAF monohydrate was dried in vacuo at room temperature for 2.5 h, placed under an argon atmosphere, and then dissolved in THF (250 mL). A filtered solution of dry, degassed polymer **5** (5.00 g in 80 mL dry THF) was added dropwise over 30 min to the rapidly stirred solution of TBAF monohydrate. A thick yellow gum immediately precipitated from the reaction mixture. After rapidly stirring for 6.5 h at room temperature, anhydrous methanol (100 mL) was then syringed into the reaction mixture. The resulting cloudy suspension was stirred for a further 36 h under argon before the off-white solid was isolated by suction-filtration using a medium porosity glass frit. After washing with methanol (2 x 10 mL) and hexanes (2 x 10 mL), the precipitate was dried in vacuo for 48 h to afford quantitative yields of polymer **7** as an amorphous off-white polymer which is insoluble in common solvents. Consequently, it has not been well characterized spectroscopically. Polymer **7** is extremely hygroscopic and should be stored in dessicator. PXRD: amorphous (no sharp reflections). Anal. Calcd for $(C_6H_8O_2)_n$: C, 64.27; H, 7.19. Found: C, 62.20; H, 7.84; N, 0.55; Si, below detection limit (100 ppm).

(b) Acetylation of Polymer 7

A 50-mL capacity, thick-walled glass Schlenk tube with a 8 mm PTFE valve was charged with a stirbar, finely powdered polymer **7** (0.553 g), and a grain of DMAP. The

solids were degassed in vacuo, placed under an argon atmosphere, and suspended in pyridine (6.0 mL, 74 mmol). Acetic anhydride (2.6 mL, 28 mmol) was added by syringe, and the slurry was stirred at 80 °C for 1.5 h, or until the reaction mixture cleared. The resulting clear yellow-orange mixture was then cooled to ambient temperature, and the volatiles were removed in vacuo. The remaining yellow glassy solid was dissolved in methylene chloride (50 mL) and washed sequentially with saturated aqueous $NaHCO_3$ (25 mL) and saturated NaCl (25 mL) solutions. The organic phase was dried over anhydrous Na_2SO_4, concentrated to approximately 5 mL, and then added dropwise to stirred hexanes (150 mL) containing a grain of BHT to precipitate the polymer. The pale yellow precipitate was isolated by suction-filtration, washed with more hexanes, and dried in vacuo overnight. Yield: 0.968 g of completely acetylated polymer **6** (93% over two steps, based on starting polymer **5**). ^{1}H NMR (400 MHz, $CDCl_3$): δ 5.6–6.0 (2H), 5.0–5.4 (2H), 2.5–2.9 (2H), 1.8–2.2 (6H). ^{13}C NMR (100 MHz, $CDCl_3$): δ 169 (C=O), 127 (C=C), 71 (C–OR), 36 (C–C=C), 21 (CH_3). Anal. Calcd for $(C_{10}H_{12}O_4)_n$: C, 61.22; H, 6.16. Found: C, 60.45; H, 6.14. IR (neat): 1745, 1233, 1054, 1024 cm^{-1}. PXRD: amorphous (two amorphous halos centered at 10.4 and 18.9 Å.)

Preparation of the Stereoregular Benzoate Derivative of Polymer 7

A 50-mL capacity, thick-walled glass Schlenk tube fitted with an 8 mm PTFE valve was charged with a stirbar, finely powdered polymer **7** (0.103 g) and a grain of DMAP. The solids were degassed in vacuo and placed under an argon atmosphere, and suspended in pyridine (5.0 mL, 60 mmol) to give a light grey slurry. Degassed benzoic anhydride (2.09 g, 9.20 mmol) was then quickly added to the reaction vessel under a light argon flush. The flask was sealed, and the reaction mixture was stirred at 80 °C for 18 h. During that time, the suspended polymer in the initial slurry dissolved, affording a clear pale yellow solution. The mixture was then cooled to ambient temperature, and the volatiles were removed in vacuo. The remaining glassy solid was dissolved in methylene

chloride (25 mL) and washed successively with saturated aqueous NaCl (2 x 25 mL), deionized water (2 x 25 mL), saturated aqueous $NaHCO_3$ (25 mL) and deionized H_2O (2 x 25 mL). The organic phase was dried over anhydrous Na_2SO_4, concentrated to approximately 5 mL, and added dropwise to stirred hexanes (50 mL) containing a grain of BHT to precipitate the polymer. The pale yellow powder was re-precipitated by the same procedure, isolated by suction-filtration, washed with more hexanes, and dried in vacuo overnight. Yield: (97%) of the benzoate derivative of polymer **7**. ^1H NMR (400 MHz, CD_2Cl_2): δ7.2–7.9 (10H), 6.3 (2H), 5.6 (2H), 3.2 (2H). PXRD: amorphous.

References and Notes

(1) Ballard, D. G. H.; Courtis, A.; Shirley, I. M.; Taylor, S. C. *J. Chem. Soc., Chem. Commun.* **1983**, 954.

(2) Ballard, D. G. H.; Courtis, A.; Shirley, I. M.; Taylor, S. C. *Macromolecules* **1988**, *21*, 294.

(3) Internal report from ICI Chemicals and Polymers Ltd., Runcorn, U. K., based on neutron scattering analysis of PPP performed at Durham University.

(4) In describing the stereochemistry of the different repeat units possible for polymers of derivatives of compound **1**, the following labelling scheme is used: A two number prefix is used to describe the regiochemistry of the linkages (e.g., 1,4- or 1,2-linked) and a series of four italicized letters is used to indicate the absolute configuration (i.e., *R* or *S*) of the four stereocenters on the repeat units, as read from left to right with the cyclohexene ring laying flat and the cis heteroatom functionalities pointing up. See Figure 2 for an example of this labelling system.

(5) McKean, D. R.; Stille, J. K. *Macromolecules* **1987**, *20*, 1787.

(6) Frey, D. A.; Hasegawa, M.; Marvel, C. S. *J. Polym. Sci., Part A* **1963**, *1*, 2057.

(7) LeFebvre, G.; Dawans, F. *J. Polym. Sci., Part A* **1964**, *2*, 3277.

(8) Cassidy, P. E.; Marvel, C. S.; Ray, S. *J. Polym. Sci., Part A* **1965**, *3*, 1553.

(9) For a brief overview of transition-metal catalyst systems which perform stereospecific polymerization of 1,3-butadiene, see: Odian, G. *Principles of Polymerization,* 2nd ed.; John Wiley and Sons: New York, 1981; p 631. Also see reference 10.

(10) Atlas, S. M. Mark, H. F. *Cat. Rev.* **1976**, *13*, 1.

(11) Dolgoplosk, B. A.; Beilin, S. I.; Korshak, Y. V.; Makovetsky, K. L.; Tinyakova, E. I. *J. Polym. Sci., Polym. Chem. Ed.* **1973**, *11*, 2569.

(12) Dolgoplosk, B. A.; Beilin, S. I.; Korshak, Y. V.; Chernenko, G. M.; Vardanyan, L. M.; Teterina, M. P. *Eur. Polym. J.* **1973**, *9*, 895.

(13) Bevza, T. I.; Pokatilo, N. A.; Teterina, M. P.; Dolgoplosk, B. A. *Vysokomol. Soedin.* **1968**, *A10*, 207.

(14) Borge-Visse, F.; Dawans, F. *J. Polym. Sci., Polym. Chem. Ed.* **1980**, *18*, 2481.

(15) Dawans, F.; Durand, J. P. *Macromol. Synth.* **1985**, *9*, 19.

(16) Dawans, F. Belg. Patent. 719 790, 1967.

(17) Hadjiandreou, P.; Júlemont, M.; Teyssié, P. *Macromolecules* **1984**, *17*, 2455.

(18) Durand, J. P.; Dawans, F. Teyssié, P. *J. Polym. Sci., Part B* **1968**, *6*, 757.

(19) Yakovlev, V. A.; Dolgoplosk, B. A.; Tinyakova, E. I.; Yakoleva, O. N.; *Yvsokomol. Soedin.* **1969**, *A11*, 1645.

(20) Porri, L.; Aglietto, M. *Makromol. Chem.* **1976**, *177*, 1465.

(21) Monomer **4** can also be polymerized with similar nickel-π-allyl complexes containing a relatively non-basic ancillary ligand (i.e., bis[(η^3-allyl)-pentafluorophenoxynickel(II)] and bis[(η^3-allyl)pentafluorobenzoatonickel(II)]). However, $(ANiTFA)_2$ was found to be the easiest to prepare and the most active polymerization catalyst.

(22) Viscotek GPC analysis was performed by the Analytical and Physical Sciences Group at ICI Chemicals and Polymers Ltd., Runcorn, U. K.

(23) Comparative 500 MHz ^{1}H NMR spectra of **5** and radically polymerized oligomers of **4** were provided by Denis Ballard and David Haddleton at ICI Chemicals and Polymers Ltd., Runcorn, U. K.

(24) Due to the complexity in assigning the tacticities possible for polymers of derivatives of **1**, a simple labelling scheme analogous to that used to describe the tactic structures of polypropylene and polyacetaldehyde is employed. The term isotactic refers to a backbone with the same repeat unit connectivity throughout and a symmetry plane relating the stereocenters of adjacent units. The term syndiotactic refers to a backbone with an alternating connectivity and a C_2 axis relating the stereocenters of adjacent units. See: Odian, G. *Principles of Polymerization,* 2nd ed.; John Wiley and Sons: New York, 1981; pp 566–574.

(25) The conformation of cyclohexene is described as a half-chair with a similar staggered structure as that shown in Figure 20. Half-chair forms undergo rapid conformational interconversion with an activation energy for ring inversion of 5.3 kcal/mol. This activation energy is approximately one-half that for the ring inversion of cyclohexane. See: Carey, F. A.; Sundberg, R. J. *Advanced Organic Chemistry, Part A: Structure and Mechanisms,* 3rd ed.; Plenum: New York, 1990; pp 131–141.

(26) Vertogen G.; de Jeu, W. *Thermotropic Liquid Crystals, Fundamentals*; Springer–Verlag: Berlin, 1988; Chapter 1.

(27) STM samples were prepared by the following procedure: A 0.5 g/L solution of **5** in HPLC grade hexanes was prepared and filtered through a 0.2 μm porosity filter unit. A 10-μL aliquot of the filtered solution was then dropped onto the surface of a piece of freshly cleaved HOPG (0.5 x 0.5 cm), and the solvent was allowed to evaporate.

(28) Chain lengths of 400–700 Å were observed in the STM images (Figure 21) of a sample of **5** made using a monomer-to-catalyst ratio of 80:1 and a monomer

concentration of 1.5 M in chlorobenzene. M_n values of approximately 38,000 (DP = 150) were obtained from Viscotek GPC analysis of samples produced under the same reaction conditions, corresponding to a calculated chain length of approximately 540 Å from computer modeling.

(29) Although much controversy has erupted over artifacts seen by STM on HOPG such as graphite fibrils (see: Chang, H.; Bard, A. J. *Langmuir* **1991**, *7*(6), 1143), rodlike structures with the dimensions observed in our STM experiments have not been observed before. In addition, these structures were not observed later when imaging polymer **6**, a polymer not expected to have a rodlike secondary structure.

(30) Typically, structures were built up from a single energy minimized repeat unit by expanding successively to a dimer, tetramer, octamer, etc., minimizing at each step using MM2 or Dreiding force-fields in Biograf Version 2.20. The roughly minimized structures (usually 23-mers) were then finally minimized over 1000 iterations using MM2 parameters and BatchMin Version 3.1d. For **5** with the 1,4-*SSRR* isotactic structure, a final energy of 94.3 kJ/mol was obtained after 1000 iterations (6261 cpu seconds) of energy minimization using MM2 parameters.

(31) For a brief overview of features characteristic of a chain addition process, see: Cowie, J. M. G. *Polymers: Chemistry and Physics of Modern Materials,* 2nd ed.; Chapman and Hall: New York, 1991; p 81.

(32) For a review of features characteristic of a "living" polymerization process, see: Quirk, R. P.; Lee, B. *Polym. Int.* **1992**, *27*(4), 359.

(33) Ring-deuterated, (d_6)-**4** was synthesized from d_6-**1**, which is obtained from the microbial oxidation of d_6-benzene by *Pseudomonas putida.*

(34) Assignments for the IR bands used to qualitatively gauge the molecular weight of PPP were obtained from: Kovacic, P.; Jones, M. B. *Chem. Rev.* **1987**, *87*, 357. Also see reference 35.

(35) Gordon, A. J.; Ford, R. A. *The Chemist's Companion*; John Wiley and Sons: New

York, 1972; p 189.

(36) Sogah, D. Y.; Webster, O. W. *Macromolecules* **1986**, *19*, 1775.

(37) Risse, W.; Grubbs, R. H. *Macromolecules* **1989**, *22*, 1558.

(38) Chung, T. C. *Chemtech*, **1991**, *21*(8), 496, and references therein.

(39) Kim, S.; Lee, W. J. *Synth. Commun.* **1986**, *16*(6), 659.

(40) The propionate and hexanoate derivatives of **7** were synthesized by Curtis A. Hastings.

(41) In the absence of conformational flexibility as assumed for the parent polymer **5**, the cyclohexene rings of the repeat units would assume a locked half-chair conformation which is completely asymmetric. See Figure 20 and reference 25.

(42) LALLS analysis of **6** was performed by the Analytical and Physical Sciences Group at ICI Chemicals and Polymers Ltd., Runcorn, U. K.

(43) STM samples of polymer **6** were prepared according to the procedure outlined in reference 27 except that HPLC grade THF was used to dissolve the polymer instead of HPLC grade hexanes.

(44) Molecular modeling of the 1,4-*SSRR* isotactic and syndiotactic structures possible for **6** was performed on a very simple level using Biograf Version 2.20 to build the structures and MM2 force-field parameters to minimize them. Typically, the structures were built up from a single minimized repeat unit by expanding successively to a dimer, tetramer, octamer, etc., minimizing at each step using MM2 or Dreiding force-fields. The roughly minimized structures (usually 32-mers) were then finally minimized over 1000 iterations using MM2 parameters and BatchMin Version 3.1d.

CHAPTER 3

Aromatization of Poly(*p*-phenylene) Precursors: The Effects of Precursor Stereochemistry and Acid Catalysts

Introduction

In the previous chapter, we described the synthesis of a 1,4-linked, stereoregular precursor to poly(*p*-phenylene) (PPP) using transition-metal-catalyzed polymerization.[1] This stereoregular acetoxy polymer (**1**)[2] should yield 100% *para*-polyphenylene whereas a similar precursor (**2**) with irregular backbone stereochemistry made by radical polymerization[3-5] only affords polyphenylene oligomers (Figure 1).[6]

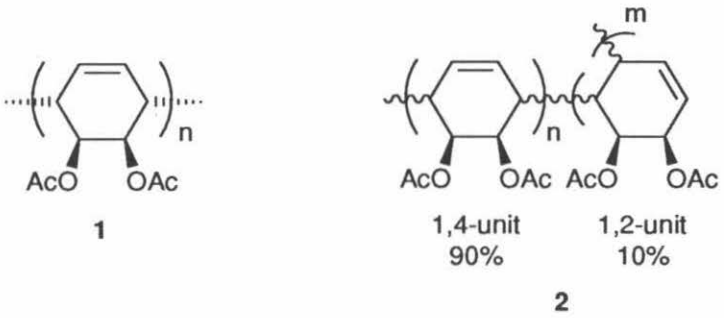

Figure 1. The 1,4-linked stereoregular PPP precursor **1** made by transition-metal-catalyzed polymerization and the irregular PPP precursor **2** made by radical polymerization.

This chapter examines the second part of the precursor process: the conversion of the intermediate polymers to the final material. In this case, the conversion of the two precursors **1** and **2** to PPP involves the thermally-induced elimination of acetic acid (Figure 2).

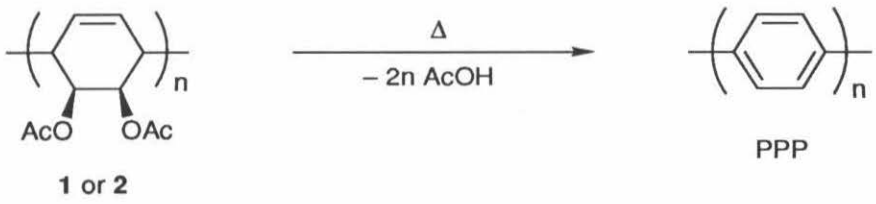

Figure 2. The thermal conversion of precursors **1** and **2** to PPP.

Since this elimination reaction is believed to proceed via a cis-six-membered ring transition state,[4] the 1,4-stereoregular structure of polymer **1** should be much better suited for the facile formation of high quality PPP (Figure 3) than the irregular structure of polymer **2**.

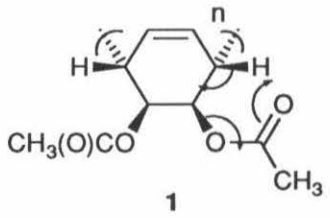

1

Figure 3. The optimum repeat unit stereochemistry for the cis-pyrolytic elimination of acetic acid.

Unfortunately, we have discovered that thermal conversion of these two PPP precursors is not a straight-forward process. Studies on the bulk pyrolysis process revealed that two competing reactions occur during the pyrolysis of the PPP precursors: (1) thermally-induced acid elimination leading to PPP formation and (2) thermal depolymerization leading to chain fracturing. The relative rates of these two reactions ultimately determine the molecular weight of the PPP formed. They depend heavily on the stereochemistry of the precursor polymers, but they can be altered by the presence of acid catalysts. Characterization of the polyphenylenes made by the acid-catalyzed and uncatalyzed bulk pyrolysis of these two PPP precursors revealed that *only* the 1,4-stereoregular precursor **1** pyrolyzed in the presence of acid catalysts affords high quality PPP. This chapter describes the effect of precursor stereochemistry and acid catalysts on the rates of these two competing pyrolysis reactions and on the quality of the PPP formed.

Results and Discussion

Preliminary pyrolysis studies of thin films of polymer **1** cast on NaCl crystals initially demonstrated that this stereoregular PPP precursor consistently affords high quality PPP films (see Chapter 2).[1] The IR spectra of the resulting PPP films typically showed an intense band at 806 cm^{-1} due to the C–H out-of-plane bending of 1,4-phenylene repeat units and only very weak bands at 760 and 697 cm^{-1} due to similar C–H bending modes in monosubstituted phenyl endgroups.[7] In contrast, pyrolysis of similarly processed films of polymer **2** gave inconsistent results.[1] The IR spectra of the resulting PPP films often exhibited repeat unit and endgroup bands with relative intensities characteristic of oligomeric material. In addition, an additional band at 789 cm^{-1} characteristic of 1,2-units was also often observed in the IR spectra.[7] However, drastically different results were obtained when the bulk pyrolysis of the two polymers was monitored by thermal gravimetric analysis (TGA).

Thermal gravimetric analysis monitors the weight loss of a material as a function of increasing temperature. Ideally, both acetoxy polymers **1** and **2** should lose 61.2% of their original weight if complete conversion to PPP occurs during the heating process. However, TGA of pressed pellets or free-flowing powders of **1** revealed that the polymer typically loses between 76 and 89% of its original weight during pyrolysis (Figure 4a). In addition, IR analysis of the TGA product revealed that only PPP oligomers are produced during bulk pyrolysis. An IR band at 1717 cm^{-1} due to residual carbonyl groups is also often observed in the bulk pyrolysis product of **1**, indicating that acid elimination is incomplete despite the fact that excessive weight loss is observed. In contrast, the radically polymerized analogue **2** loses only slightly more weight than expected for complete PPP formation (Figure 4b). IR analysis of the TGA residue of **2** confirmed that only PPP oligomers are formed. Additional TGA and IR analysis experiments with polymers **1** and **2** containing 10 wt % NaCl indicated that the presence

Figure 4. TGA profiles of (a) stereoregular PPP precursor **1** and (b) radically polymerized PPP precursor **2**.

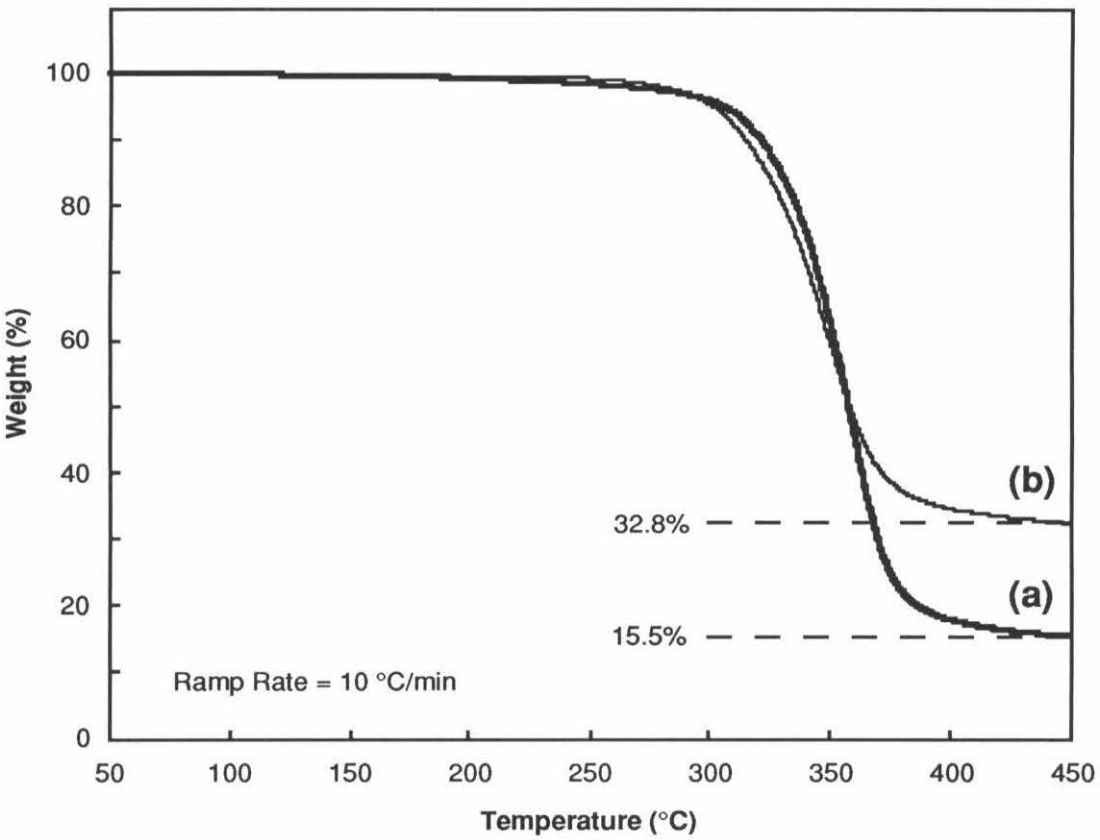
100
80
60
40
20
0
Weight (%)
50
100
150
200
250
300
350
400
450
Temperature (°C)
(b)
32.8%
(a)
15.5%
Ramp Rate = 10 °C/min

of NaCl in the polymers does not improve the excessive mass loss or the quality of the final products. Consequently, NaCl itself does not appear to be responsible for the discrepancies observed between bulk and thin film pyrolysis.[8]

These TGA and IR results indicate that other reactions besides aromatization must be occurring during the bulk pyrolysis of the two PPP precursors. In addition, the stereochemistry of the precursors has a profound effect on the nature and extent of these side reactions and the quality of the PPP produced.

(A) The Effect of Polymer Stereochemistry on the Pyrolysis Process

In order to elucidate the nature of the differences between the TGA profiles of polymers **1** and **2**, the bulk pyrolysis of the two acetoxy polymers was examined by thermal gravimetric analysis–mass spectrometry (TGA–MS).[9] TGA–MS analysis not only monitors the weight loss of a material as a function of increasing temperature, but it also identifies the volatile compounds lost during the heating process using a mass spectrograph. The TGA-MS profiles of polymers **1** and **2** are presented in Figures 5 and 6, respectively. The TGA–MS profile of polymer **1** (Figure 5) shows that the stereoregular polymer **1** loses approximately 89% of its weight upon heating to 500 °C. More importantly, it shows that the major elimination products are small aromatic compounds such as benzene and phenol rather than the desired product, acetic acid. On the other hand, the TGA–MS profile of **2** (Figure 6) shows that this radically polymerized polymer only loses approximately 65% of its original mass upon heating to 500 °C and that the major elimination product is acetic acid. The elimination products from **2** still contain a substantial fraction of benzene and phenol, but the proportion of these aromatic side-products is significantly smaller than in the case of **1**.

From these TGA–MS results, two things can be inferred: First, the pyrolysis of the two PPP precursors does not involve just a single process. Instead, there appear to

Figure 5. TGA–MS profile of polymer **1**.

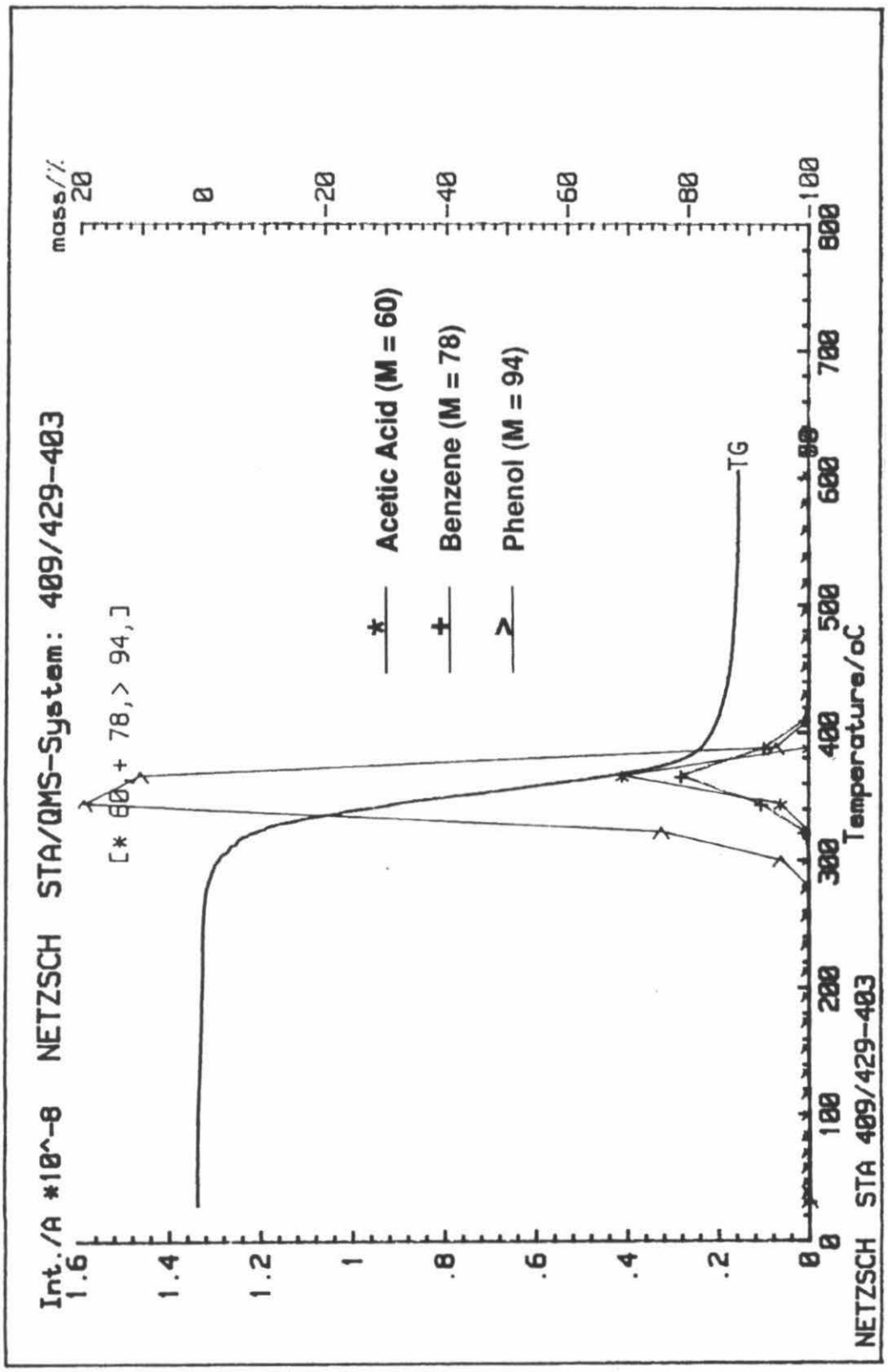
Int./A *10^-8
NETZSCH STA/QMS-System: 409/429-403
mass/%
Acetic Acid (M = 60)
Benzene (M = 78)
Phenol (M = 94)
TG
Temperature/oC
NETZSCH STA 409/429-403

Figure 6. TGA–MS profile of polymer **2**.

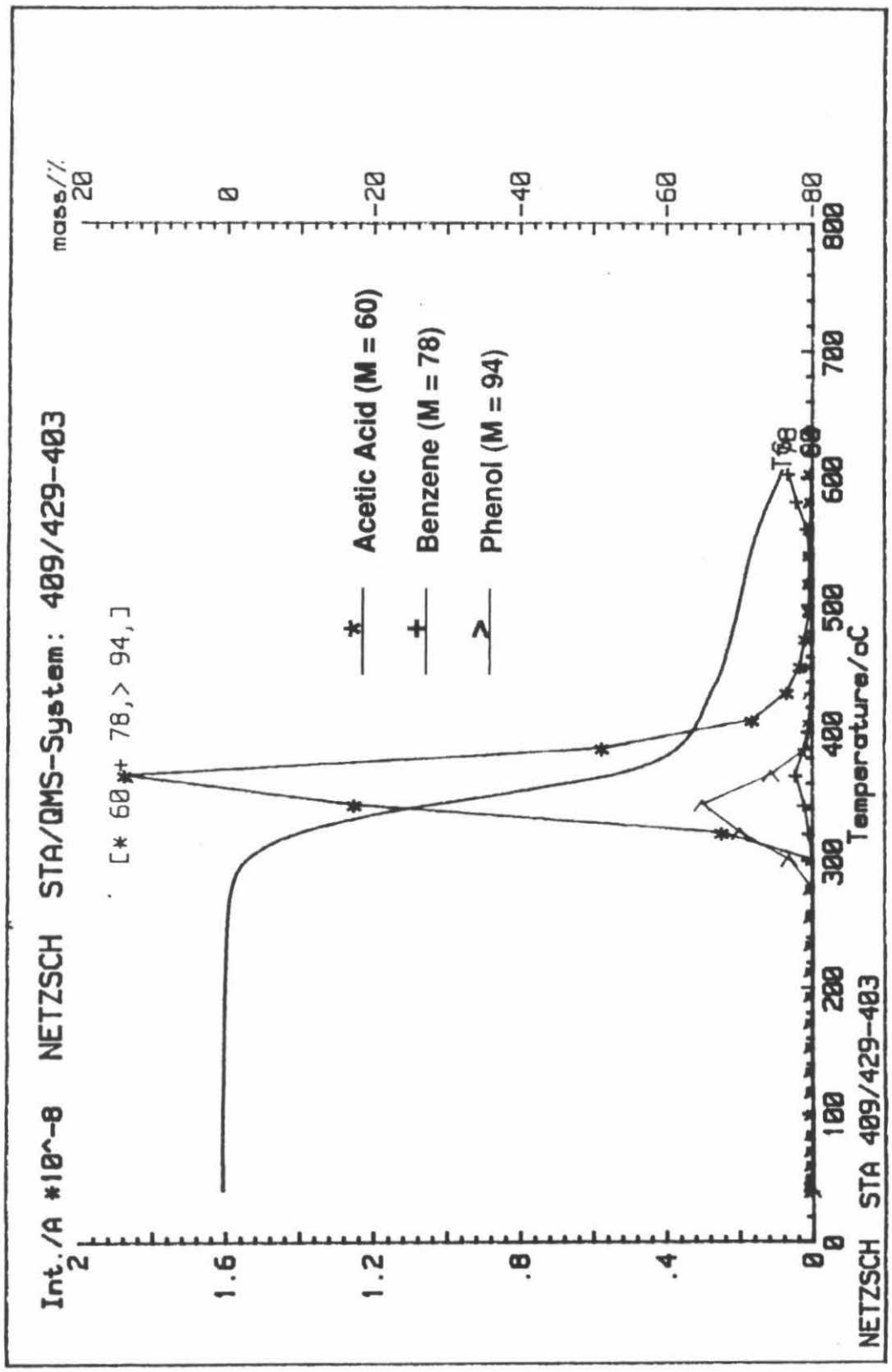
Int./A *10^-8
NETZSCH STA/QMS-System: 409/429-403
mass/%
[* 60,+ 78,> 94,]
Acetic Acid (M = 60)
Benzene (M = 78)
Phenol (M = 94)
Temperature/oC
NETZSCH STA 409/429-403

be two types of competing reactions occurring during pyrolysis: (1) thermal depolymerization resulting in backbone fracturing and the evolution of small aromatic molecules, and (2) thermally-induced acid elimination resulting in PPP formation and the evolution of acetic acid (Figure 7).

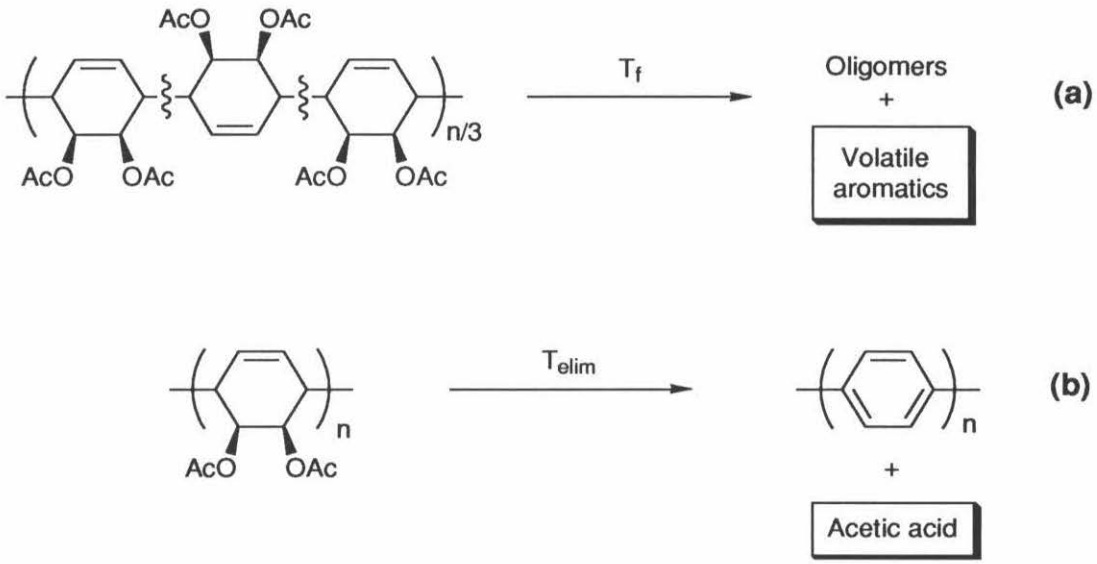

Figure 7. The two competing processes in the pyrolysis of **1** and **2**: (a) thermal depolymerization; (b) aromatization (thermally-induced acid elimination). The boxed items are the compounds detected by mass spectrometry in TGA–MS analysis.

Second and most important, the relative rates of these two competing reactions are highly dependent upon the stereochemistry of the polymers. For the completely 1,4-linked stereoregular polymer **1**, the rate of depolymerization is much greater than the rate of acid elimination during pyrolysis. For polymer **2** with its random backbone stereochemistry and 10% 1,2-units, the reverse is true. In other words, by virtue of its stereoregular structure, the onset temperature for backbone fracturing (T_f)[10] for **1** is lower than the onset temperature for acetic acid elimination (T_{elim}). Consequently, as **1** is heated to higher temperatures, it undergoes a greater amount of backbone fracturing relative to PPP formation. In contrast, the irregular backbone stereochemistry of **2** apparently elevates T_f slightly above T_{elim} so that aromatization is the dominant process as **2** is heated to higher

temperatures. However, significant backbone fracturing still occurs as indicated by the presence of benzene and phenol in the MS profile (Figure 6).

Although we have managed to synthesize a highly 1,4-linked, stereoregular PPP precursor with the optimum stereochemistry for cis-elimination, the inherent thermal instability of the stereoregular backbone results in depolymerization before substantial aromatization can occur.

(B) The Effect of Acids on the Pyrolysis Process

In order to produce high quality bulk PPP from polymer **1**, aromatization catalysts were employed to lower T_{elim} below T_f by selectively accelerating the acid elimination reaction. Inorganic Lewis acids such as $ZnCl_2$ were found to catalyze the aromatization process. $ZnCl_2$ was a trace contaminant in early batches of **1** made using the $ZnCl_2$/acetyl chloride process.[11] These samples containing approximately 1.6 wt % $ZnCl_2$ exhibited TGA weight losses consistent with complete conversion to PPP. The effect of small quantities of $ZnCl_2$ on the TGA-MS profile of polymer **1** is quite pronounced. For example, the addition of 2 wt % $ZnCl_2$ to a sample of **1** made by a Zn-free route[12] has a dramatic effect on both the mass loss and the composition of the volatiles evolved during pyrolysis (Figure 8). Instead of losing 89% of its weight upon pyrolysis as in the case of the pristine material, the polymer containing $ZnCl_2$ only loses approximately 60% of its original weight (cf. Figures 5 and 8). This weight loss value is close to that expected for complete conversion to PPP (accounting for the amount of $ZnCl_2$ in the mixture). In addition, the only elimination product generated in the presence of $ZnCl_2$ is acetic acid, thus indicating that only aromatization is occurring. As can be seen from the MS profile in Figure 8, benzene and phenol are barely detectable during the pyrolysis. Apparently, $ZnCl_2$ selectively accelerates the acid elimination (aromatization) reaction and lowers its onset temperature below that of thermal depolymerization. This

Figure 8. TGA–MS profile of polymer **1** containing 2 wt % $ZnCl_2$.

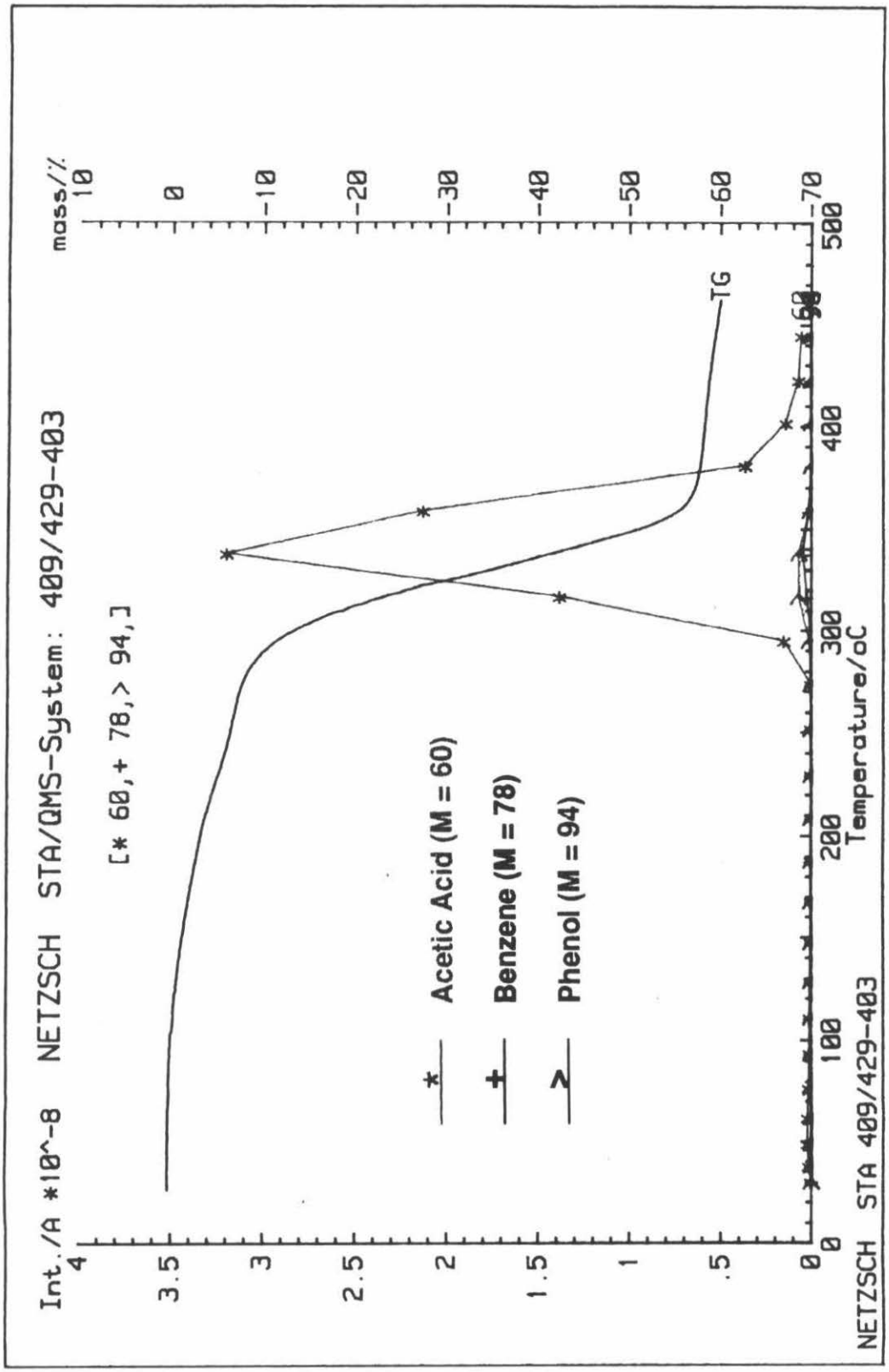
Int./A *10^-8
NETZSCH STA/QMS-System: 409/429-403
[* 60,+ 78,> 94,]
mass/%
TG
Acetic Acid (M = 60)
Benzene (M = 78)
Phenol (M = 94)
Temperature/oC
NETZSCH STA 409/429-403

temperature reduction effect is small with only 2 wt % $ZnCl_2$ in the polymer (cf. Figures 5 and 8), but it becomes more pronounced with increasing wt % of $ZnCl_2$ (Figure 9).

Zinc chloride also catalyzes the aromatization of polymer **2**. As can be seen from Figure 10, the addition of 10 wt % $ZnCl_2$ to polymer **2** lowers the aromatization temperature and stabilizes the weight loss of the material during pyrolysis as in the case of polymer **1**. This catalytic effect on both PPP precursors is also exhibited by the other zinc halides (i.e., $ZnBr_2$ and ZnI_2). Unfortunately, the one drawback in using the zinc halides as aromatization catalysts is the fact that these compounds are difficult, if not impossible, to remove from the insoluble PPP matrix even by repeated washing.[13]

Organic Brønsted acids were also found to catalyze the aromatization of both polymers **1** and **2**. Recently, Wilson and co-workers discovered that nonvolatile, strong Brønsted acids such as 3,4-dichlorobenzenesulfonic acid (DCBSA) and *p*-toluenesulfonic acid are able to reduce the aromatization temperature and improve the mass loss during the pyrolysis of the radically polymerized PPP precursor **2** (Figure 11).[14] However, they did not observe any difference in the IR spectra of the thin PPP films made by the catalyzed and uncatalyzed pyrolysis of **2**. When the same organic acids were added to the stereoregular PPP precursor **1**, a similar catalytic effect was also observed. As can be seen from the TGA profiles in Figure 12, the addition of 5 wt % DCBSA to **1** lowers the T_{elim} of the polymer from approximately 330 °C, where a combination of depolymerization and acid elimination simultaneously occurs in the pristine material, to approximately 180 °C. This temperature regime is well below the temperature where volatile aromatics are evolved (Figure 5). The observed weight loss (65%) during the pyrolysis of **1** with 5 wt % DCBSA approaches the value expected for complete conversion of **1** to PPP, assuming that all of the organic acid catalyst is also boiled away during the pyrolysis. Unfortunately, the addition of larger amounts of DCBSA does not lower the T_{elim} of either PPP precursor much below 170 °C. However, there are two advantages in using organic Brønsted acids over inorganic Lewis acids such as $ZnCl_2$:

Figure 9. A plot of onset temperature of acid elimination (T_{elim}) as a function of the wt % of $ZnCl_2$ added to polymer **1**.

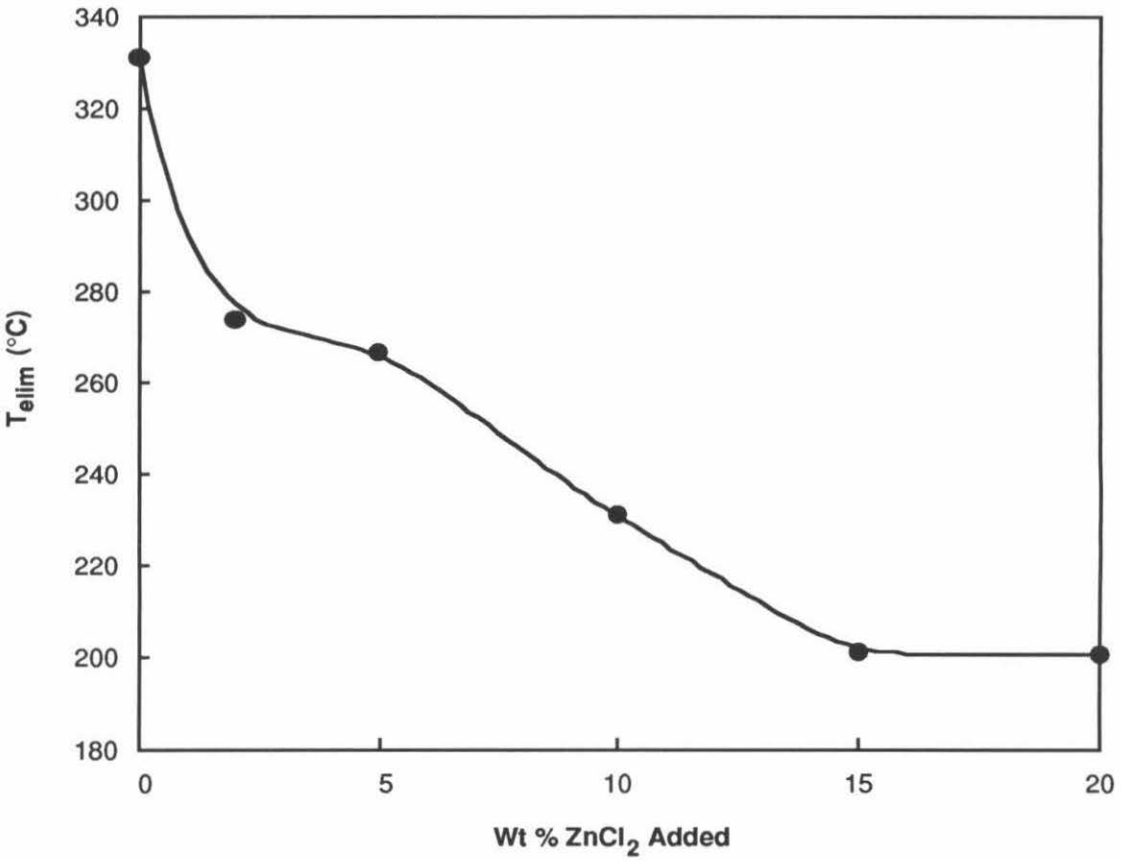
340
320
300
280
260
240
220
200
180
T_{elim} (°C)
0
5
10
15
20
Wt % $ZnCl_2$ Added

Figure 10. TGA profiles of (a) pristine polymer **2** and (b) polymer **2** containing 10 wt % $ZnCl_2$.

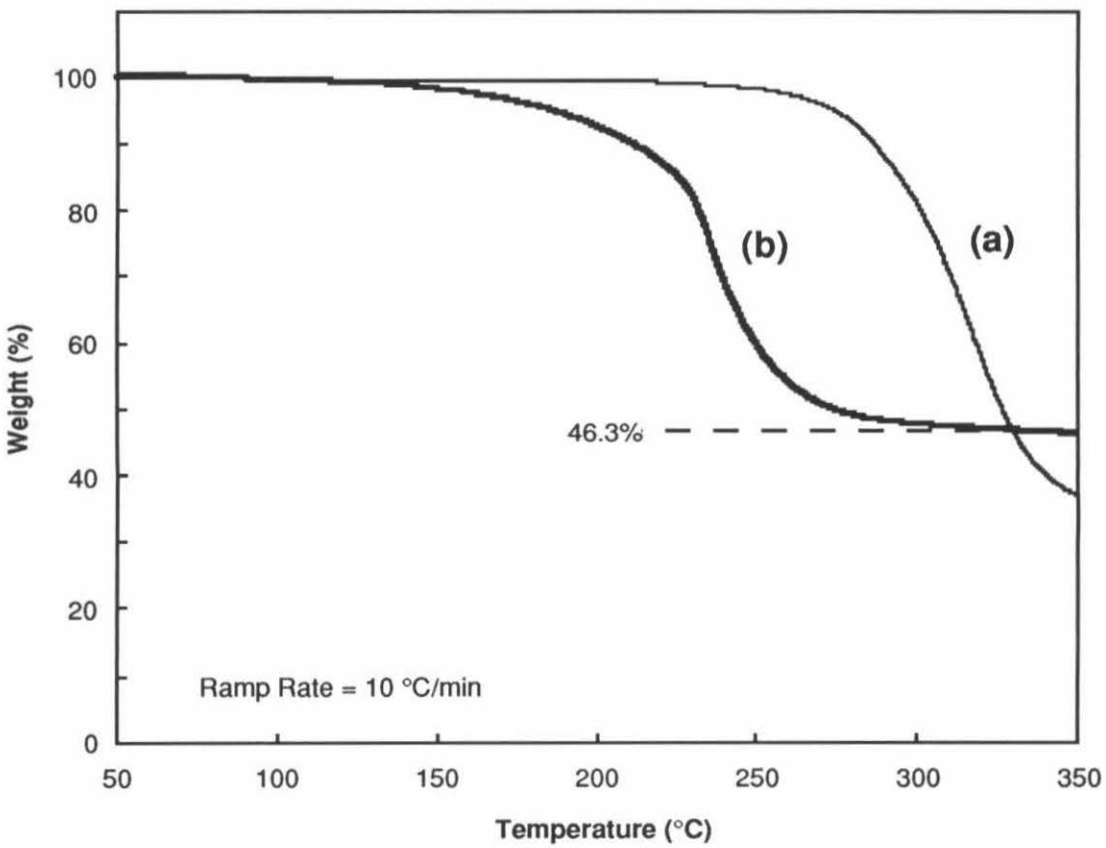
100
80
60
40
20
0
Weight (%)
(b)
(a)
46.3%
Ramp Rate = 10 °C/min
50
100
150
200
250
300
350
Temperature (°C)

Figure 11. TGA profiles of (a) pristine polymer **2** and (b) polymer **2** containing 5 wt % DCBSA.

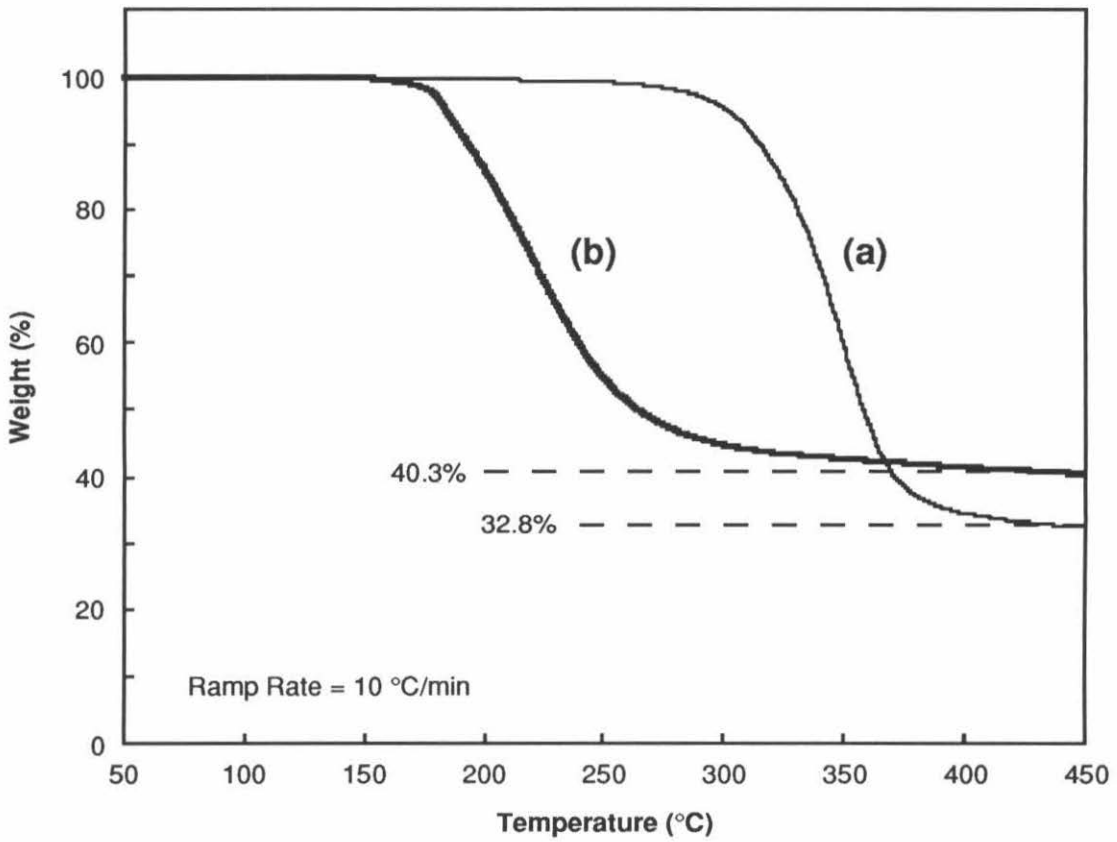
100
80
60
40
20
0
Weight (%)
(b)
(a)
40.3%
32.8%
Ramp Rate = 10 °C/min
50
100
150
200
250
300
350
400
450
Temperature (°C)

Figure 12. TGA profiles of (a) pristine polymer **1** and (b) polymer **1** containing 5 wt % DCBSA.

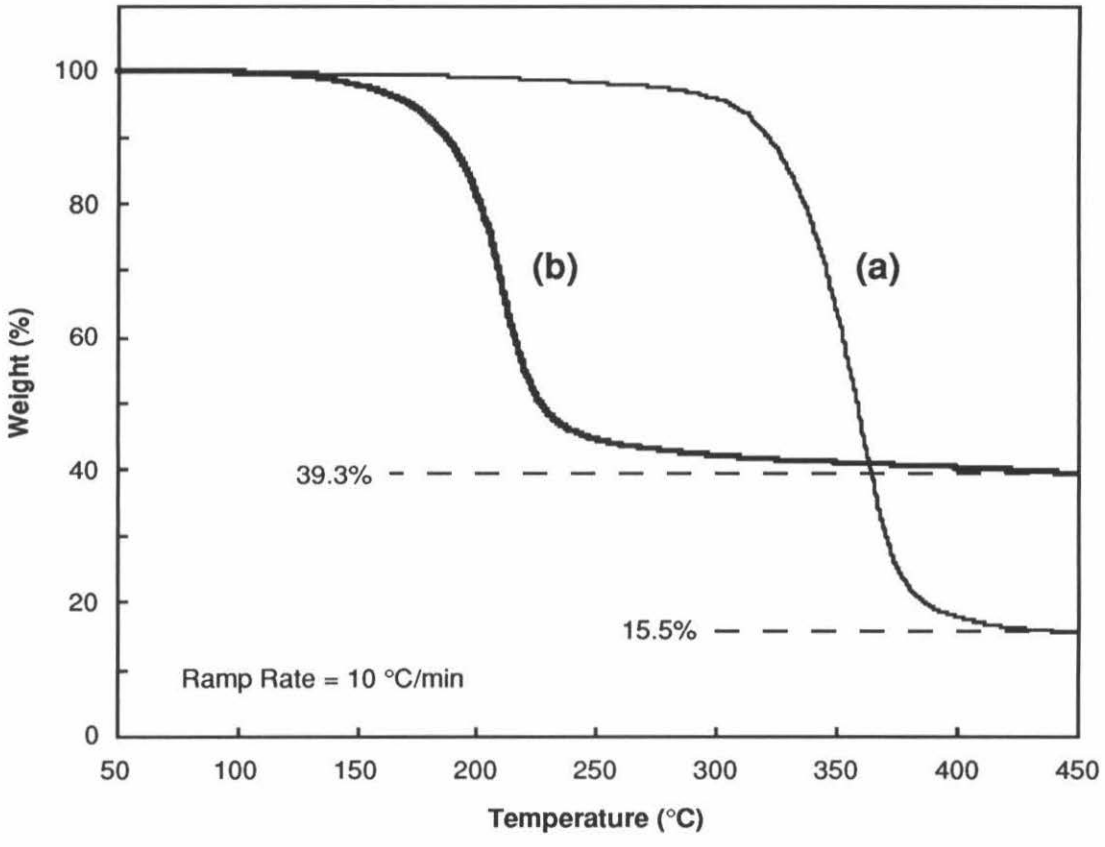
100
80
60
40
20
0
Weight (%)
(b)
(a)
39.3%
15.5%
Ramp Rate = 10 °C/min
50
100
150
200
250
300
350
400
450
Temperature (°C)

(1) The catalytic effect is more pronounced with the organic acids than $ZnCl_2$ on both a per weight and a per mole basis (see Figures 9 and 12b).[15] (2) The organic acids can be easily removed from the final product by simply heating the resulting PPP to higher temperatures.[13,16]

It should be noted that Lewis acids and Brønsted acids also catalyze the aromatization of some of the other derivatives of polymers **1** and **2** mentioned in Chapter 2.[17,18] However, the acid-catalyzed aromatization of the acetoxy polymers **1** and **2** provides the most efficient route to PPP in terms of overall mass loss upon conversion to polyphenylene[17] and in terms of the quality of the final product.[18]

(C) The Effect of Precursor Stereochemistry and Acid Catalysts on the Quality of the Poly(*p*-phenylene) Formed.

IR Analysis

IR analysis is generally used to determine the structure and molecular weight of PPP samples.[19-22] Typically, the regiochemistry and the molecular weight of polyphenylene chains can be qualitatively determined by comparing the relative intensities of two sets of bands in the IR spectrum of the material: (1) a band at approximately 810 cm^{-1}, which is due to the C–H out-of-plane bending of the 1,4-substituted benzene repeat units, and (2) two bands at approximately 760 and 697 cm^{-1}, which are due to the C–H out-of-plane bending modes of the monosubstituted benzene endgroup units of the polymer (Figure 13).

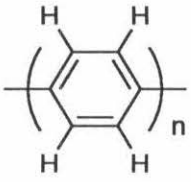

PPP repeat unit
(C–H) $_{o\text{-}o\text{-}p}$ bend: ~810 cm^{-1}

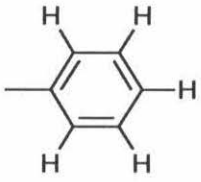

PPP endgroup unit
(C–H)$_{o\text{-}o\text{-}p}$ bends: ~760, 697 cm^{-1}

Figure 13. The repeat and endgroup units of PPP: Characteristic IR bands.

For high molecular weight, completely 1,4-linked polyphenylene chains, the intensity of the 810 cm^{-1} band should be much greater than the two endgroup bands. In addition, as the number of consecutive 1,4-linked phenylene units increases, the position of the IR band due to the PPP repeat units shifts to lower wavenumbers. These two trends can be seen in the IR spectra of a series of three *p*-oligophenyls (Figure 14).

Although initial TGA and TGA–MS studies indicated that Brønsted and Lewis acids catalyze the thermally-induced acid elimination of both acetoxy polymers **1** and **2**, IR analysis of the products revealed that high molecular weight, completely 1,4-polyphenylene is formed *only* by the acid-catalyzed aromatization of the completely 1,4-linked precursor **1**. As can be seen from Figures 15a and 15b, the IR spectra of the PPP samples made from the DCBSA- and $ZnCl_2$-catalyzed aromatization of **1** are dominated by an intense band at 806 cm^{-1}. The two endgroup bands at 760 and 696 cm^{-1} are extremely small in comparison. In sharp contrast, the IR spectra of the polyphenylene samples prepared from polymer **2** using the same catalysts exhibit repeat unit and endgroup bands with relative intensities characteristic of only very short runs of 1,4-phenylene units (Figures 16a and 16b). Furthermore, they both exhibit an additional IR band at 789 cm^{-1} which is characteristic of the C–H bending of 1,2-linked phenylene units.[7] Apparently, the irregular stereochemistry of polymer **2** results in the formation of substantial amounts of 1,2-phenylene units when aromatized in the presence of the acid

Figure 14. The IR spectra (KBr mull) of (a) *p*-terphenyl, (b) *p*-quaterphenyl, and (c) *p*-sexiphenyl.

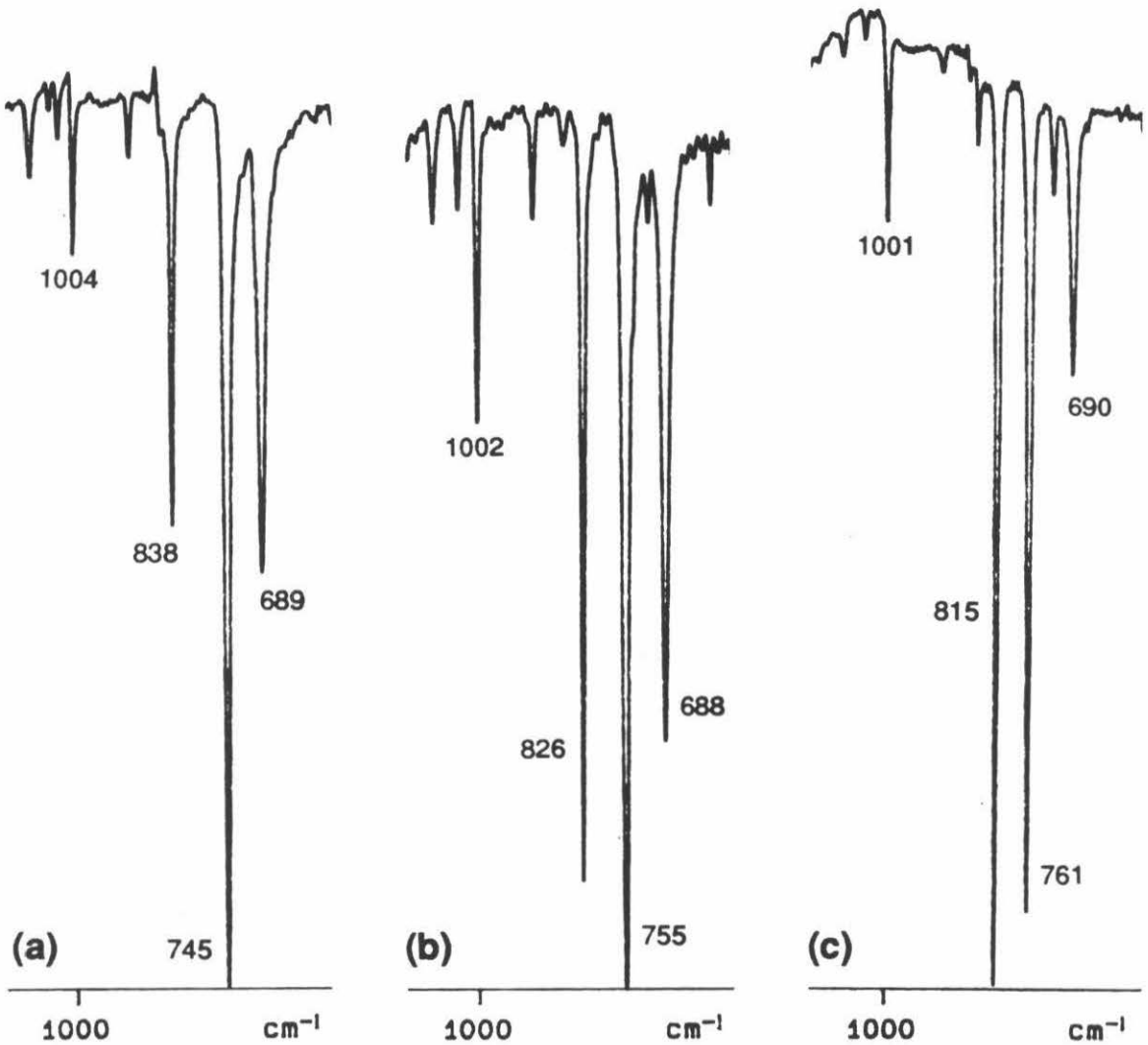
1004
838
689
745
(a)
1000
cm⁻¹
1002
826
755
688
(b)
1000
cm⁻¹
1001
690
815
761
(c)
1000
cm⁻¹

Figure 15. The IR spectra (KBr mull) of the polyphenylene samples made from the bulk pyrolysis of polymer **1** containing (a) 5 wt % DCBSA, (b) 10 wt % $ZnCl_2$, and (c) no aromatization catalysts.

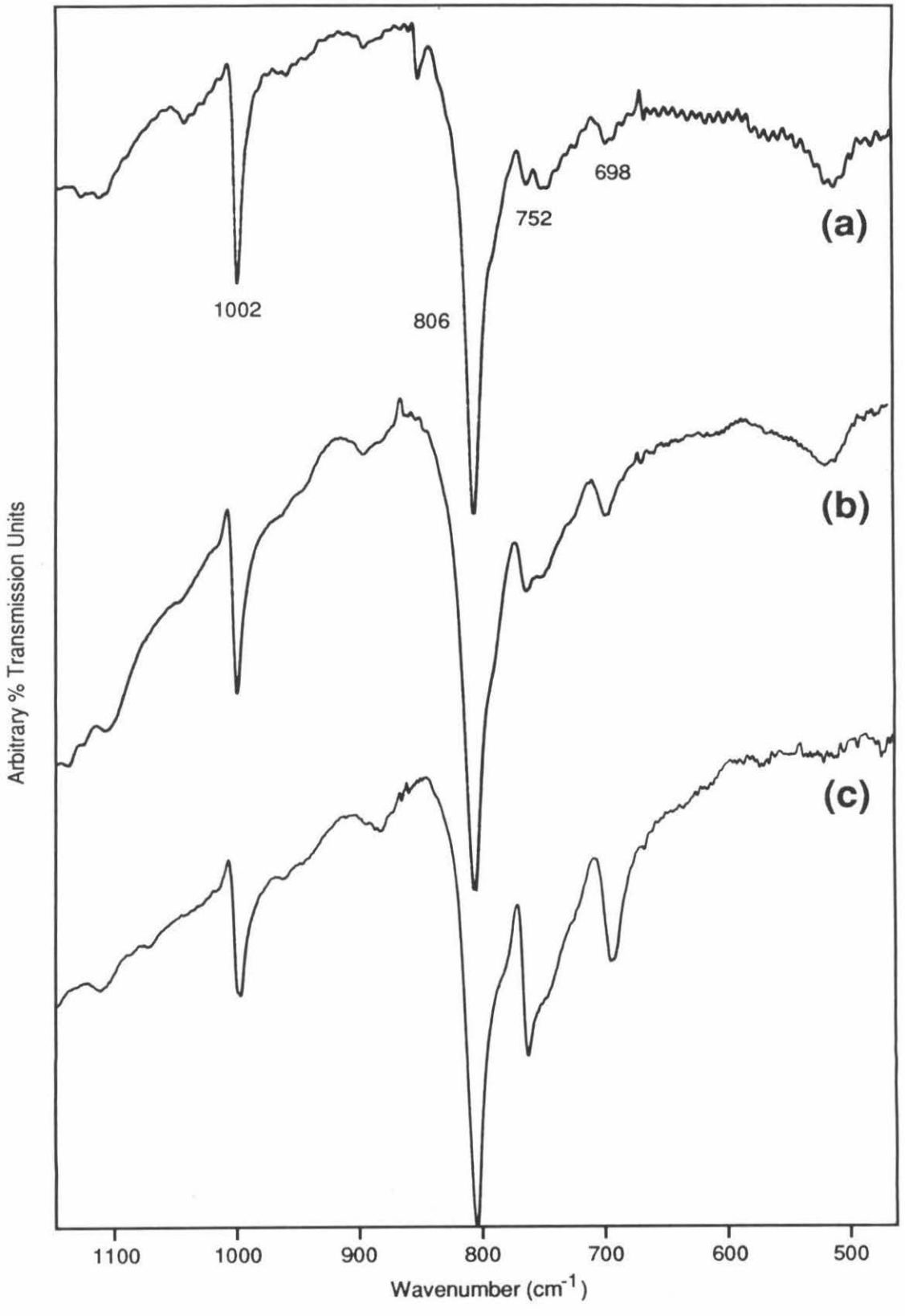
1002
806
752
698
(a)
(b)
(c)
Arbitrary % Transmission Units
1100
1000
900
800
700
600
500
Wavenumber (cm-1)

Figure 16. The IR spectra (KBr mull) of the polyphenylene samples made from the bulk pyrolysis of polymer **2** containing (a) 5 wt % DCBSA, (b) 10 wt % $ZnCl_2$, and (c) no aromatization catalysts.

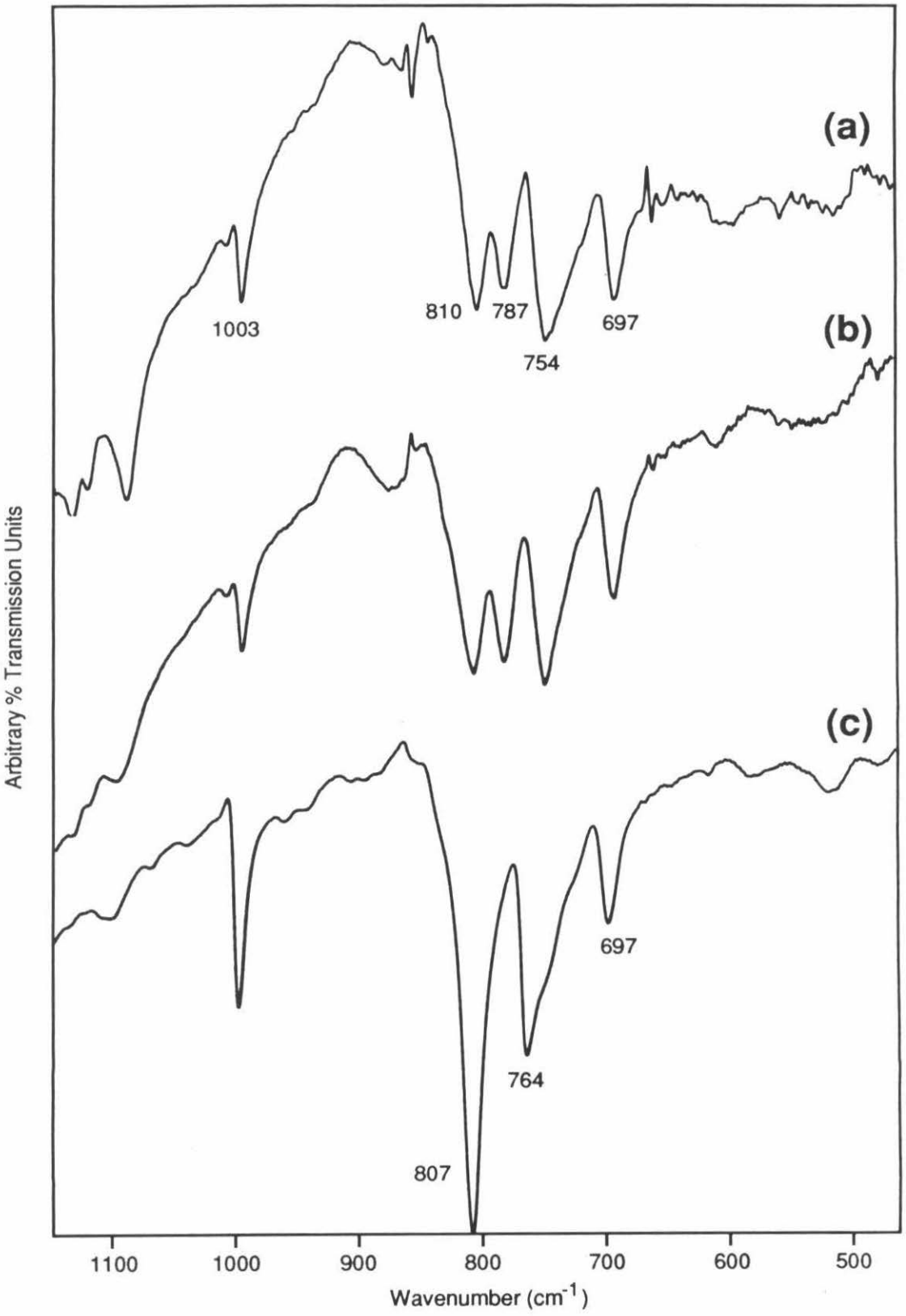
(a)
1003
810
787
754
697
(b)
(c)
807
764
697
Arbitrary % Transmission Units
1100
1000
900
800
700
600
500
Wavenumber (cm-1)

catalysts. On the other hand, the IR spectra of the PPP samples produced from the bulk pyrolysis of the pristine polymers **1** and **2** indicate that they are only oligomeric in nature and contain no 1,2-units (Figures 15c and 16c). Judging by the relative intensities of the repeat unit and endgroup bands, the molecular weights of these PPP oligomers are only slightly higher than *p*-sexiphenyl (Figure 14c). These observations are consistent with the earlier TGA–MS results obtained on the pristine precursors. Although acids catalyze the thermal aromatization of both precursor polymers, it is the regiochemical structure of the precursor that determines the structure of the polyphenylene formed.

It is interesting to note that in earlier studies on the organic acid-catalyzed pyrolysis of **2**, Wilson et al. found that the acid-catalyzed product was not significantly different by IR analysis from material obtained by the pyrolysis of the pristine polymer when thin films were compared.[14] However, our current IR studies indicate that the polyphenylene samples produced by the acid-catalyzed bulk pyrolysis of **2** are structurally very different from the samples made using the pristine polymer. These differences suggest that in thin films where the surface area-to-mass ratio is very high, even the relatively nonvolatile organic acids used sublime away before reaching the temperatures required for catalyzed acid elimination. In pressed pellets or powders where the surface area to mass ratio is much smaller, the organic acid is better confined and unable to sublime away during the heating up cycle. Consequently, organic acids apparently have no effect when used in the pyrolysis of thin films. This assumption is supported by the fact that the IR spectra of thin polyphenylene films obtained from **2** with and without 5 wt % DCBSA were found to be virtually identical, whereas a film made from **2** containing $ZnCl_2$ (which is extremely nonvolatile (bp = 732 °C)) exhibits the same four band pattern in the 650–810 cm^{-1} region of the IR spectrum as samples made from the acid-catalyzed bulk pyrolysis of **2** (cf. Figures 17a, b, c).

Figure 17. The IR spectra of polyphenylene films on NaCl crystals made from the pyrolysis of thin films of **2** containing (a) 5 wt % DCBSA, (b) 10 wt % $ZnCl_2$, and (c) no aromatization catalysts.

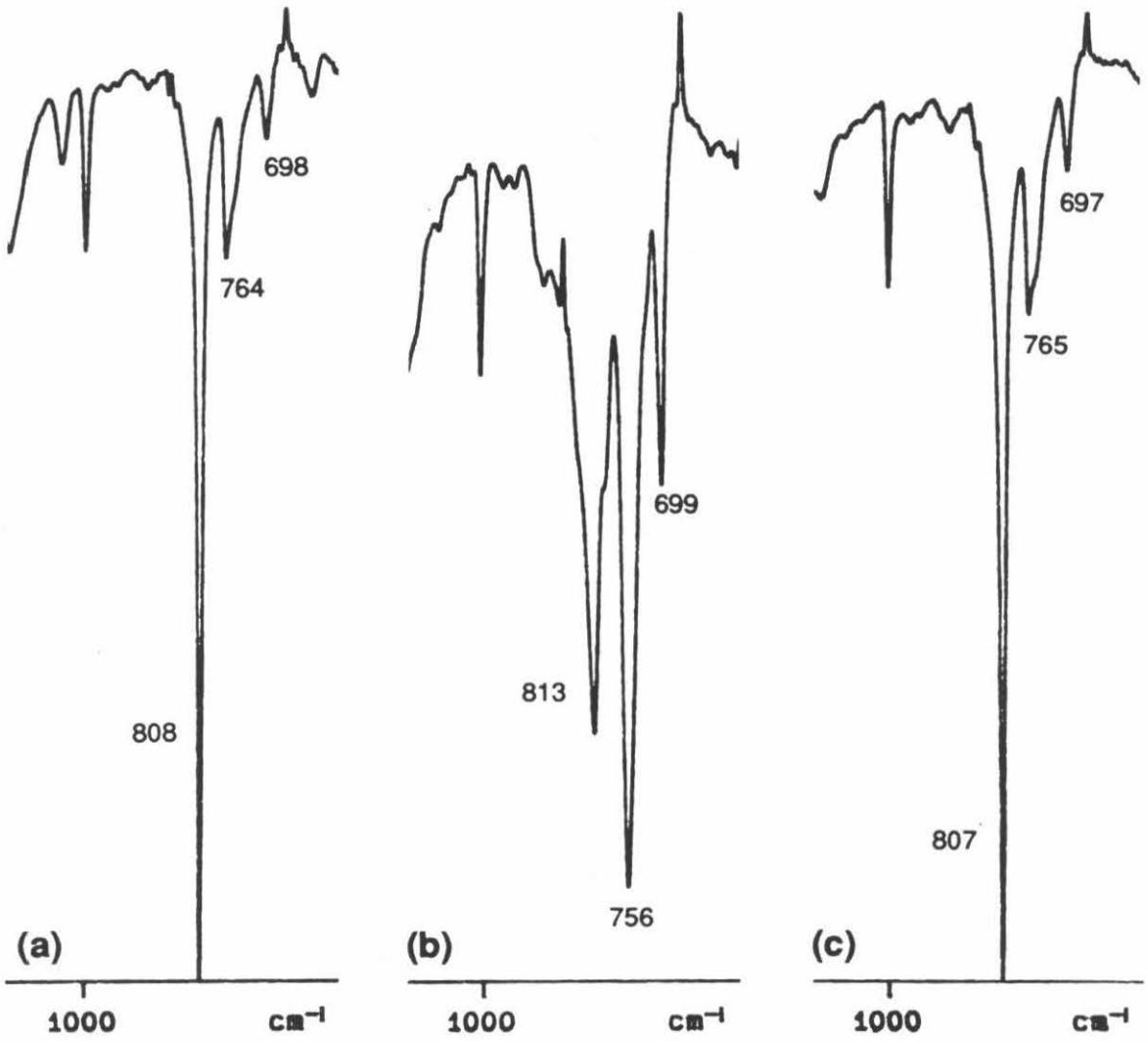
698
764
808
(a)
1000
cm⁻¹
699
813
756
(b)
1000
cm⁻¹
697
765
807
(c)
1000
cm⁻¹

Morphology

The acid catalysts used to catalyze the aromatization of **1** and **2** also have a dramatic effect on the morphology of the final products. When pressed pellets of **1** and **2** containing DCBSA or $ZnCl_2$ are pyrolyzed, both the high quality PPP made from **1** and the irregular polyphenylene made from **2** are formed as resilient black foams (Figures 18a and 19a), which are completely amorphous by powder X-ray diffraction (PXRD) analysis. The foams have roughly the same shape as the original pressed pellets, but their dimensions are larger due to added interior void volume produced by the rapid evolution of acetic acid. Often, the interior of these polyphenylene foams are filled with lustrous, flaky fibers (Figures 18a,b). In contrast, when pressed pellets of the pristine precursors are pyrolyzed, the resulting PPP oligomers are obtained as brittle orange–brown films which are semicrystalline by PXRD analysis (Figures 20a and 20b). Apparently, without acid catalysts to accelerate the aromatization reaction, the pristine precursors flow and lose their original shape as they undergo a combination of acid elimination and depolymerization.

To our knowledge, the high quality PPP samples made by the acid-catalyzed aromatization of **1** are the only examples of completely amorphous PPP. PPP made by previous synthetic routes have been almost always semicrystalline.[18-21] Because of this difference in morphology, the molecular weight of the PPP samples made by the acid-catalyzed aromatization of **1** may actually be substantially higher than that of previous PPP samples if compared by IR analysis. The intensities of the IR bands used for determining the relative amount of phenylene endgroups actually shrink relative to the intensity of the repeat unit band when semicrystalline PPP samples are annealed to higher crystalline perfection.[19,23] Since higher crystallinity favors weaker endgroup bands, the chain lengths of our amorphous, high quality PPP samples may actually be underestimated by IR analysis compared to semicrystalline materials.

Figure 18. Scanning electron microscope photographs of the cross-section of a high quality PPP foam made from the bulk pyrolysis of a pressed powder pellet of **1** containing 5 wt % DCBSA: (a) low magnification; (b) high magnification.

(a)

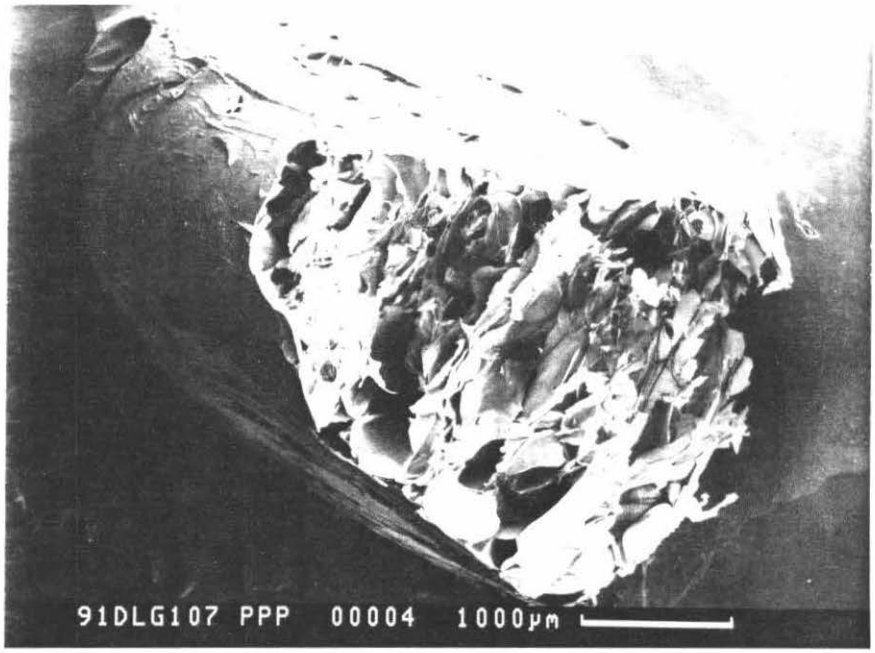

(b)

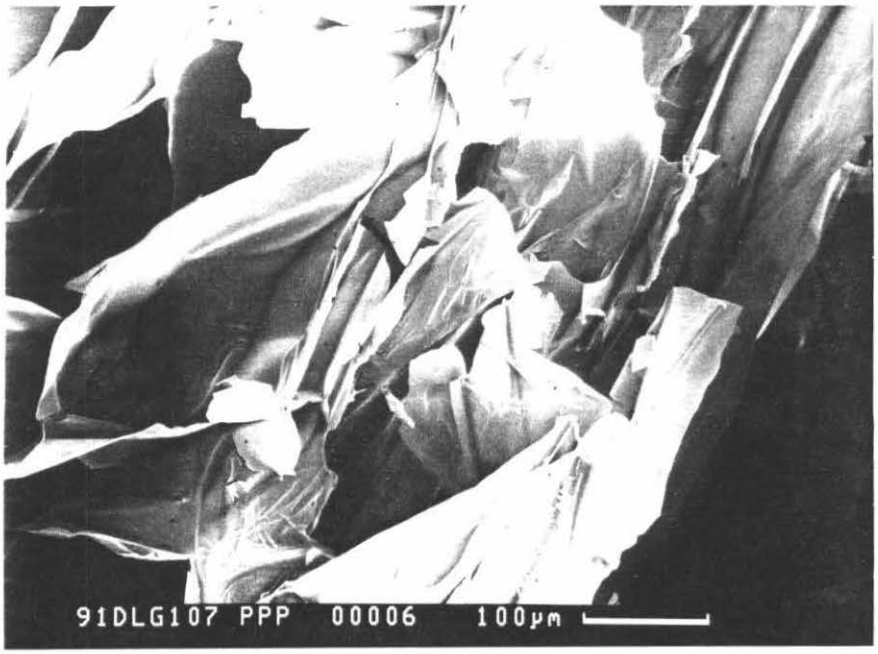

Figure 19. Scanning electron microscope photographs of the cross-section of a high quality PPP foam made from the bulk pyrolysis of a pressed powder pellet of **1** containing 10 wt % $ZnCl_2$ (a) low magnification; (b) high magnification.

(a)

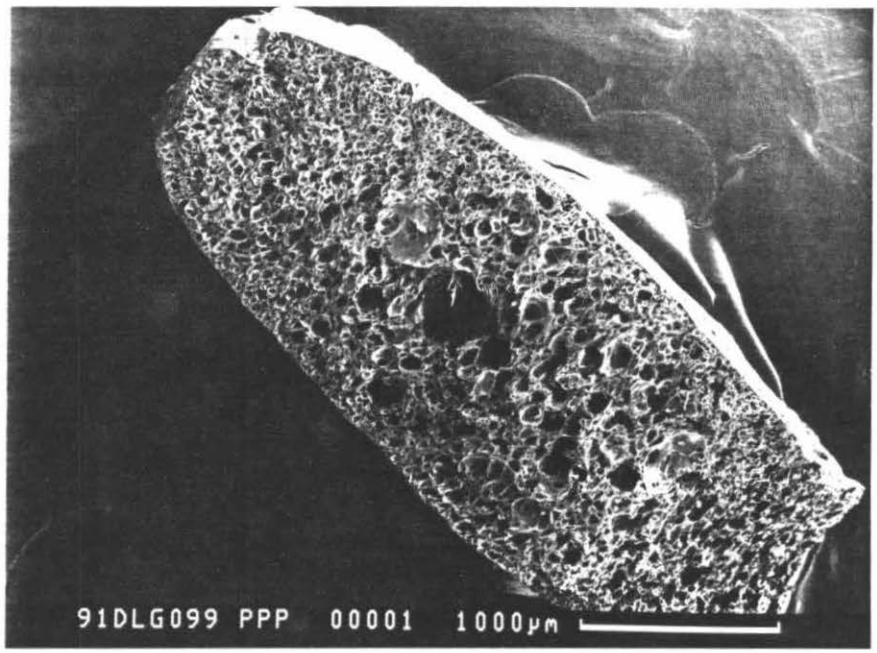

(b)

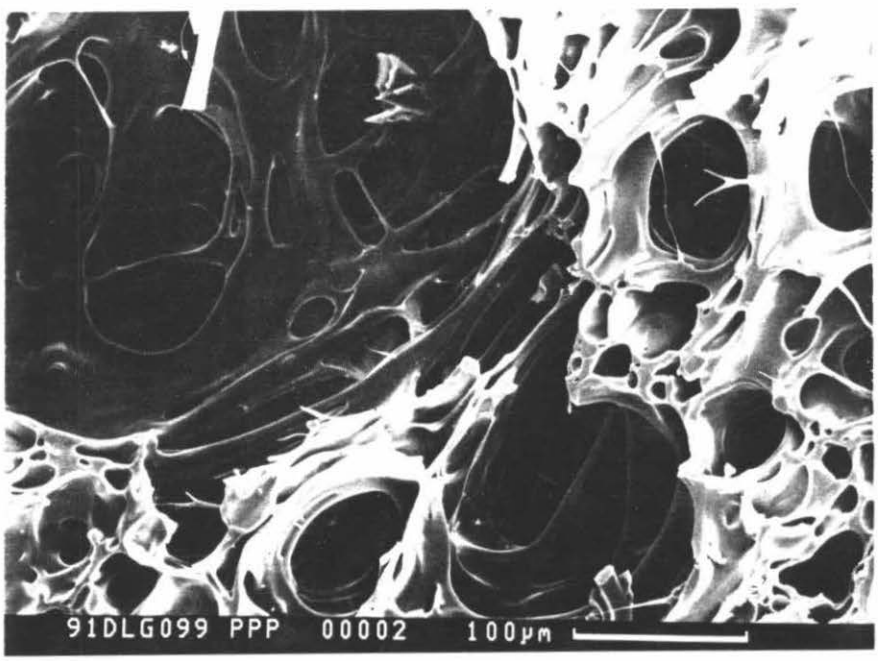

Figure 20a. PXRD profile of the PPP oligomers obtained from the uncatalyzed bulk pyrolysis of polymer **1**. The peaks at 4.149 and 3.747 Å are diffractometer artifacts. Assignments for the observed reflections can be found in reference 4.

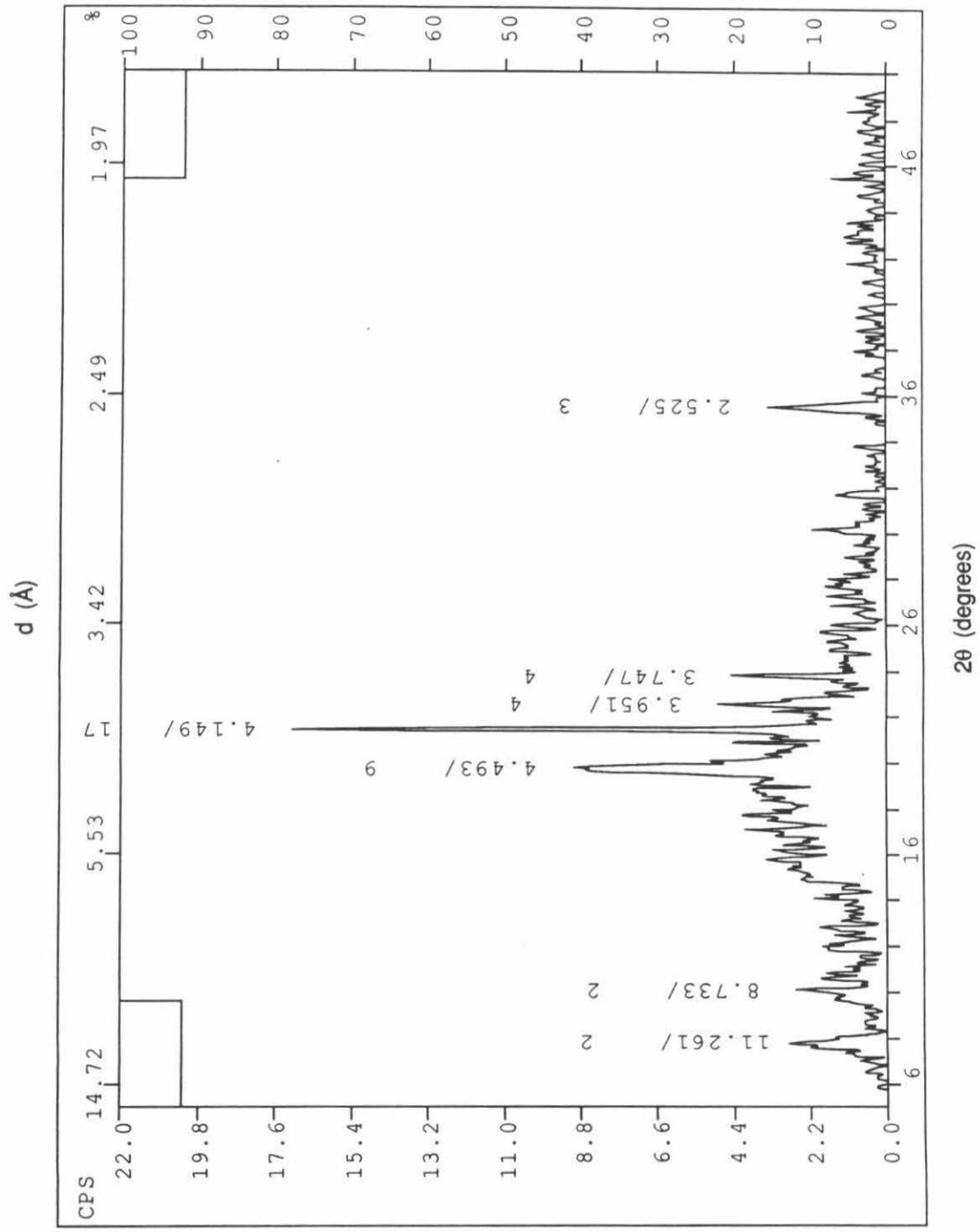
CPS
14.72
5.53
3.42
2.49
1.97
d (Å)
%
22.0
19.8
17.6
15.4
13.2
11.0
8.8
6.6
4.4
2.2
0.0
100
90
80
70
60
50
40
30
20
10
0
6
16
26
36
46
2θ (degrees)
11.261/ 2
8.733/ 2
4.493/ 9
4.149/ 17
3.951/ 4
3.747/ 4
2.525/ 3

Figure 20a. PXRD profile of the PPP oligomers obtained from the uncatalyzed bulk pyrolysis of polymer **2**. Assignments for the observed reflections can be found in reference 4.

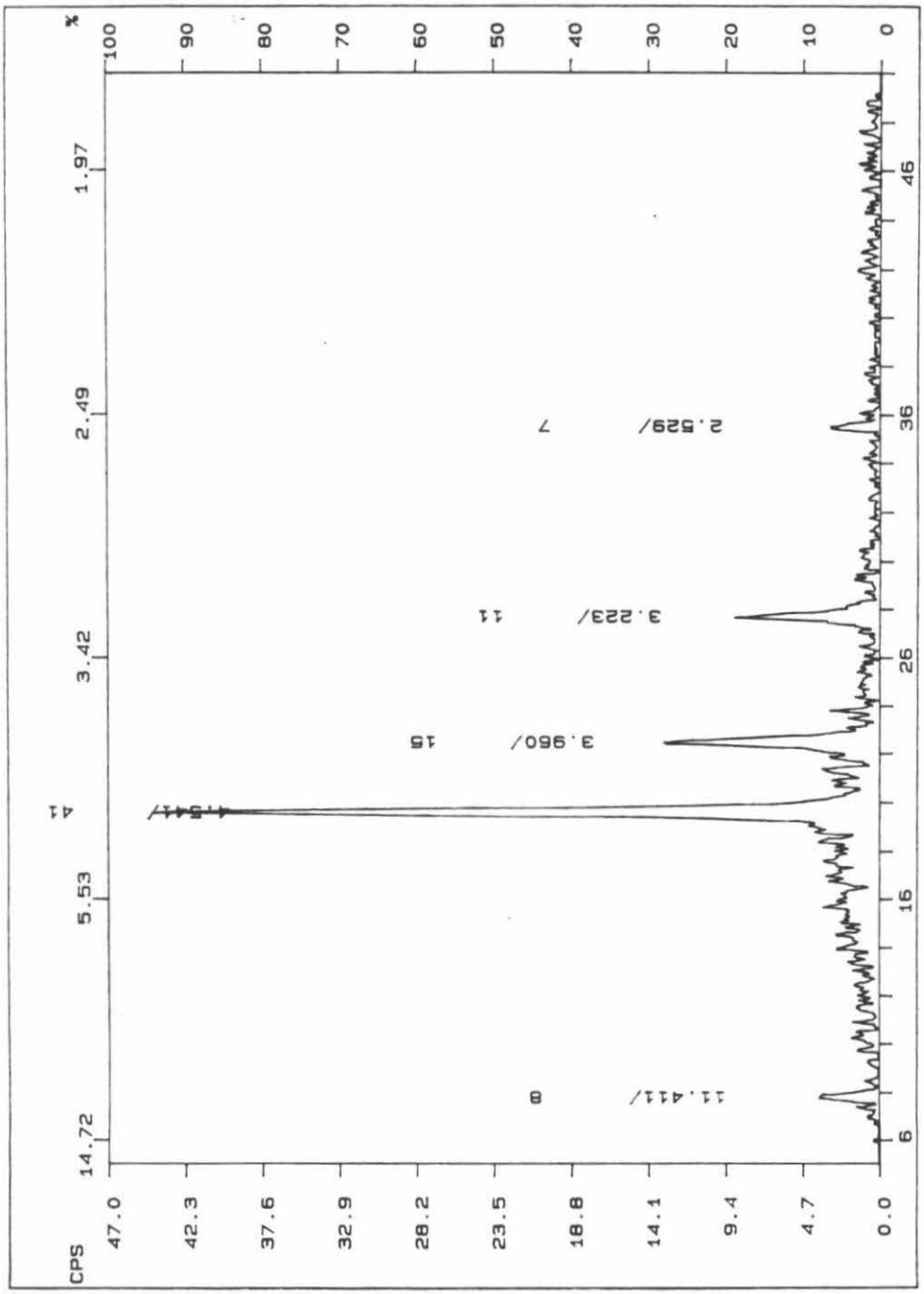
d (Å)
2θ (degrees)
CPS
%
14.72
5.53
3.42
2.49
1.97
47.0
42.3
37.6
32.9
28.2
23.5
18.8
14.1
9.4
4.7
0.0
100
90
80
70
60
50
40
30
20
10
0
6
16
26
36
46
11.412/
3.960/
3.223/
2.529/

^{13}C CPMAS Solid-State NMR Analysis

In order to confirm the differences in chain length inferred from IR analysis, the polyphenylene samples made from **1** and **2** were also analyzed by ^{13}C cross-polarization magic angle spinning (CPMAS) NMR spectroscopy. Due to the inherent insolubility and chemical inertness of PPP, the number of physical and chemical techniques for characterizing the material other than IR analysis is rather limited. Recently, ^{13}C CPMAS solid-state NMR spectroscopy has been used by several research groups to characterize and determine the approximate molecular weight of PPP samples.[24-27] Typically, both PPP and *p*-oligophenyls are characterized by two signals at 128 and 139 ppm in their ^{13}C solid-state NMR spectra. These resonances are due to the protonated and nonprotonated aromatic carbon atoms in the compounds, respectively (Figure 21).

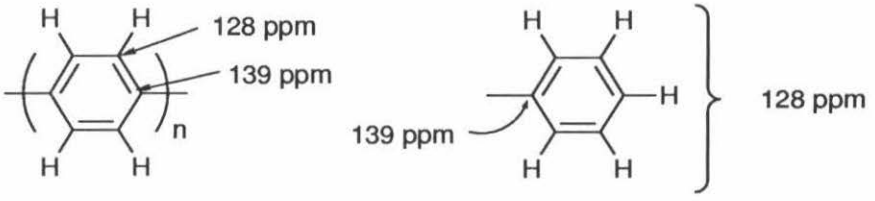

Figure 21. The two types of aromatic carbons observed by ^{13}C CPMAS NMR spectroscopy for PPP and oligophenyls.

Ideally, the ratio of the integrals of these two ^{13}C resonances can be used to semi-quantitatively determine the chain length of PPP and *p*-oligophenyls.[24] As shown in Table I, the ratio of protonated to nonprotonated aromatic carbons (r) decreases with the number of consecutive phenyl rings in the chains (n) according to Eq. 1.

Table I. The ratio of protonated to nonprotonated aromatic carbons as a function of the number of phenyl rings for a series of *p*-oligophenyls.

Compound	Chain Length (n)	Ratio of protonated to nonprotonated carbons (r)
biphenyl	2	5.0
p-terphenyl	3	3.5
p-quaterphenyl	4	3.0
p-sexiphenyl	6	2.6

$$r = \frac{2n+1}{n-1} \qquad (1)$$

For an infinitely long PPP chain, r should approach a minimum value of 2. Consequently, the integral ratio of these two carbon resonances in the ^{13}C NMR spectrum can be used to extrapolate the average chain length of the sample. However, this technique loses precision with longer chain lengths because the relationship between r and n is asymptotic. Thus, this method cannot be used to precisely gauge PPP chain lengths above n = 6, but it can be used to differentiate between low oligomers and chains longer than *p*-sexiphenyl.

Only five of the six polyphenylene samples made by the catalyzed and uncatalyzed pyrolysis of **1** and **2** were analyzed by ^{13}C CPMAS NMR spectroscopy. The polyphenylene sample made by the pyrolysis of pristine **1** was not analyzed by this technique because TGA-MS and IR analysis revealed that this sample is obviously oligomeric in nature. Also, because of the large amount of chain fracturing that occurs during the uncatalyzed bulk pyrolysis of **1** (Figure 5), it was difficult to synthesize enough of the resulting PPP oligomers to pack an NMR sample rotor (10–15% pyrolysis yield).

Initially, ^{13}C CPMAS NMR experiments were performed on *p*-quaterphenyl and *p*-sexiphenyl as NMR standards in order to determine pulse parameters that would give accurate integral ratios. The ^{13}C NMR spectra of the five polyphenylene samples taken with these pulse parameters (10 ms contact pulse, 6 ms ^{1}H 90° pulse) and a pulse delay of

5 s are presented in Figure 22. All five polyphenylene samples exhibit only the two sets of ^{13}C resonances at 128 and 139 ppm characteristic of PPP and *p*-oligophenyls. (The small signals on either side of the main resonances are spinning sidebands.) There are no signals due to residual carbonyl groups (160–190 ppm) or saturated carbon centers (10–50 ppm). Unfortunately, the linewidths of the ^{13}C peaks are so broad that it is only possible to differentiate between protonated and nonprotonated carbons but not identify any carbon centers belonging to 1,2-, or 1,3-linked aromatic units. Thus, it is not possible to confirm the regiochemical differences observed by IR analysis between the polyphenylene samples using this technique. However, two distinct sets of differences can be seen in the five spectra. First, the spectra of the four polyphenylene samples made by acid-catalyzed aromatization of precursors **1** and **2** (Figures 22a–d) have extremely poor resolution and signal-to-noise compared to that of the PPP oligomers made from the uncatalyzed pyrolysis of **2** (Figure 22e). Second, the spectra of the two high quality PPP samples made by the acid-catalyzed aromatization of **1** (Figures 22a and 22b) show an integral ratio of nearly 1:1, which is below the theoretical minimum value expected for PPP. The spectra of the other three samples (Figures 22c–e), on the other hand, exhibit approximately the expected 2:1 integral ratio. The ^{13}C integrals of the five spectra are listed in Table II.

Table II. The integral ratios of protonated (128 ppm) and nonprotonated (139 ppm) carbons in the ^{13}C CPMAS NMR spectra in Figure 22.

Polyphenylene ^{13}C CPMAS Spectrum	Composition of Precursor	Integral Ratio[a] ($I_{128\ ppm}/I_{139\ ppm}$)
Figure 21a	**1** + 5 wt % DCBSA	1.05
Figure 21b	**1** + 10 wt % $ZnCl_2$	1.22
Figure 21c	**2** + 5 wt % DCBSA	1.84
Figure 21d	**2** + 10 wt % $ZnCl_2$	1.75
Figure 21e	pristine **2**	1.91

(a) Integrals were obtained by the standard integration procedures on the NMR spectrometer. These values were checked by deconvoluting and curve-fitting selected spectra to obtain more accurate integral values.

Figure 22. ^{13}C CPMAS NMR spectra of the polyphenylene samples obtained from the bulk pyrolysis of (a) polymer **1** containing 5 wt % DCBSA, (b) polymer **1** containing 10 wt % $ZnCl_2$, (c) polymer **2** containing 5 wt % DCBSA, (d) polymer **2** containing 10 wt % $ZnCl_2$, and (e) pristine polymer **2**.

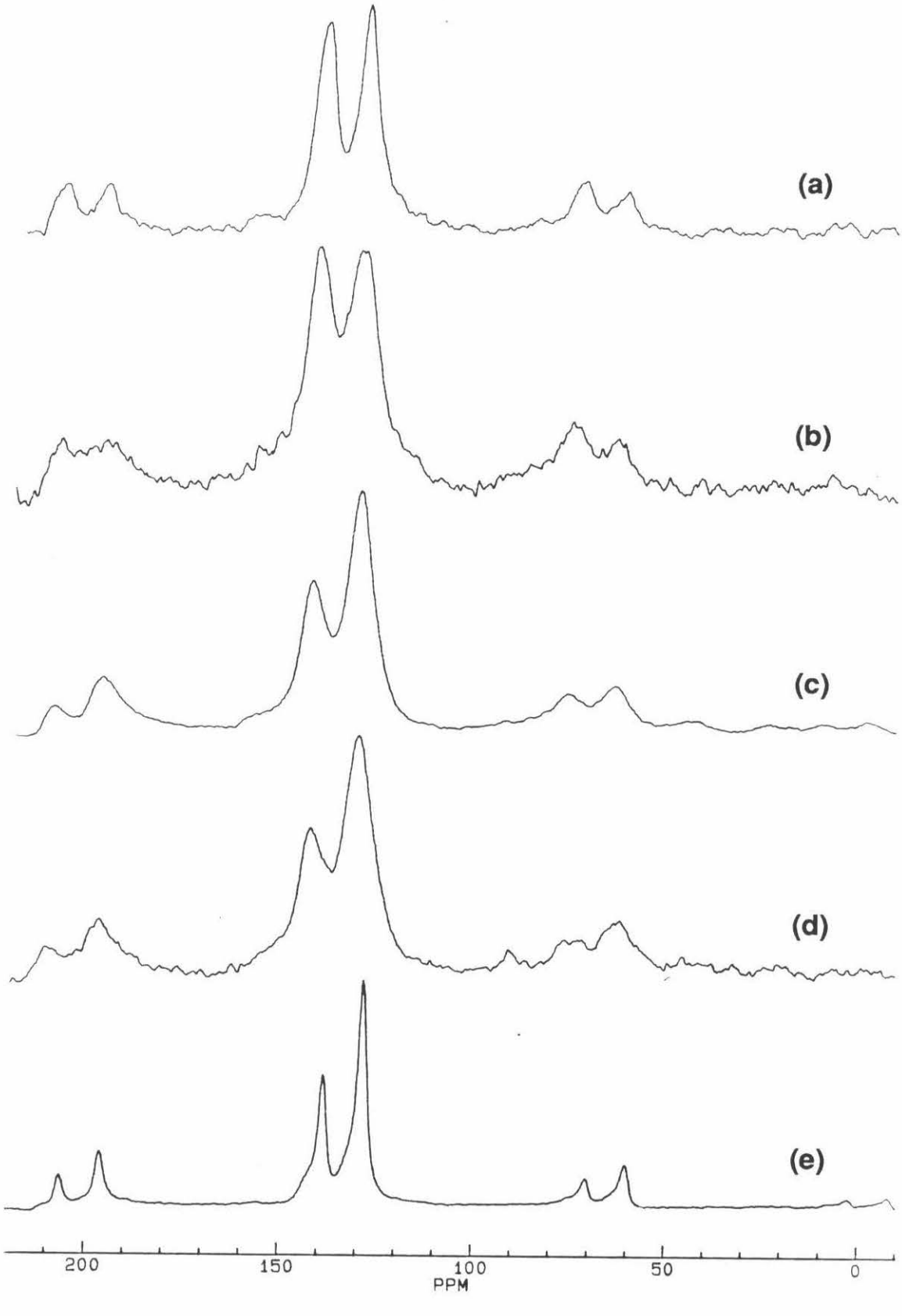

phenomenon. The irregular polyphenylene samples made from the acid-catalyzed aromatization of **2** and the PPP oligomers made by the uncatalyzed pyrolysis of **2** all exhibit a nearly 2:1 integral ratio using the same pulse parameters. In addition, even

The first difference observed in the five spectra was of instrumental origin and can be attributed to the difference in morphology between the acid-catalyzed polyphenylene samples and the PPP oligomers. The acid-catalyzed polyphenylene samples are all completely amorphous while the PPP oligomers are partially crystalline. Since the original pulse parameters were optimized on semicrystalline *p*-quaterphenyl and *p*-sexiphenyl standards, they were probably not ideal for the amorphous samples. ^{13}C CPMAS NMR Spectra with better signal resolution and signal-to-noise were obtained for the two amorphous polyphenylene samples made from the DCBSA-catalyzed aromatization of **1** and **2** by using a much shorter contact pulse of 1 ms (Figures 23a and 23b). Proton spin–lattice relaxation time (^1H T_1) experiments indicated that these two amorphous samples have ^1H T_1 values of 0.64 and 0.15 s, respectively, so the 5 s pulse delay initially employed was more than enough to permit complete relaxation of the magnetization between pulses.[28] Unfortunately, even with the updated pulse parameters, better quality spectra and accurate ^1H T_1 values could not be obtained for the two polyphenylene samples made by the $ZnCl_2$-catalyzed aromatization of **1** and **2** . Possibly, the large amount of residual $ZnCl_2$ in the samples (approximately 25 wt %) may have a detrimental effect on the quality of the spectra obtained.

The second anomaly, involving lower than theoretical integral ratios for the two types of aromatic carbons, has been also been encountered by other researchers using ^{13}C CPMAS NMR spectroscopy to characterize PPP.[26] The cause of these anomalous intensity distributions has been attributed to either instrument problems[24] or a high degree of π-conjugation in the polymers.[26] It is unlikely that the cause of the anomalous intensity distributions observed in our study is instrumental in origin since only the two high quality PPP samples made by the acid-catalyzed aromatization of **1** exhibit this phenomenon. The irregular polyphenylene samples made from the acid-catalyzed aromatization of **2** and the PPP oligomers made by the uncatalyzed pyrolysis of **2** all exhibit a nearly 2:1 integral ratio using the same pulse parameters. In addition, even

Figure 23. Improved ^{13}C CPMAS NMR spectra of (a) the amorphous, high quality PPP obtained from the DCBSA-catalyzed bulk aromatization of **1** and (b) the amorphous, irregular polyphenylene obtained by the DCBSA-catalyzed bulk pyrolysis of **2**. Both spectra were taken with a contact pulse of 1 ms and a recycle delay of 5 s.

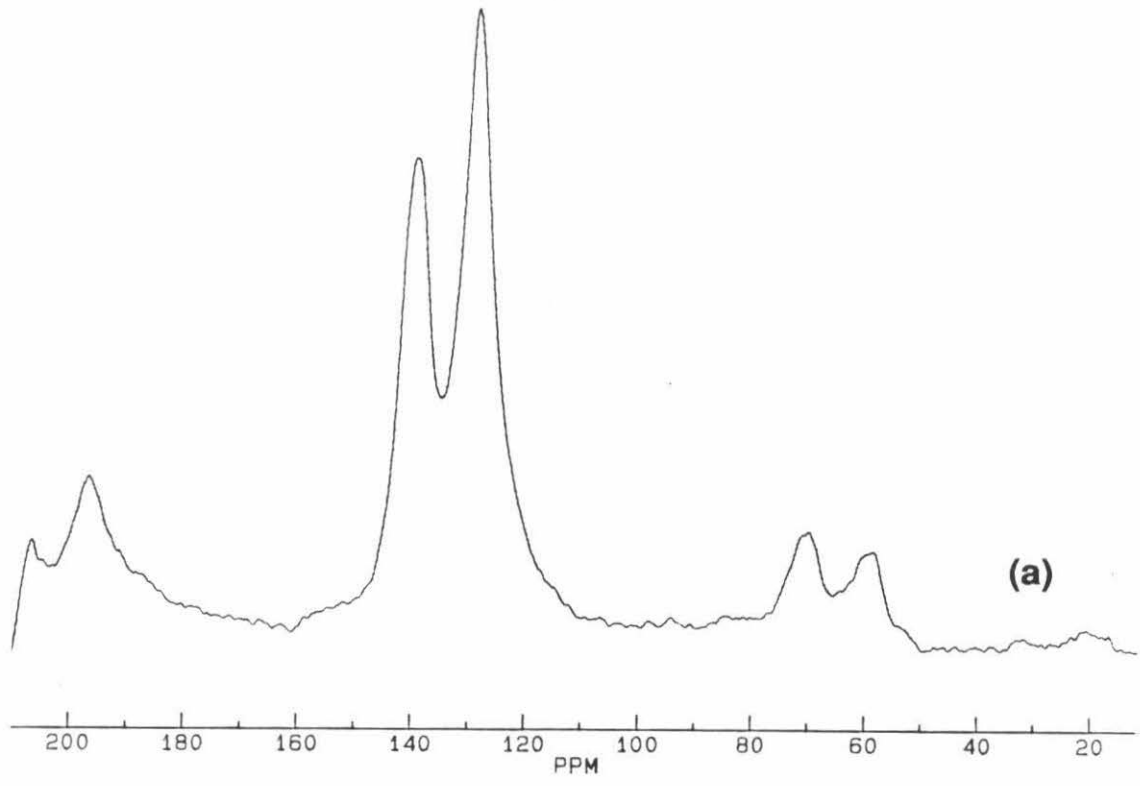
(a)
200
180
160
140
120
100
80
60
40
20
PPM

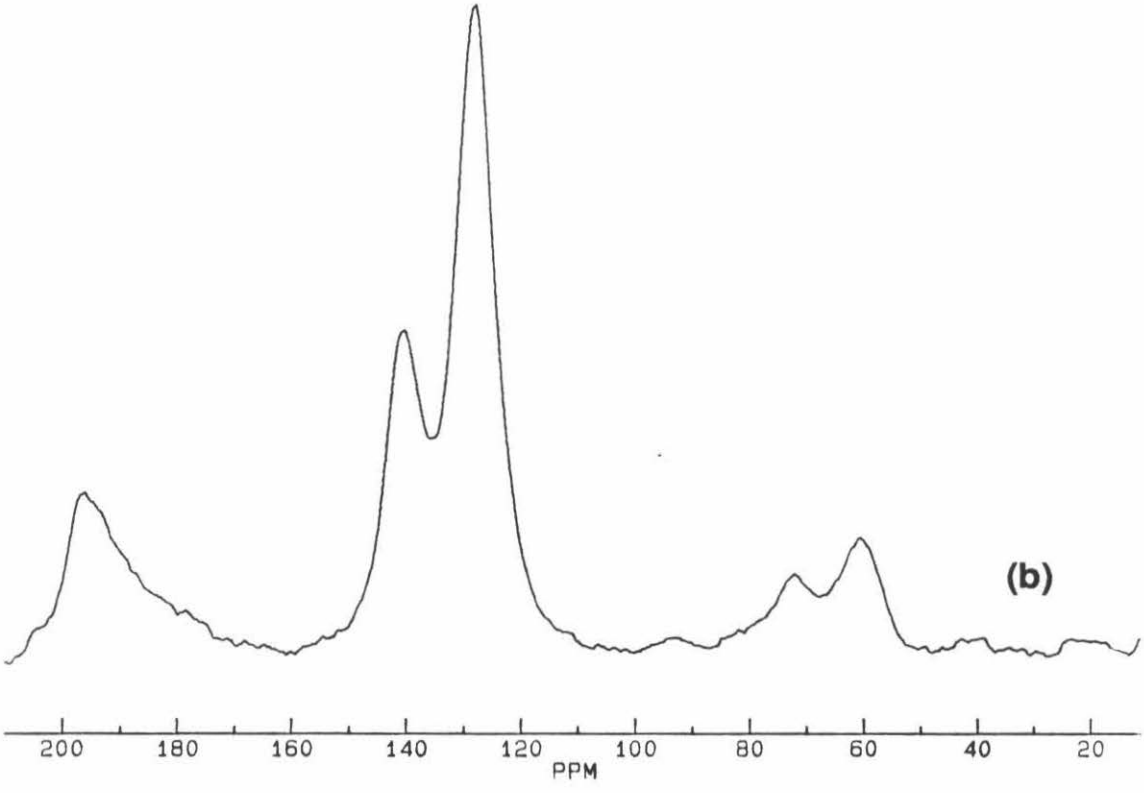
(b)
200
180
160
140
120
100
80
60
40
20
PPM

with the pulse parameters optimized for amorphous samples, the anomalous intensity distributions do not change significantly (Figure 23a). More likely, the cause of this anomaly must be molecular in origin because IR analysis has established that the PPP samples made by the DCBSA- and $ZnCl_2$-catalyzed aromatization of **1** are predominantly 1,4-linked and much higher molecular weight than the other polyphenylene samples analyzed. Whether this structural difference and the observed anomalous intensity distribution implies a higher degree of conjugation in the samples has yet to be proven.

Although the conclusions that can be drawn from this preliminary ^{13}C CPMAS NMR study are rather limited, it is quite obvious that the high quality PPP samples identified by IR analysis behave very differently in the NMR spectrometer compared to the other polyphenylenes.

Thermal Stability

Although different combinations of precursor and acid catalyst produce different qualities of polyphenylene, the thermal stabilities of the samples are quite similar. The thermal stabilities of the six polyphenylene samples made by the catalyzed and uncatalyzed bulk pyrolysis of **1** and **2** were determined by TGA, and are summarized in Table III.

Table III. Thermal stabilities of the polyphenylene samples made by the catalyzed and uncatalyzed bulk pyrolysis of polymers **1** and **2**.

Polyphenylene Preparation		Polyphenylene Thermal Stability [b]	
Precursor Composition	Pyrolysis Conditions [a]	% Wt Loss @ 500 °C	Onset of Decomposition (°C)
1 + 5 wt % DCBSA	A	3–5	545
1 + 10 wt % $ZnCl_2$	B	15	418
pristine **1**	A	6	487
2 + 5 wt % DCBSA	A	5	526
2 + 10 wt % $ZnCl_2$	B	16	434
pristine **2**	A	4	549

(a) A: 100 °C (1 h) —> (2 °C/min) —> 300 °C (5 h) —> (2 °C/min) —> 400 °C (0.1 h).
B: 100 °C (1 h) —> (2 °C/min) —> 340 °C (5 h).
(b) TGA was performed with a ramp rate of 10 °C/min from 100 °C to 700 °C.

As can be seen from Table III, the thermal stabilities of the polyphenylene samples made by uncatalyzed and DCBSA-catalyzed aromatization of **1** and **2** are virtually identical. They all begin to slowly decompose near 500 °C. These decomposition temperatures are in good agreement with the thermal stabilities of PPP samples made by other routes in the literature.[19] However, the high quality PPP and the irregular polyphenylene made using $ZnCl_2$ exhibit lower thermal stabilities. This may be the result of the approximately 25 wt % $ZnCl_2$ residue in the two samples. The interaction of a strong Lewis acid such as $ZnCl_2$ with the π-electrons of the polyphenylenes may cause the polymers to decompose at a significantly lower temperature.

Magnetic Measurements

Magnetic measurements were performed on the six polyphenylene samples made from **1** and **2** in order to determine their intrinsic free spin densities.[29] All PPP samples synthesized by other methods have been found to exhibit high free spin densities on the order of 10^{16}–10^{18} spins/g in the undoped state.[19] Higher spin densities have been

correlated with increasing chain length in *p*-oligophenyls[19] and shorter ^1H T_1 values in PPP samples and *p*-oligophenyls.[24] Thus, determining the concentration of intrinsic paramagnetic defects in our polyphenylene samples may provide more information on the structure and chain length of the materials as well as the anomalous intensity distributions observed by ^{13}C CPMAS NMR analysis on some of the samples.

Magnetic measurements were performed on the six polyphenylene samples using a superconducting quantum interference device (SQUID) magnetometer. Only two of the six polyphenylene samples made from **1** and **2** were found to be intrinsically paramagnetic. The high quality PPP made from **1** with 5 wt% DCBSA and the PPP oligomers made from pristine **2** have spin densities of 10^{19} and 10^{20} spins/g, respectively. These spin densities are comparable to those observed by electron spin resonance (ESR) spectroscopy for other PPP materials in the literature.[19] However, the magnetic measurements on these two materials reveal very high cooperativity between the unpaired spins. The spin states of the two samples were calculated to be 3.4 for the high quality PPP made from DCBSA-catalyzed aromatization of **1** and 6.5 for the PPP oligomers made from pyrolysis of pristine **2**.[30] In addition, the PPP oligomers made by the pyrolysis of pristine **2** demonstrated hysteresis at low temperature. This behavior is indicative of long range ordering of the spins enforced by the π-network. These surprising results for the two materials were reproducible over several different batches of the polymers.

The exact nature of the extremely stable paramagnetic species found in PPP has been a matter of great speculation. Factors as chain length, steric factors, the formation of charge–transfer complexes, and the presence of structural defects such as polynuclear aromatic structures have been found to influence the concentration of unpaired spins in PPP.[19] Although the paramagnetic behavior of PPP is a very complex phenomenon, three things can be inferred from correlating the SQUID results on our six polyphenylene

samples with data obtained by IR analysis and ^{13}C CPMAS NMR spectroscopy. First, the presence of diamagnetic impurities such as $ZnCl_2$ in the material appears to have a detrimental effect on the spin density of the sample. Both the high quality PPP samples made by the DCBSA- and $ZnCl_2$-catalyzed aromatization of **1** are similar in structure and morphology by IR and PXRD analysis; however, only the former displays a high spin concentration. The only difference between the two high quality PPP samples is that the latter sample contains approximately 25 wt % $ZnCl_2$ as a residue from the $ZnCl_2$-catalyzed aromatization reaction. The PPP made using DCBSA as the aromatization catalyst, on the other, is virtually free of catalyst residues because the organic acid is removed during the pyrolysis process by heating to elevated temperatures. Second, the presence of structural defects such as 1,2-units in the polyphenylene also appears to have a detrimental effect on the spin concentration. Both samples made from the DCBSA- and $ZnCl_2$-catalyzed aromatization of **2** contain a significant amount of 1,2-units as indicated by IR analysis; however, both are diamagnetic despite the fact that the former sample does not contain residual $ZnCl_2$. In addition, PPP oligomers having no 1,2-units but made from the uncatalyzed pyrolysis of the same precursor display a very high spin density. Lastly, it appears that crystallinity favors higher spin concentrations and a higher overall spin state. Although IR analysis has shown that the high quality PPP made by the DCBSA-catalyzed aromatization of **1** is composed of longer PPP chains than the PPP oligomers made from the uncatalyzed pyrolysis of **2**, the PPP oligomers have a spin density nearly 20 times higher. The only difference between the two materials other than chain length is that PPP oligomers are semicrystalline while the high quality PPP is completely amorphous. The increased order of the semicrystalline PPP oligomers may be partially responsible for the higher spin density and higher degree of cooperativity between the unpaired spins despite its lower molecular weight. It should be noted that doped C_{60} has also shown cooperative magnetic behavior;[31] thus π-stacking interactions may act to establish a ferromagnetic exchange field in a number of systems.

UV–Visible Absorption Spectroscopy

UV–visible absorption spectroscopy was also used to characterize the different polyphenylene samples made from the PPP precursors **1** and **2**. The position of the UV–visible absorption maximum (λ_{max}) of PPP samples has been used to gauge the approximate molecular weight and the extent of conjugation of the materials, and detect the presence of structural defects.[19,20,22] The λ_{max} of *p*-oligophenyls increases asymptotically with increasing chain length.[19] The maximum value that λ_{max} can reach has been calculated to be 339 nm for an infinitely long PPP chain.[32,33] Unfortunately, the λ_{max} can only be used to extrapolate the approximate chain length of higher *p*-oligophenyls because the relationship between λ_{max} and linear chain length loses precision with higher molecular weight materials.[19] Also, structural defects in runs of 1,4-phenylene units are also known to shift the λ_{max} of PPP samples and oligophenyl compounds. For example, excessively large λ_{max} values as high as 379–395 nm have been measured for PPP samples made by the Kovacic method and have been attributed to the presence of polynuclear aromatic defects.[19] In contrast, the presence of 1,2- and 1,3-phenylene units in oligophenyls is known to lower the λ_{max} and the extent of conjugation compared to the completely 1,4-linked analogues.[22,34-36]

Because of the opaqueness of our bulk polyphenylene samples, the UV–visible absorption spectra of the materials were obtained using thin transparent films of the materials baked onto quartz transmission windows. The spectra are presented in Figures 24 and 25. Some unexpected observations can be made from a quick comparison of these spectra: (1) Both the polyphenylene samples obtained by the DCBSA- and $ZnCl_2$-catalyzed aromatization of **2** have been shown by IR analysis to contain a substantial amount of 1,2-units; however, only the $ZnCl_2$-catalyzed thin film (Figure 25c) exhibits the lower λ_{max} expected from these non-linear defects. (2) Both the PPP films made

Figure 24. UV–visible absorption spectra of polyphenylene films made from the pyrolysis of thin films of polymer **1** containing (a) 5 wt % DCBSA, (b) 10 wt % $ZnCl_2$, and (c) no aromatization catalysts. The wavelength scale is in nanometers.

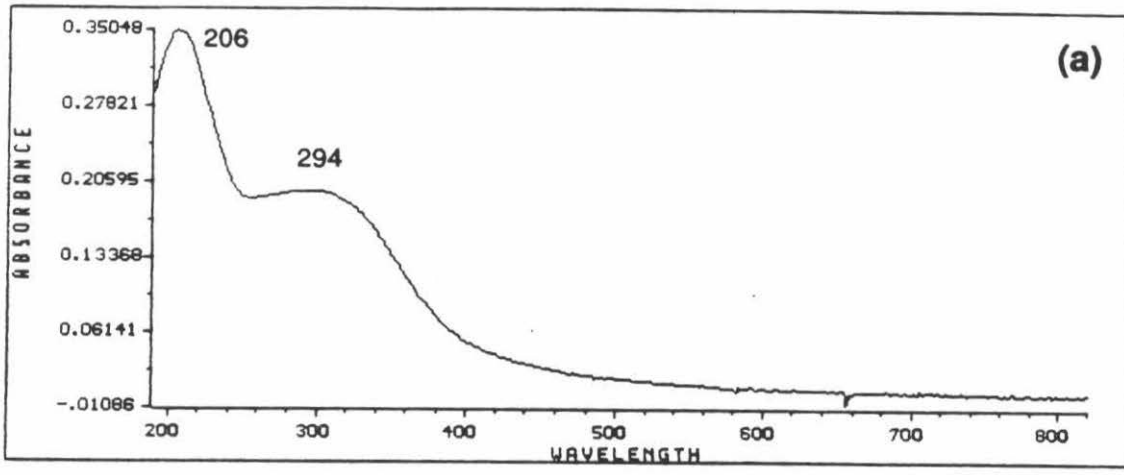
(a)
206
294
0.35048
0.27821
0.20595
0.13368
0.06141
-.01086
ABSORBANCE
200
300
400
500
600
700
800
WAVELENGTH

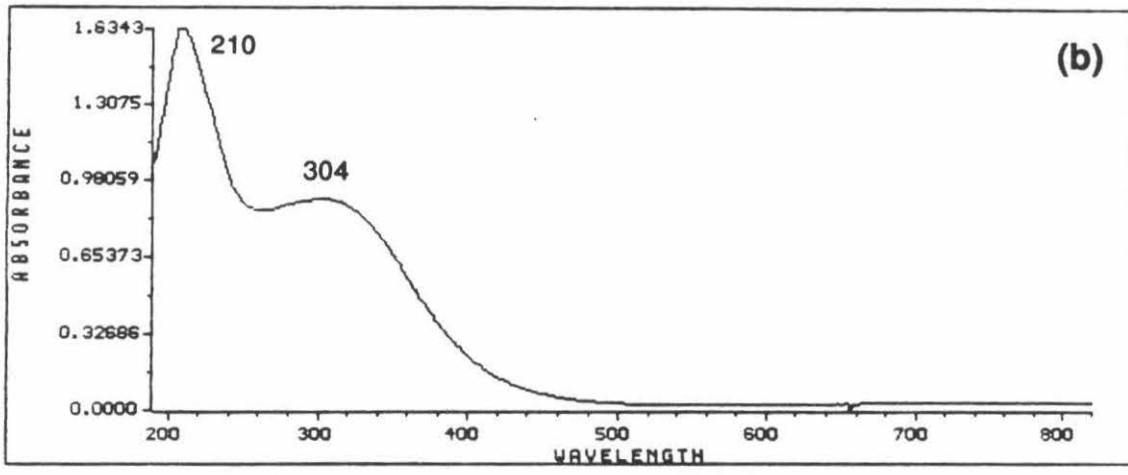
(b)
210
304
1.6343
1.3075
0.98059
0.65373
0.32686
0.0000
ABSORBANCE
200
300
400
500
600
700
800
WAVELENGTH

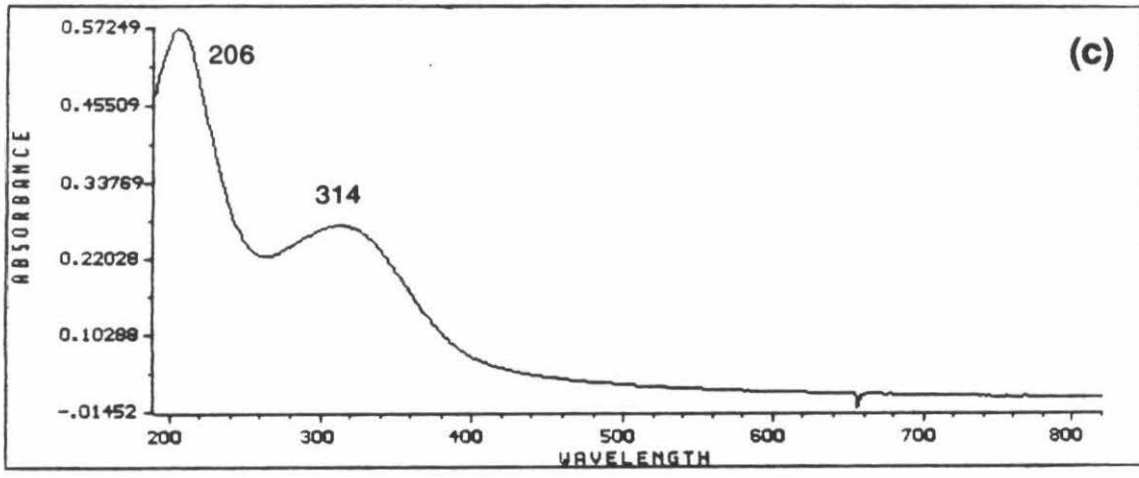
(c)
206
314
0.57249
0.45509
0.33769
0.22028
0.10288
-.01452
ABSORBANCE
200
300
400
500
600
700
800
WAVELENGTH

Figure 25. UV–visible absorption spectra of polyphenylene films made from the pyrolysis of thin films of polymer **2** containing (a) 5 wt % DCBSA, (b) 10 wt % $ZnCl_2$, and (c) no aromatization catalysts. The wavelength scale is in nanometers.

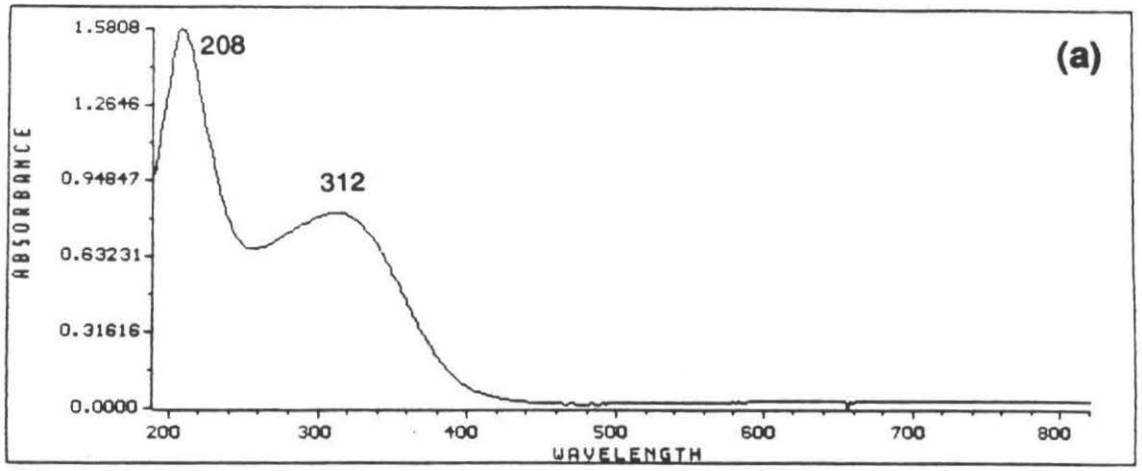
(a)
208
312
1.5808
1.2646
0.94847
0.63231
0.31616
0.0000
ABSORBANCE
200
300
400
500
600
700
800
WAVELENGTH

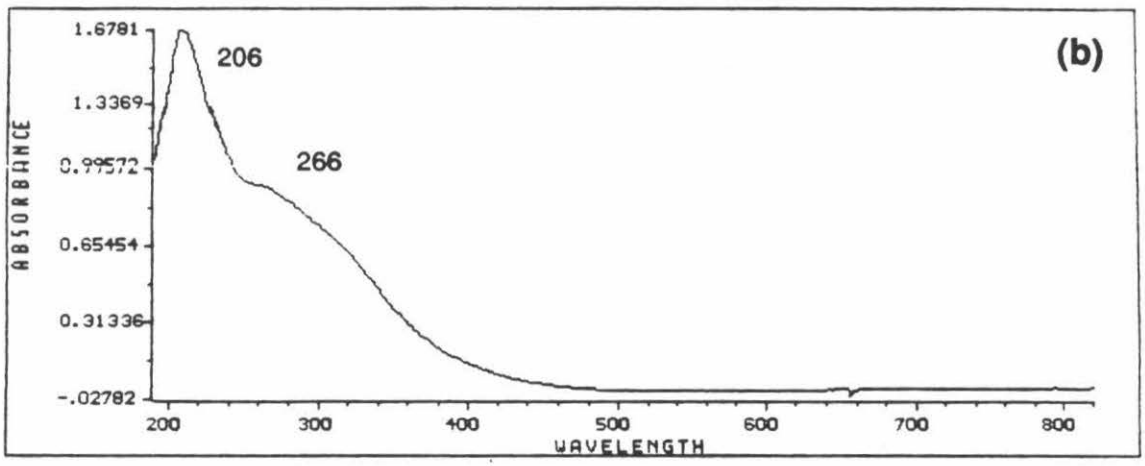
(b)
206
266
1.6781
1.3369
0.99572
0.65454
0.31336
-.02782
ABSORBANCE
200
300
400
500
600
700
800
WAVELENGTH

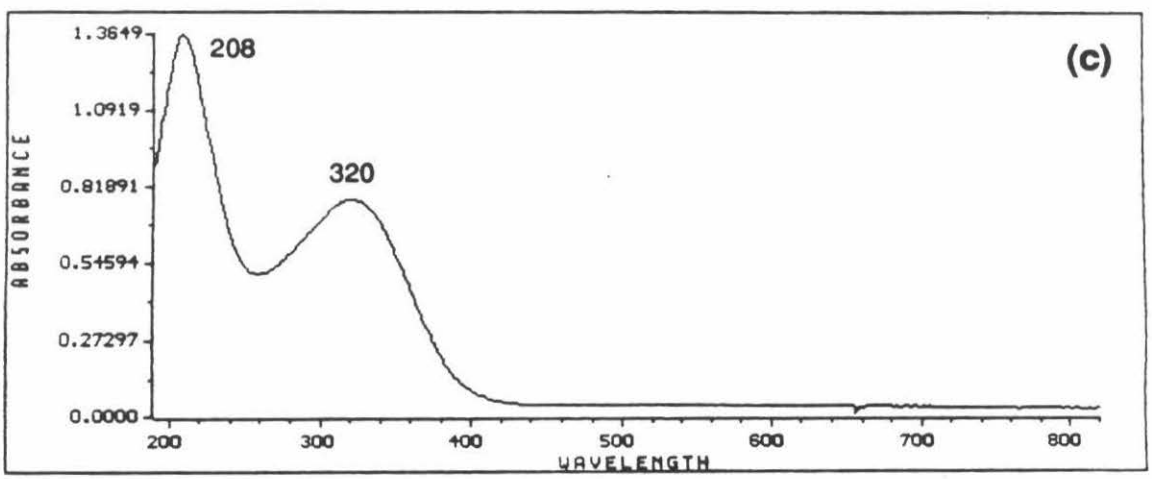
(c)
208
320
1.3649
1.0919
0.81891
0.54594
0.27297
0.0000
ABSORBANCE
200
300
400
500
600
700
800
WAVELENGTH

from the DCBSA- and $ZnCl_2$-catalyzed aromatization of the stereoregular precursor **1** have approximately the same λ_{max} (305–310 nm) as the PPP oligomers made from the pyrolysis of the pristine precursors. This observation is unexpected because IR analysis has confirmed that the PPP samples made by the acid-catalyzed aromatization of **1** have a higher molecular weight than the oligomers made by pyrolysis of the pristine precursors (see IR analysis section). Judging from the λ_{max} values, these PPP samples only have a linear chain length and an extent of conjugation comparable to that of *p*-sexiphenyl (λ_{max} = 318 nm).[35]

However, caution must be used when interpreting these results obtained from samples made by thin film pyrolysis. First of all, samples made by pyrolysis of thin films of the precursors containing organic acids (e.g., DCBSA) to catalyze the aromatization process are probably not representative of the polyphenylenes made using the same acids in a bulk pyrolysis process. That is, organic acid catalysts have been shown to have no effect on the quality of the resulting polyphenylene in thin film pyrolysis of the precursors. These results have been previously observed in studies by Wilson et al.[14] and in our IR studies. Apparently, the organic acid catalysts tend to sublime away prematurely before the onset of aromatization in thin films. Although IR analysis has shown that bulk pyrolysis of **2** containing acid catalysts produces material with a substantial percentage of 1,2-units, only the polyphenylene film made from **2** containing $ZnCl_2$, an extremely nonvolatile catalyst, exhibits the lower λ_{max} expected for a material with substantial 1,2-units (Figure 25b). In all likelihood, both the polyphenylene films made by the DCBSA-catalyzed thin film aromatization of **1** and **2** are probably the same materials as that obtained by uncatalyzed pyrolysis of the two precursors. Thus, UV–visible analysis on thin films is not a reliable technique in this case.

Secondly, higher λ_{max} values for even the high quality PPP films made with an extremely nonvolatile acid catalyst such as $ZnCl_2$ may not be possible due to morphological limitations. The λ_{max} of some conjugated polymers has been observed to

shift depending on the order in the material. For example, the λ_{max} of poly(1,4-phenylene-vinylene) (PPV) is related to the degree of long range order and crystallinity of the material.[37,38] Thus, the reason why even the high quality PPP film made by $ZnCl_2$-catalyzed aromatization shows the same or slightly lower λ_{max} than the PPP oligomers may lie in the fact that the $ZnCl_2$-catalyzed material is completely amorphous while the oligomers are semicrystalline (cf. Figures 24b and 24c). Unfortunately, the inherent intractability of PPP made by direct routes and the poor quality of materials made from previous precursor routes[19] have made it difficult to determine whether changes in morphology and crystallinity have as dramatic an effect on the λ_{max} of PPP as they have for that of PPV. With our new precursor methodology ,which affords high quality PPP, it may be possible to do this in the near future.

Because of the inherent problems in acid-catalyzed thin film pyrolysis and the likely dependence of λ_{max} on morphology and crystallinity, UV–visible spectroscopy on thin films of the polyphenylenes reveals little about the structure and molecular weight of the bulk materials.

Preliminary Doping and DC Conductivity Measurements

Poly(*p*-phenylene) forms highly conductive charge–transfer complexes upon doping with strong electron acceptors (e.g., AsF_5) and electron donors (e.g., alkali metals).[19,20] In fact DC conductivities of up to 500 S/cm have been measured for AsF_5-doped pressed pellets of PPP made by the oxidative cationic polymerization of benzene.[19,20] In order to compare the conductivities of the polyphenylene samples made by our route, preliminary doping experiments were performed and conductivity measurements were taken.

Usually, doping and DC conductivity experiments on PPP samples are performed on pressed powder pellets due to the intractable nature of the material.[20] Unfortunately,

due to the unique morphology of our acid-catalyzed polyphenylene samples, void-free, pressed pellets could not be obtained.[39] Consequently, preliminary doping and conductivity experiments had to be performed on two types of polyphenylene samples. That is, the acid-catalyzed polyphenylene samples were all doped and analyzed as the foams obtained directly from bulk pyrolysis of pressed pellets of the precursors. On the other hand, the PPP oligomers obtained by uncatalyzed pyrolysis of **1** and **2** were doped as spin-coated films on quartz. It was not possible to process all of the samples into a single form for a truly comparative study because only the acid-catalyzed samples form foams whereas the samples made from the pristine precursors flow into films. Studies were not performed on thin films of all the samples because it has been observed that thin film pyrolysis of the precursors containing organic acids does not give PPP representative of that obtained in the catalyzed bulk process.

The six polyphenylene samples were doped by exposing them to approximately 240 torr of AsF_5 for 50–60 minutes. During the doping process, only the flaky interior of the high quality PPP foam made from the DCBSA-catalyzed aromatization of precursor **1** changed from a lustrous tan color to a deep blue-green color. The interior of all the other polyphenylene pellets became slightly darker but did not lose all of their lustrous appearance. The PPP oligomer films baked onto quartz discs did not exhibit any color change. Only the high quality PPP sample made from the DCBSA-catalyzed aromatization of stereoregular precursor **1** was found to exhibit an appreciably high electrical conductivity of approximately 10^{-2}–10^{-1} S/cm. All of the other five doped polyphenylene samples made from **1** or **2** were found to be highly insulating ($\leq 10^{-7}$ S/cm). Because of the amorphous, void-filled structure of the sample, the conductivity value measured should be considered a lower limit.[20] Significantly higher conductivities may well be possible if the sample is doped for longer periods of time, or if it can processed into an oriented, void-free form.[40]

Summary

The quality of the poly(*p*-phenylene) (PPP) produced from the thermal conversion of two acetoxy-functionalized polymers **1** and **2** (Figure 1) depends on the stereochemistry of the polymer and the presence of aromatization catalysts. The thermal conversion of these precursors to PPP involves two competing reactions: (1) thermal depolymerization of the polymer, and (2) thermally-induced acid elimination resulting in PPP formation. The relative rates of these two processes, which ultimately determine the molecular weight of the final product, depend heavily upon the stereochemistry of the polymer backbone. For the 1,4-linked, stereoregular precursor **1**, made by transition-metal-catalyzed polymerization, the rate of thermal depolymerization is much faster than the rate of acid elimination during the pyrolysis process. Consequently, this material fractures to a greater degree than it aromatizes during heating despite the fact that the stereochemistry of the polymer is ideal for facile cis-pyrolytic acid elimination. On the other hand, for the radically polymerized analogue **2**, containing random backbone stereochemistry and regiochemical defects, the reverse relationship is true. Although depolymerization still takes place during the pyrolysis of the radically polymerized polymer, the thermal stability of the irregular polymer backbone is greater so the relative amount of backbone fracturing is less than that of aromatization. Brønsted and Lewis acids are able to overcome this problem by selectively catalyzing the acid elimination reaction of both precursor polymers. They lower the onset temperature of the aromatization process to temperatures well below that at which thermal depolymerization can occur. However, characterization of the resulting polyphenylene materials indicates that the regiochemical structure of the polyphenylene produced by the acid-catalyzed aromatization process depends entirely on the stereochemistry of the precursor polymer. *Only* the the acid-catalyzed aromatization of the 1,4-linked, stereoregular polymer **1** yields high quality, high molecular weight PPP.

The high quality PPP produced by the acid-catalyzed aromatization of **1** exhibits properties similar to those of PPP samples in the literature. However, it is completely amorphous whereas PPP samples made by other routes are almost always semicrystalline. Since the physical and chemical properties of PPP and many other conjugated polymers depend highly on sample morphology, processing techniques for this material will have to be developed before its optimum properties can be realized. Our new precursor route to PPP employing polymer **1** is ideal for these studies since it offers processability as well as a high quality product.

Experimental Section

General Considerations

All manipulations were performed in the air unless otherwise specified. Reagents, gases, and solvents were used without further purification unless otherwise specified. Drying of polymers prior to pyrolysis or analysis was performed on a Schlenk line using conventional vacuum line techniques. Air- and/or water-sensitive compounds were stored in a nitrogen filled Vacuum Atmospheres drybox.

Materials

Solvents such as THF and hexanes were obtained from Fisher Scientific or EM Science. 3,4-Dichorobenzenesulfonic acid (DCBSA) was purchased from Eastern Chemicals. Zinc chloride (99.999%) was purchased from Aldrich and stored in the drybox. *p*-Toluenesulfonic acid, 2,6-di-*tert*-butyl-4-methylphenol (BHT) (99+%), *p*-terphenyl, *p*-quaterphenyl were all purchased from Aldrich. *p*-Sexiphenyl was purchased from TCI America. Argon (UN1006) for tube furnace pyrolysis and TGA experiments was obtained from Liquid Air. Arsenic pentafluoride was purchased from Ozark–Mahoning. NaCl, KBr, and quartz transmission windows (25 mm x 2 mm discs) were all purchased from Wilmad. Polymer **1** was synthesized according to the procedures outlined in the previous chapter. Polymer **2** (batch 12871/80) was graciously donated by ICI Chemicals and Polymers Ltd., Runcorn, U. K.

Preparation of PPP Precursor/Catalyst Mixtures for Pyrolysis and TGA Studies

Typically, a mixture of PPP precursor containing a specified wt % of acid catalyst was prepared by dissolving the appropriate amount of precursor polymer in THF, syringing in the appropriate amount of catalyst in the form of a stock solution in THF, and coprecipitating the two dispersed components by decanting the mixture into a

nonsolvent (e.g., pentane or hexanes). For example, to prepare a mixture containing 10 wt % of $ZnCl_2$ in polymer **1**, first the polymer (0.360 g) was dissolved in THF (6 mL). With rapid stirring, 1.20 mL of a 0.033 g/mL stock solution of $ZnCl_2$ in dry THF was syringed into the polymer solution. The pale yellow polymer/catalyst solution was then added dropwise to approximately 75 mL of rapidly stirred hexanes containing a grain of antioxidant (BHT). The resulting off-white precipitate was isolated by suction-filtration, washed with fresh hexanes, and then dried overnight in vacuo. The off-white powder was stored in a vial with a PTFE-lined cap and parafilmed to exclude atmospheric moisture. The amount of $ZnCl_2$ (or any other acid catalyst added) was confirmed by elemental analysis of the mixture at Oneida Research Services, Inc., Whitesboro, NY.

Preparation of Supported Thin Films of Precursor/Catalyst Mixtures for Pyrolysis

An approximately 15 wt % solution of a pristine PPP precursor or a precursor/catalyst mixture was prepared by dissolving 0.100 g of the powder in 0.6 mL of THF. The viscous polymer solution was then clarified by passing through a small plug of glass microfibre paper (Whatman) in a transfer pipette. Four to five drops of the clarified solution were then placed on top of a 25 mm x 2 mm disc (NaCl, KBr, or quartz), and spin-coated at 1.6–1.7 x 10^3 rpm for 30 s using a Headway Research spin-coater. Thirty seconds of additional spinning after initial film formation was usually employed to dry the films. Transparent films (up to 10 μm in thickness) were typically obtained on the substrate discs by this procedure.

Preparation of Pressed Pellets for Bulk Pyrolysis

The pristine PPP precursor or a precursor polymer/catalyst mixture (100–150 mg) was loaded as a fine powder into a 1.3 cm I.D. KBr pellet die (Aldrich). The die was placed in a Carver Laboratory Press (Mini "C", 12 ton capacity), and 10000 lbs load was applied to the die under light vacuum for approximately 0.5–1 min to obtain a firm free-

standing pellet approximately 1 mm in thickness.

Bulk Pyrolysis of PPP Precursors

Pyrolysis of supported thin films or pressed pellets of the PPP precursors polymers was performed using a Lindberg Model 55437 Moldatherm, three-zone, hinged tube furnace with a 3 in I.D. by 43 in long quartz tube insert. Temperatures within the three zones were controlled by a Eurotherm 818 Controller/Programmer to control the middle zone and two Eurotherm 847 Digital Controllers for the two end zones acting as slave terminals in a feedback loop with the middle controller.

Pressed pellets and supported thin films were placed on flat glass supports inside the quartz tube near the center of the furnace heating area. All samples were dried at 100 °C for 1 h under argon flush prior to the actual pyrolysis run which is also performed under argon flush. The temperature program for the pyrolysis of pristine PPP precursors or precursors containing organic acids as aromatization catalysts is as follows:

100 °C (1 h) —> (2 °C/min) —> 300 °C (5 h) —> (2 °C/min) —> 400 °C (0.1 h) —> (10 °C/min) —> 50 °C (0.5 h).

A slightly different temperature program was usually employed for PPP precursor mixtures containing $ZnCl_2$ as the aromatization catalyst:

100 °C (1 h) —> (2 °C/min) —> 340 °C (5 h) —> (10 °C/min) —> 50 °C (0.5 h)

Both temperature programs yield the same quality product.

Precise mass losses during the bulk pyrolysis of pressed pellets using the aforementioned temperature programs were obtained by either measuring the mass of the pellets before and after heating, or by using thermal gravimetric analysis, mimicking the

temperature programs used with the TGA7 thermal analysis system

Thermal Gravimetric Analysis (TGA)

Thermal gravimetric analysis was performed on powders or pieces of pressed pellets using a Perkin–Elmer PC Series TGA7. Conventional % weight loss vs. temperature profiles were obtained using PC Series TGA7 Multitasking Software, Version 2.1. TGA conditions for these profiles involved heating the samples under argon flush in a platinum sample holder from 50 or 100 °C at a ramp rate of 10 °C/min to a final temperature of 350, 450 or 700 °C. All TGA samples were dried for 30 min at 100 °C under argon flush in the apparatus prior to analysis.

Thermal Gravimetric Analysis–Mass Spectrometry (TGA–MS)

TGA–MS analysis was performed at ICI Chemicals and Polymers, Runcorn, U. K. using a Netzsch STA/QMA–System: 409/429-403. Samples were analyzed under a flow of helium (60 cc/min) in a platinum crucible. Samples were typically heated from ambient temperature at 10 °C/min to a final temperature of either 500 or 600 °C.

Scanning Electron Microscopy (SEM)

Scanning electron microscope images of the PPP pellets were obtained on a CamScan scanning electron microscope. PPP pellets were generally cut in two by a razor to expose the interior of the pellet. The cleaved pellets were then mounted onto stainless steel stubs with graphite paint and gold-coated prior to loading into the SEM sample chamber.

Powder X-Ray Diffraction (PXRD)

Wide angle powder X-ray diffraction on PPP samples was performed on ground-up pellets using a Scintag/USA PAD V diffractometer. Sample preparation involved

adhering powdered samples onto one side of 25 x 2 mm glass disc mounts with petroleum jelly. The mounted samples were spun and step-scanned for 5 or 10 seconds every 0.04 degrees over the 2θ range of 5 to 50 degrees. The PXRD spectra obtained by this procedure were all background corrected.

Infrared (IR) Analysis

IR spectra of PPP samples and *p*-oligophenyls were obtained using a Perkin–Elmer 1600 Series FT–IR Spectrometer over the spectral range 4400–450 cm^{-1} with a resolution of 2 cm^{-1}. Spectra were taken under a stream of nitrogen on thin films on NaCl or KBr crystals, or KBr mulls. All spectra were background corrected by subtracting the spectra of either a blank NaCl or KBr disc, or a blank KBr pellet from the sample spectra.

^{13}C CPMAS Solid-State NMR Analysis

^{13}C CPMAS solid-state NMR spectra were obtained on a Bruker MSL-200 (200.13 MHz ^{1}H, 50.32 MHz ^{13}C) spectrometer. NMR samples were prepared by powdering the samples with an agate mortar and pestle and packing them into 0.5 cm O.D. zirconium oxide rotors mated with Kel-F caps. If insufficient sample was available to pack a rotor completely, the sample was diluted with alumina (Fluka). Rough shimming of the spectrometer field prior to the runs was performed on a static sample of H_2O in a rotor. The Hartmann–Hahn condition was tuned by optimizing the shape of the free induction decay trace of a sample of adamantane, followed by further shimming of the field on the adamantane sample. ^{13}C CPMAS NMR spectra of PPP and *p*-oligophenyls were obtained on samples spun at 3.4–3.5 kHz at a temperature of 300 K. Common pulse parameters employed for all samples were a ^{1}H 90° pulse of 6 μs and a dwell time of 4 μs. Typically, 800–7000 scans were taken. Spectra of semicrystalline PPP and *p*-oligophenyl samples were obtained using a contact time of 10 ms and an

acquisition time of 100 ms, whereas optimum spectra of amorphous PPP samples were obtained using a contact time of 1 ms and an acquisition time of 200 ms. A recycle delay time of 5 s was more than adequate for all the PPP samples, but longer recycle delays on the order of 100–400 s were required for *p*-quaterphenyl and *p*-sexiphenyl because of their much longer ^{1}H T_1 values. Generally a line broadening factor of 50 Hz was applied to all FID's prior to Fourier transformation to improve the signal-to-noise level in the displayed spectra.

^{1}H T_1 values were calculated for some of the PPP samples using the inversion–recovery method.[24,41,42] For each sample, several spectra were taken with different variable delay times (τ) but with the same number of scans using the following pulse sequence:

$$180° - \tau - \text{(cross-polarization pulse sequence)}$$

For the series of spectra, the absolute intensity of the peak at 128 ppm as a function of τ was curve-fitted to extrapolate a value for ^{1}H T_1.

Magnetic Measurements

Magnetic measurements on PPP samples were performed using a Quantum Design Model MPMS Magnetic Property Measurement System. Samples were ground up using an agate mortar and pestle and loaded into 0.65 cm O.D. x 18 cm long delrin sample tubes in the drybox to exclude oxygen. Magnetic measurements on the samples were typically made over the range of 0–55 kG at constant temperature (1.8 K) and over the temperature range of 1.8–300 K at constant external field (5 kG). A control experiment performed on a sample of precursor polymer **1**, which was not expected to have significant spin density, did not show any magnetic behavior.

UV–Visible Absorption Spectroscopy

UV–visible absorption spectra were taken with a Hewlett–Packard Model 8452A Diode Array Spectrophotometer. Samples were prepared by spin-coating 6–8 drops of filtered precursor or precursor/catalyst solutions (20 mg in 0.5 mL THF) onto 25 x 2 mm quartz discs using a spinning speed of 1000 rpm and a spinning time of 30 s. The supported thin films were then pyrolyzed according to the procedure outlined in the pyrolysis section. UV–visible absorption spectra of the resulting transparent, light brown films were taken in the air over the spectral range of 190–820 nm, using a blank quartz disc as the background correction.

AsF_5 Doping

AsF_5 doping of the PPP samples was performed according to the procedure of Swager.[43] Due to the toxicity of the dopant, a dedicated single-manifold vacuum line in a high-speed fumehood containing a charcoal filter was used. All valves on the line were constructed of PTFE, and all connections for attaching glassware were Viton O-ring seals. The O-rings were coated with Halocarbon grease (Halocarbon Products Corp.) to provide extra resistance to strong oxidizers. Pressure in the line was measured using an electronic gauge system specially designed for use with corrosive gases: a MKS Instruments AA01000A pressure transducer and a PDRC-1B readout/power supply unit with a precision of 0.1 torr. Both the pressure transducer and the AsF_5 tank were connected to the line via separate metal-to-glass seals. Samples for exposure to AsF_5 were loaded in thick-walled glass, wide-bore doping chambers containing O-ring seals and a PTFE valve to control gas flow.

A typical doping experiment first involved degassing the entire line under dynamic vacuum up to the AsF_5 tank while heating the glass sections with heat guns. Under static vacuum, 300 torr of AsF_5 was slowly admitted into the line. The dopant was then condensed into a cold finger immersed in liquid nitrogen and degassed for 15 min

under dynamic vacuum. With the AsF_5 still frozen in the cold finger, the doping chambers containing the polyphenylene samples were attached to the line and thoroughly degassed under dynamic vacuum for approximately 30 min. With the entire system under static vacuum, the AsF_5 in the cold finger was allowed to slowly warm up to room temperature and fill the manifold and the doping chambers with a total pressure of 238 torr of dopant. After approximately 50 min of exposure, the excess AsF_5 was condensed back into the cold finger. The cold finger was then detached from the line, and the excess AsF_5 was quenched with acetone while still in the solid or liquid state. The doped samples were degassed for a further 8–10 h under dynamic vacuum to remove any traces of excess dopant before transferring them to the drybox for DC conductivity measurements.

DC Conductivity Measurements

All DC conductivity measurements on doped polyphenylene samples were performed in the drybox using a four-in-line probe system[20] consisting of a Signatone four-in-line probe head (probe spacing of 0.15 cm), a Signatone combination sample support/probe arm, two Kiethley Model 197 Autoranging Digital Multimeters, and a Power Designs Model 605 Precision Power Source. DC conductivity values (σ) were obtained by placing the four probes on the surface of the doped pellets or films, measuring the resulting current (i) and voltage drop (v), and applying these measurements to Eq. 2:[20]

$$\sigma = \frac{1}{2\pi S} \times \frac{i}{v} \qquad (2)$$

This equation applies for samples thicker than the probe spacing (S).[20] Sample thicknesses were measured with a Fowler Digitrix II electronic caliper for the pellets, or a Dektak 3030 profilometer for the supported thin films. Reported DC conductivity values

were an average of a series of measurements taken over a range of applied voltages (0.1–1.5 V) from the power supply. Initial measurements were performed on a commercial Si wafer (σ = 100–200 S/cm) to confirm the accuracy of the detection circuit prior to actual measurements on the doped samples. Generally, conductivity values lower than 10^{-7} S/cm could not be measured accurately due to the limitations of the detection circuit.

References and Notes

(1) For a brief overview of this synthesis, also see: Gin, D. L.; Conticello, V. P.; Grubbs, R. H. *J. Am. Chem. Soc.* **1992**, *114*(8), 3167.

(2) Polymer **1** is believed to be a highly isotactic or syndiotactic polymer with the repeat unit depicted in Figure 1. See Chapter 2 for the assignment of the structure of **1**.

(3) Ballard, D. G. H.; Courtis, A.; Shirley, I. M.; Taylor, S. C. *Macromolecules* **1988**, *21*, 294.

(4) Ballard, D. G. H.; Courtis, A.; Shirley, I. M.; Taylor, S. C. *J. Chem. Soc., Chem. Commun.* **1983**, 954.

(5) McKean, D. R.; Stille, J. K. *Macromolecules* **1987**, *20*, 1787.

(6) Internal report from ICI Chemicals and Polymers Ltd., Runcorn, U. K., based on neutron-scattering analysis of the PPP performed at Durham University.

(7) Gordon, A. J.; Ford, R. A. *The Chemist's Companion*; John Wiley and Sons: New York, 1972; p 189.

(8) The differences observed between thin film and bulk pyrolysis of the PPP precursors may be the result of a surface effect. The crystalline surface of the NaCl transmission windows may enhance the aromatization of the thin precursor films.

(9) TGA–MS analysis was performed by George Wilkinson at ICI Chemicals and

Polymers Ltd., Runcorn, U. K.

(10) This onset temperature for backbone fracturing or depolymerization (T_f) is very similar to the ceiling temperature (T_c) observed for many radically polymerized polyolefins. T_c is the temperature at which the opposing rates of polymerization and depolymerization are equal, and the monomer is in equilibrium with the polymer. (See: Odian, G. *Principles of Polymerization,* 2nd ed.; Wiley–Interscience: New York, 1981; pp 268–271.) In the case of the PPP precursors, however, use of the term T_c is technically incorrect because at the temperatures employed for the pyrolysis process, any monomer regenerated by depolymerization is immediately decomposed to the more stable aromatic analog, as observed by MS. Consequently, once depolymerization begins, it is a one-way process, and a monomer–polymer equilibrium does not exist.

(11) The preparation of **1** by treatment of the corresponding trimethylsilyl ether derivative with acetyl chloride and $ZnCl_2$ is described in Chapter 2 of this thesis.

(12) The preparation of polymer **1** by a Zn-free route is also described in Chapter 2 of this thesis.

(13) Elemental analysis of thoroughly washed polyphenylene samples made using 10 wt % $ZnCl_2$ as an aromatization catalyst showed that the samples contain a large percentage of material which is neither carbon nor hydrogen and is assumed to be $ZnCl_2$. Zinc analysis could not be performed on these samples due to their insolubility.

(14) Wilson, D. R.; Jathavedam, H.; Thomas, N. W.; *Contemporary Topics in Polymer Science*; Salome, J. C.; Riffle, J. S., Eds.; Plenum: New York, 1991; Vol. 7. We thank D. R. Wilson for a preprint of this article.

(15) The greater temperature reduction effect observed for DCBSA is probably due to the fact DCBSA (dihydrate) melts at 71–72 °C—and is thus better able to diffuse through the precursor polymer matrix at a lower temperature—than $ZnCl_2$, which

melts at 283 °C. See: *CRC Handbook of Chemistry and Physics,* 65th ed.; Weast, R. C.; Astle, M. J.; Beyer, W. H., Eds.; Chemical Rubber Company: Baton Rouge, 1985; p C-122 and p B-159.

(16) Elemental analysis of polyphenylene samples made using 5 wt % DCBSA showed that these samples contain only trace amounts of residual sulfur and chlorine (less than 0.5 wt %) after heating to a maximum temperature of 400 °C during pyrolysis. Also, TGA of DCBSA revealed that this acid is completely sublimed or boiled away at temperatures higher than 300 °C. $ZnCl_2$ cannot be removed from the polyphenylene samples in the same manner because it boils at 732 °C, above the decomposition temperature of PPP itself. See: *CRC Handbook of Chemistry and Physics,* 65th ed.; Weast, R. C.; Astle, M. J.; Beyer, W. H., Eds.; Chemical Rubber Company: Baton Rouge, 1985; p B-159.

(17) Lewis acids and Brønsted acids were also found to generally catalyze the aromatization of other ester-functionalized derivatives of **1** and **2**, such as the stereoregular benzoate derivative of **1** described in Chapter 2. However, in terms of mass loss upon conversion to PPP, use of the acetoxy polymers **1** and **2** is still the most efficient route to PPP because acetic acid is the smallest acid that can be eliminated in the series of possible ester derivatives for the best weight yield upon aromatization.

(18) Nonvolatile Lewis and Brønsted acids were also tested on the other functionalized derivatives of polymers **1** and **2** mentioned in Chapter 2. They either have no beneficial effect on the pyrolysis process, or they only produce low quality PPP. For example, DCBSA and $ZnCl_2$ have no effect on the pyrolysis of the methoxycarbonyl derivative of polymer **2** made by the ICI process (see references 3 and 4). This pyrolysis of this derivative is base-catalyzed (see references 4 and 14). $ZnCl_2$ has no effect on the pyrolysis of the trimethylsilyl ether derivative of polymer **1**, but strong Brønsted acids catalyze the thermal hydrolysis of this

polymer to the corresponding stereoregular hydroxy polymer in the presence of trace amounts of water. Both DCBSA and $ZnCl_2$ catalyze the thermal dehydration of the stereoregular hydroxy derivative of **1**, but IR and TGA analyses indicated that only low quality PPP oligomers are formed by this process.

(19) Kovacic, P.; Jones, M. B. *Chem. Rev.* **1987**, *87*, 357, and references therein.

(20) Elsenbaumer, R. I.; Shacklette, L. W. In *Handbook of Conducting Polymers*; Skotheim, T. A., Ed.; Marcel–Dekker: New, York, 1986; Vol. 1, Chapter 7, and references therein.

(21) Speight, J. G.; Kovacic, P.; Koch, F. W. *J. Macromol. Sci., Rev. Macromol. Chem.* **1971**, *C5*(2), 295, and references therein.

(22) Noren, G. K.; Stille, J. K. *Macromol. Rev.* **1971**, *5*, 385, and references therein.

(23) Yaniger, S. I.; Rose, D. J.; McKenna, W. P.; Eyring, E. M. *Macromolecules* **1984**, *17*, 2579.

(24) Murray, D. P.; Dechter, J. J.; Kispert, L. D. *J. Polym. Sci., Polym. Lett. Ed.* **1984**, *22*, 519.

(25) Barbarin, F.; Berthet, G.; Blanc, J. P.; Fabre, C.; Germain, J. P.; Hamdi, M.; Robert, H. *Synth. Met.* **1983**, *6*, 53.

(26) Brown, C. E.; Khoury, I.; Bezoari, M D.; Kovacic, P. *J. Polym. Sci., Polym. Chem. Ed.* **1982**, *20*, 1697.

(27) Brown, C. E.; Jones, M. B.; Kovacic, P. *J. Polym. Sci., Polym. Lett. Ed.* **1980**, *18*, 653.

(28) Typically, recycle delays of at least five times ^1H T_1 are required to ensure complete relaxation of the magnetization between scans. See: Sanders, J. K. M.; Hunter, B. K.; *Modern NMR Spectroscopy, A Guide for Chemists*; Oxford University: Oxford, 1987, p 43.

(29) Magnetic measurements were performed by S. Josh Jacobs at the California

Institute of Technology.

(30) Carlin, R. L. *Magnetochemistry*; Springer–Verlag: New York, 1986; Chapter 1.

(31) Allemand, P. -M.; Khemani, K. C.; Koch, A.; Wudl, F.; Holczerk, K.; Donovan, S.; Grüner, G.; Thompson, J. D. *Science* **1991**, *253*, 301.

(32) Davydov, A. S. *Zh. Eksp. Teor. Fiz.* **1948**, *18*, 515.

(33) Suzuki, H. *Bull. Chem. Soc. Jpn.* **1969**, *33*,109.

(34) Ibuki, E.; Ozasa, S.; Fujioka, Y.; Kitamura, H. *Chem. Pharm. Bull.* **1980**, *28*(5), 1468.

(35) Ozasa, S.; Hatada, N.; Fujioka, Y.; Ibuki, E. *Bull. Chem. Soc. Jpn.* **1980**, *53*(9), 2610.

(36) Ibuki, E.; Ozasa, S.; Murai, K. *Bull. Chem. Soc. Jpn.* **1975**, *48*(6), 1868.

(37) Stenger-Smith, J. D.; Lenz, R. W.; Wegner, G. *Polymer* **1989**, *30*, 1048.

(38) Bradley, D. D. C. *J. Phys. D: Appl. Phys.* **1987**, *20*, 1389.

(39) Attempts to form void-free, pressed powder pellets of the DCBSA- and $ZnCl_2$-catalyzed polyphenylene samples using a KBr pellet die and 10^5 lbs applied load were unsuccessful. The powders could be compacted under pressure, but the resulting pellets would not hold together. Attempts to form void-free pellets of the DCBSA- and $ZnCl_2$-catalyzed polyphenylene samples by pyrolyzing the precursor/catalyst mixtures under pressure in a heated KBr pellet die also failed. The samples were simply extruded out of the pellet die as they aromatized.

(40) Conductivities measured for compacted powder pellets of a polycrystalline material can be up to 100 times lower than that of a completely space-filled, single-crystalline material. See reference 20.

(41) Kowalewski, J.; Levy, G. C.; Johnson, L. F.; Palmer, L. *J. Magn. Reson.* **1977**, *26*, 533.

(42) Sullivan, M. J.; Maciel, G. E. *Anal. Chem.* **1982**, *54*, 1615.

(43) Swager, T. M. Ph.D. Thesis, California Institute of Technology, 1987.

SUMMARY OF THE PROCESS

A New Route to Poly(*p*-phenylene): Stereoregular Precursors via Transition-Metal-Catalyzed Polymerization

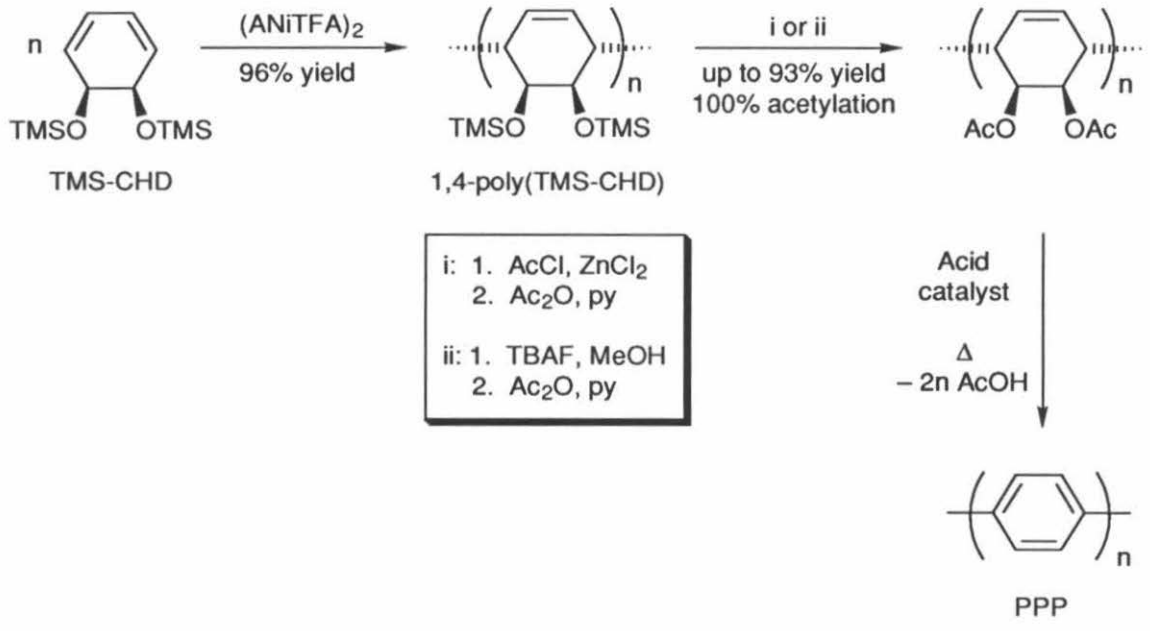

1,4-Linked, stereoregular precursors to PPP are synthesized by transition-metal-catalyzed polymerization of heteroatom-functionalized 1,3-cyclohexadienes. *cis*-5,6-Bis(trimethylsiloxy)-1,3-cyclohexadiene (TMS-CHD), a derivative of a microbial oxidation product of benzene, is polymerized stereospecifically by bis[(η^3-allyl)trifluoroacetatonickel(II)] with yields up to 96%. Not only does this polymerization system afford a highly 1,4-linked, stereoregular polymer, but it also has the potential for molecular weight control. The resulting polymer, [1,4-poly(TMS-CHD)], is a soluble, processable, semicrystalline material. Although 1,4-poly(TMS-CHD) cannot be pyrolyzed to yield PPP directly, the trimethylsilyl ethers on the polymer can be transformed to better leaving groups such as acetates to give the corresponding stereoregular acetoxy polymer (100% acetylation; 93% overall yield). Due to the relatively low thermal stability of the stereroregular backbone, aromatization of this acetoxy polymer to high quality PPP requires Lewis or Brønsted acid catalysts. Acids lower the onset temperature of the acid elimination process to a temperature regime well below that at which depolymerization can occur. The high quality PPP produced by the acid-catalyzed aromatization of the

stereoregular acetoxy polymer exhibits properties comparable to those of PPP samples in the literature. However, the material is completely amorphous whereas PPP samples made by other routes are almost always semicrystalline. Since the physical and chemical properties of PPP and many other conjugated polymers depend highly on sample morphology, processing techniques for this material will have to be developed before its optimum properties can be realized. Fortunately, our new route to PPP offers processability as well as a high quality product.